Organometallic compounds of osmium for cancer therapy

Shirley Hui Zhi Shirley Lee

NANYANG TECHNOLOGICAL UNIVERSITY

ORGANOMETALLIC COMPOUNDS OF OSMIUM FOR CANCER THERAPY

COMPOSES ORGANOMETALLIQUES D'OSMIUM POUR LA THERAPIE DU CANCER

LEE HUI ZHI SHIRLEY

School of Physical and Mathematical Sciences (CBC)
and Ecole Doctorale, Ecole Polytechnique
2015

ORGANOMETALLIC COMPOUNDS OF OSMIUM FOR CANCER THERAPY

LEE HUI ZHI SHIRLEY

BSC (Hons, 2nd upper), 2011

Nanyang Technological University

A THESIS SUBMITTED FOR THE DEGREE OF

DOCTOR OF PHILOSOPHY

NANYANG TECHNOLOGICAL UNIVERSITY (CBC)/

CHIMIE PARISTECH

SINGAPORE

2015

JURY

Tianhu LI	Associate Professor	Président
Han Vinh HUYNH	Associate Professor	Rapporteur
Christophe BIOT	Professeur	Rapporteur
Tanja WEIL	Professeur	Rapporteur
Richard D. WEBSTER	Associate Professor	Examinateur
Fabien GAGOSZ	Directeur de recherche	Examinateur
Shao FANGWEI	Associate Professor	Examinateur

Weng Kee LEONG	Associate Professor	Co-Directeur de thèse
Siden TOP	Directeur de recherche	Co-Directeur de thèse

Abstract

Cis-platin and its derivatives are the most currently used for cancer treatment. Inspired by these metallodrugs, organometallic compounds (Ti, Ru, Fe, Rh, Au…) have been developed over the years as potential candidates for anticancer drugs, some of these have entered clinical trials. Jaouen and co-workers have developed novel therapeutic agents based on ferrocene compounds analogous to tamoxifen, which show high anti-proliferative effects against two types of breast cancer cells, namely the ER+ breast carcinoma (MCF-7) and the ER- breast carcinoma (MDA-MB-231). Similarly, Leong's group has found a series of triosmium carbonyl clusters that shows anticancer activity against these two breast cancer cells. Thus, it would be interesting to study osmocene compounds analogous to tamoxifen. Cytotoxic activity of these tamoxifen analogues, as well as that of triosmium clusters, were studied.

Le cis-platine et ses dérivés sont des médicaments très utilisés pour traiter certains types de cancers. Inspirés par ces métallodrogues, des composés organométalliques (Ti, Ru, Fe, Rh, Au…) font l'objet en ce moment d'une recherche active pour leur activité anticancéreuse. Certains ont atteint le stade des tests cliniques. Le groupe du Professeur G. Jaouen a mené des travaux de recherche sur des antitumoraux basés sur les analogues ferrocéniques du tamoxifen. Ces composés sont actifs contre les cellules cancéreuses hormono-dépendantes (MCF-7) et hormonaux indépendantes (MDA-MB-231). D'un autre côté, le groupe du Professeur W. Leong a démontré que les clusters triosmium carbonylés possèdaient aussi les propriétés antitumorales contre les deux lignées cellulaires citées plus haut. Il apparaissait donc intéressant de synthétiser des analogues osmocéniques du tamoxifen jusqu'ici inconnus. L'activité cytotoxique de ces espèces et aussi celle des clusters d'osmium a été étudiée.

Acknowledgements

I would like to express my gratitude to my supervisor, Associate Professor Leong Weng Kee for his invaluable guidance, support, encouragement, and understanding. Next, I would like to extend my gratitude to my co-supervisor Dr Siden Top for his guidance and support while I am in Paris; it was indeed a wonderful experience.

I would like to express my appreciation to Prof Jaouen and Dr Anne Vessières for accepting me to their lab for this NTU-ParisTech PhD program; it was indeed an honour to be part of their research group. I would like to extend this appreciation to Dr Fabien Gagosz from Ecole Polytechnique and Prof. Didier Gourier from Chimie ParisTech for being my corresponding PhD advisors, Dr Christian Amatore, Olivier Buriez and Eric Labbé from Ecole Nationale Superieure for their kind support and expertise on the electrochemistry experiments, which aided me tremendously in this thesis study.

To my following fellow labmates, thank you for all the assistance in lab as well as the fun times we had: Jing Wei, Yuqian, Yong Jia, Ying Zhou, Zhiyong, Boyang, Garvin, Liu Yu, Kumaran, Joey, Holly, Chloe, Chandan, Marcus, Quanli, ShiinYiing and Shi Ning from Singapore group; Michele Salmain, Pigeon Pascal, Wang Yong, José Cázares-Marinero, Marie-Aude and Nathalie Durand from Paris group.

I would also like to thank the following who have given me assistance in various ways during my postgraduate studies: CBC thesis committee Prof Xing Bengang, Prof Shao Fangwei, the CBC research staffs Rakesh, Ee Ling, Derek, Wenwei, Eric from SBS, and special friends forged in Paris: Vasilieos, Xue, Ismael and Anthony for making me feel comfortable in Paris so that I can concentrate with my research work in Paris. The NTU-ParisTech Research Scholarship from NTU over the last four years is also gratefully acknowledged.

Last but not least, I would like to thank my family and friends for their love, and their full support, trust and encouragement in all my pursuits. ☺

Summary

This thesis describes studies directed at two potential classes of osmium compounds which show anticancer activity. The aim is to gain a better understanding of their structure-activity relationships and modes of action, so as to aid the development of more potent variants.

Chapter one provides a background to the biochemical basis of cancer and anticancer drugs, including the different modes of cell death. The main categories of anti-cancer drugs available in the market are surveyed, particularly, those based on organometallic compounds. Of these, two particular classes, triosmium carbonyl clusters, developed by Pr W.K Leong in Singapore, and ferrocifens, developed by Pr G. Jaouen in Paris, are of interest in this study.

Structure-activity relationship studies were conducted on the osmium carbonyl cluster $Os_3(CO)_{10}(NCMe)_2$ **2**, which has been reported to exhibit anticancer properties, in chapter two. In effect, two criteria were necessary for its activity – the availability of a vacant coordination site, and good solubility. In the course of these studies, two new classes of triosmium clusters, $Os_3(CO)_{11}(NCMe)(\mu\text{-}H)^+$ **1'** and $Os_3(CO)_9(\mu\text{-}H)(\mu\text{-}\gamma\text{-}C_6H_5O_3)$ **5**, which were structurally different from **2**, were also found to be active against cancer cells. An osmium cluster-thymidine bioconjugate was also synthesised to test the hypothesis that this species may have increased selectivity through the over-expression of thymidine kinase I in cancer cells.

The mode of action for **1'** and **5** were investigated in chapter three. Their apoptosis induction was established through various apoptosis assays. With the expectation that their targets were protein residues, their chemical reactivity towards nucleophilic aminoacids were investigated. It was found that while **2** readily reacted with thiols, **1'** required initial deprotonation and **5** required a stronger nucleophile, such as, thiolate. Identification of their reaction products in cancer cells, however, revealed a new possible target –hydroxyl residues.

Chapter four describes studies directed at the metallocifens. The osmium-based tamoxifens (osmocifens) were successfully synthesized, and characterized. A comparison with the Fe and Ru analogues concluded that osmocifens and ruthenocifens have similar cytotoxic activity and are less active than ferrocifens. For Os and Ru compounds, only the compounds bearing an amine

chain are active against cancer cells; and this suggests that the phenol and the amine derivatives might have different mode of actions. The main mechanism of action was found to be the induction of senescence, and contributing factors from the metal included its redox potential and electronegativity. The ability to form quinone methides, and their stability, were found to be important factors for the antiproliferative activity.

This study shows that osmium, which has been quite neglected, might become potential antitumor agents. In this context, this work is important as it expands the diversity in potentially usable bioorganometallics.

Résumé

Cette thèse décrit les études sur l'activité antitumorale de deux classes de complexes organométalliques d'osmium. L'objectif du travail est de trouver la relation entre la structure et l'activité cytotoxique d'une part, et d'autre part, les meilleurs composés pour cette application thérapeutique.

Le premier chapitre est un rappel des connaissances de base sur le cancer et sur quelques médicaments anticancéreux mis sur le marché. Les différents mécanismes d'action liés à la mort des cellules cancéreuses ont été discutés. Un état des lieus sur la recherche en cours concernant de nouveaux types de médicaments basés sur les complexes des métaux de transition est décrit. Deux types de complexes organométalliques ont été particulièrement examinés. Il s'agit des anologues ferrocéniques du tamoxifène, développés par le groupe du Professeur G. Jaouen à Paris, et les clusters triosmium développés par le groupe du Professeur W. Leong à Singapour. Suite aux résultats intéressants obtenus, les deux équipes ont décidé de mener une recherche commune qui est relative à l'étude d'un nouveau type de composés, il s'agit des analogues osmocéniques du tamoxifène.

Le deuxième chapitre décrit les résultats obtenus sur les clusters d'osmium. Une étude sur la relation entre structure et activité du cluster de triosmium carbonylé $Os_3(CO)_{10}(NCMe)_2$ **2**, composé présentant des propriétés cytotoxiques, a été menée. Il apparaît que la présence d'un site de coordination vacant et la bonne solubilité sont importantes pour avoir une bonne activité cytotoxique. Deux autres composés, $Os_3(CO)_{11}(NCMe)(\mu\text{-}H)^+$ **1'** et $Os_3(CO)_9(\mu\text{-}H)(\mu\text{-}\gamma\text{-}C_6H_5O_3)$ **5**, dont les structures sont très différentes, sont aussi actifs contre les cellules cancéreuses. Pour tester l'hypothèse de l'existence de la surexpression de thymidine kinase dans les cellules cancéreuses, un cluster de triosmium portant le résidu thymidine a été également étudié.

Le mode d'action de $Os_3(CO)_{11}(NCMe)(\mu\text{-}H)^+$ **1'** et $Os_3(CO)_9(\mu\text{-}H)(\mu\text{-}\gamma\text{-}C_6H_5O_3)$ **5** a été décrit dans le chapitre 3. Ces composés ont provoqué la mort cellulaire par apoptose. En considérant que la cible de ces composés est un résidu de la protéine, une étude sur la réactivité chimique avec les aminoacides nucléophiles a été menée. On trouve que **2** réagit directement sur les thiols

alors que **1'** nécessite une déprotonation préalable et que **5** nécessite un fort nucléophile, comme par exemple un thiolate. On trouve que les résidus hydroxyliques sont aussi des cibles possibles.

Le chapitre quatre est consacré aux analogues osmocéniques du tamoxifène. En suivant la méthode développée pour la synthèse des analogues ferrocéniques (ferrocifène), les analogues osmocéniques (osmocifènes) ont été obtenus. Ces composés ont permis une étude comparative entre l'activité cytotoxique des trois séries métallocéniques : ferrocifène, ruthénocifène et osmocène. D'une manière générale, les osmocènes et les ruthénocènes ont des activités similaires et plus faibles que celle des ferrocifènes. Cette étude a permis de mettre en évidence la différence d'activité entre les composés phénoliques sans chaîne aminée et les composés portant une chaîne aminée. Pour les complexes d'osmium et de ruthénium, seuls les composés aminés sont actifs alors que les composés phénoliques sont presque inactifs. Cette différence pourrait être corrélée à l'effet de sénescence observé, seuls les composés aminés provoquent la sénescence. Les propriétés électrochimiques, la formation et la stabilité des quinones méthides sont des facteurs importants qui influencent l'activité antiproliférative des complexes.

Cette étude a montré que certains types de complexes d'osmium sont actifs contre les cellules cancéreuses. Ce métal sous forme d'organométallique a jusqu'ici été peu utilisé dans ce contexte. Ce travail est important dans la mesure où il précise les possibilités de son utilisation et par suite ouvre la voie à de nouvelles orientations.

Table of Contents

List of Figures

List of Schemes

List of Tables

Abbreviations

$CDCl_3$:	Chloroform
COE:	Cyclooctene
CV:	Cyclic voltammogram
DAPI:	4',6-diamidino-2-phenylindole
DCM:	Dichloromethane
DMEM:	Dulbecco's Modified Eagle's Medium
DMSO:	Dimethylsulfoxide
DNA:	Deoxyribonucleic acid
ER:	Estrogen receptor
FACS:	Fluorescence activated cell sorting
FBS:	Feral Bovine Serum
Fe:	Iron
FITC:	Fluorescein isothiocyanate
Hex:	Hexane
IC_{50}:	50 % inhibitory Concentration
IR:	Infrared
MS:	Mass Spectrometry
NMR:	Nuclear Magnetic Resonance
Os:	Osmium
PBS:	Phosphate Buffered Saline
PI:	Propidum iodide
ppm:	Part Per Million
QM:	Quinone methide
Ru:	Ruthenium
SAR:	Structure Activity Relationship
THF:	Tetrahydrofuran
TLC:	Thin-Layer Chromatography

Infrared Spectroscopy

νco:	stretching frequency in the carbonyl region (1700 – 2200 cm^{-1})
w:	weak
m:	medium
s:	strong
vs:	very strong
sh:	shoulder

NMR shift

s:	singlet
d:	doublet
dd:	doublet doublet
q:	quartet
t:	triplet
m:	multiplet

Molecular Numbering Scheme

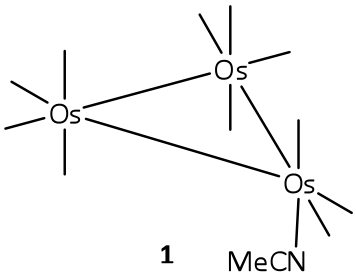

1

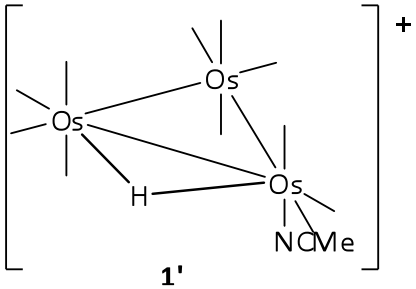

1'

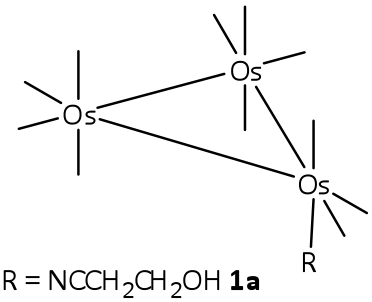

R = $NCCH_2CH_2OH$ **1a**
R = NCC_6H_4OH **1b**
R = pyridine **1c**
R = imidazole **1d**

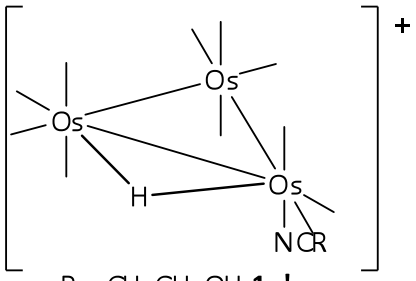

R = CH_2CH_2OH **1a'**
R = *p*-C_6H_4OH **1b'**

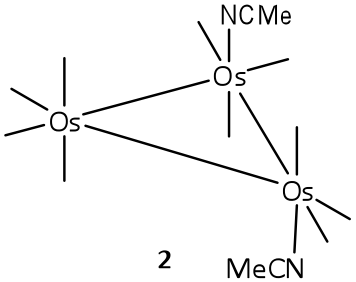

2

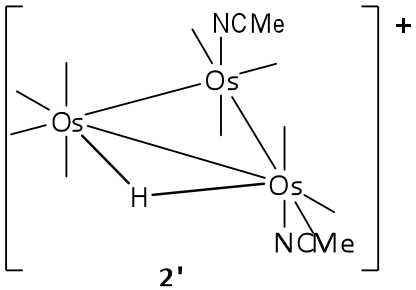

2'

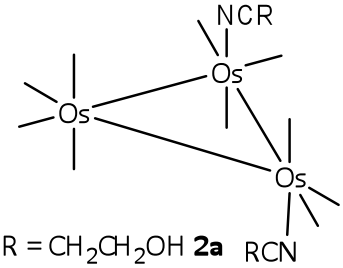

R = CH_2CH_2OH **2a**
R = *p*-C_6H_4OH **2b**

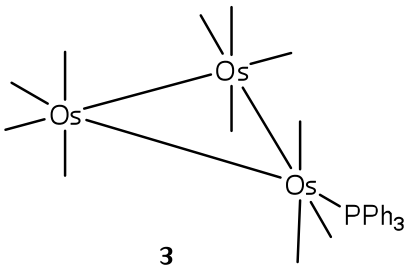

3

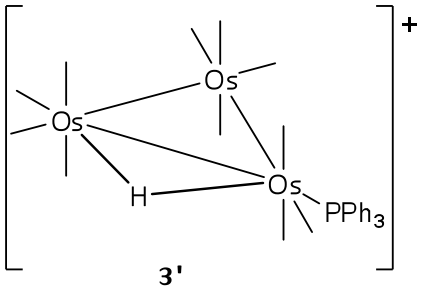

3'

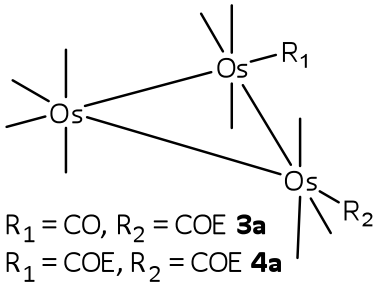

R_1 = CO, R_2 = COE **3a**
R_1 = COE, R_2 = COE **4a**

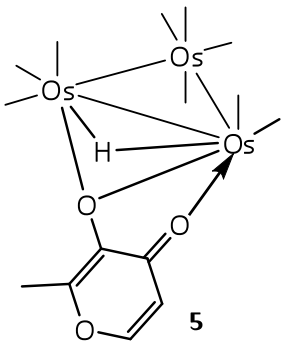

5

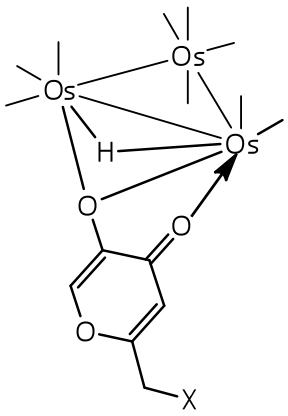

X = Cl **5a**

X = Br **5b**

X = N_3 **5c**

X = OH **5d**

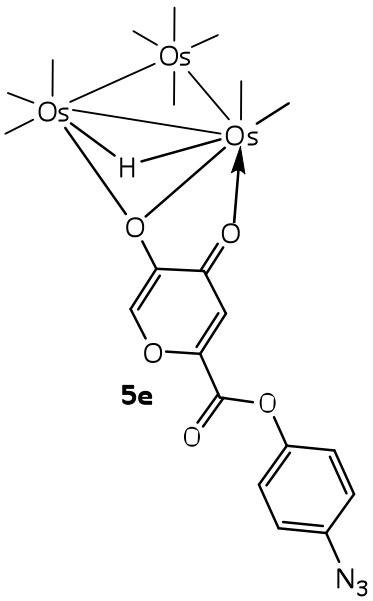

5e

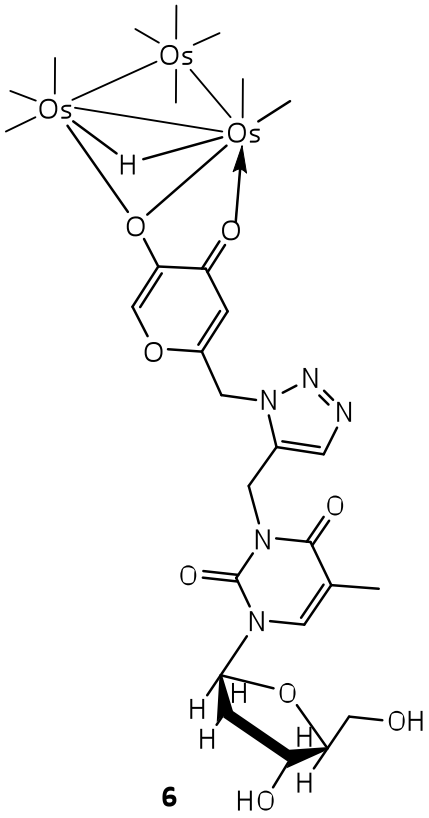

6

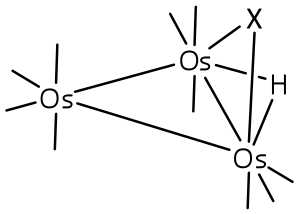

X = SCH_2CH_3 **7a**
X = SR **7a'**
X = OH **7b**
X = OR **7b'**
X = Cl **7c**

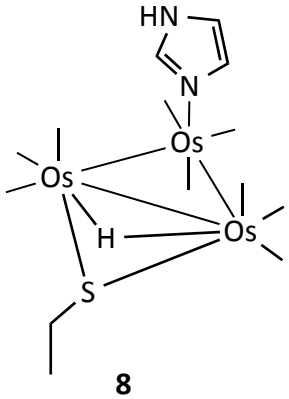

8

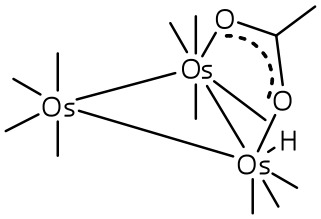

9

Chapter 4: Osmium-based Tamoxifens

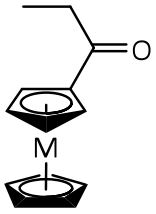

M = Fe **10**
M = Ru **11**
M = Os **12**

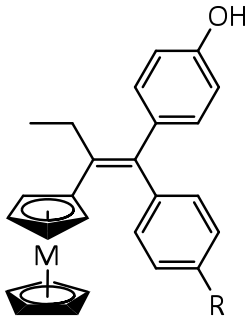

M = Fe, R = H, **10a**.
M = Fe, R = OH, **10b**.
M = Ru, R = H, **11a**.
M = Ru, R = OH, **11b**.
M = Os, R = H, **12a**.
M = Os, R = OH, **12b**.

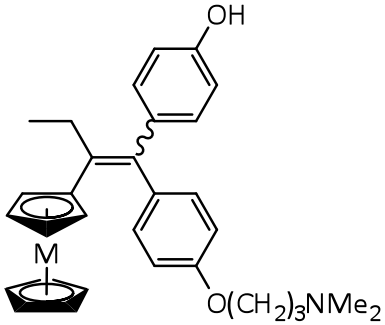

M = Fe, **10c**.
M = Ru, **11c**.
M = Os, **12c**.

List of publications

1. H. Z. S. Lee, W. K. Leong, S. Top, A. Vessieres, *Chemmedchem,* **2014**, *9*, 1453.

2. H. Z. S. Lee, O. Buriez, E. Labbe, S. Top, P. Pigeon, G. Jaouen, C. Amatore, W. K. Leong, *Organometallics*, **2014**, *33*, 4940.

3. H. Z. S. Lee, O. Buriez, F. Chau, E. Labbe, R. Ganguly, C. Amatore, G. Jaouen, A. Vessieres, W. K. Leong, S. Top, *Eur. J. Inorg. Chem*, **2015**, 4217.

Chapter 1: Cancer and use of organometallic compounds in cancer therapy

1.1 Cancer

Cancer is a class of diseases where a group of cells grow uncontrollably and do not die. There are over 100 different known cancers,[1] and they are classified by the type of cells that is initially affected. Breast cancer, which constitutes 18.2 % of reported cancer deaths worldwide, is the most common invasive cancer in females.[2] Breast cancer arises when milk-producing glands, which normally reproduce under the control of hormones, grow out of control to form a tumor. For many cancers, only 5-10 % of the cases are due to inherited genes; the BRCA1 and BRCA2 genes are examples for breast cancer.[3] The rest of the cases are due to external factors, such as, tobacco and radiation, that directly damage DNA. Damaged DNA causes a series of different gene mutations, such as activation of oncogenes (cancer causing genes) and inhibition of tumor suppressor gene functions, leading to uncontrolled cell growth. Such uncontrolled cell division is a result of interference in the normal cell cycle. In order to better understand cancer, therefore, it is necessary to understand the cell life cycle.

1.2 Cell cycle

The life cycle of a cell, which is a series of complex signaling pathways, is divided into four phases (Figure 1.1).

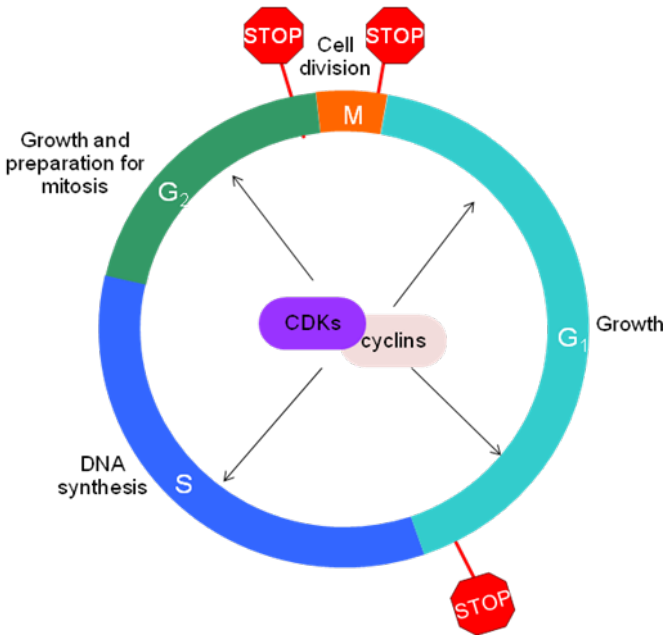

Figure 1.1. The four different stages of a life cycle.

The four phases are: G1 (gap) phase, in which the cells grow and prepare to synthesize DNA; S phase, where the cell synthesizes DNA; G2 (gap) phase, in which the cell continues to grow and prepares to divide; and finally the M or mitosis phase, during which cell division occurs. Before the cell enters each phase, it passes through a checkpoint, with specialized cell cycle regulator proteins (cyclins) and kinases (cyclin-dependent kinases) to check for DNA damage.[4] Cells with intact DNA continue to the next phase; cells with damaged DNA "commit suicide" through apoptosis. Cancer occurs when there is genetic mutation resulting in one or more of the regulatory proteins at the cell cycle checkpoints being in a "permanently molecular switch on" mode. This causes uncontrolled multiplication of the cell, resulting in tumor growth and, ultimately, cancer.

1.3 Apoptosis

As mentioned earlier, cells with damaged DNA will undergo a programmed cell death known as apoptosis. The mechanisms of apoptosis are highly complex and sophisticated, involving an energy-dependent cascade of molecular events.[5] To date, two main apoptotic pathways are recognized: The extrinsic and the intrinsic pathways (Figure 1.2).

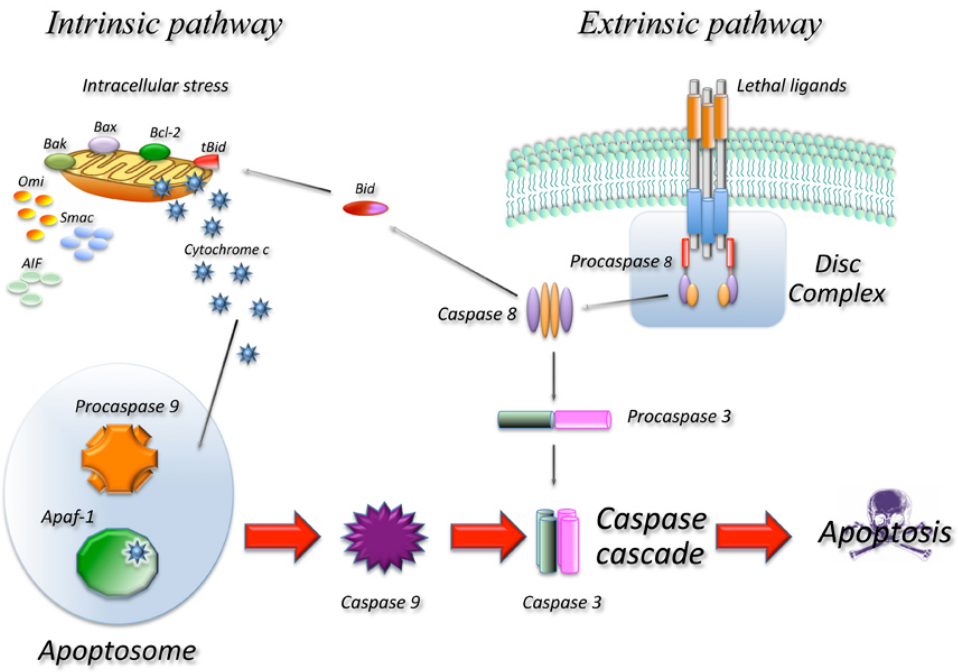

Figure 1.2. The extrinsic and intrinsic pathway of apoptosis.[6]

In both pathways, a group of cysteine proteases, called caspases, are involved. The pathways ultimately lead to the activation of caspase-3, and thence to apoptosis. The extrinsic pathway, as the name suggests, is induced by extracellular signals through the binding of ligands to specific trans-membrane receptors known as death receptors. This ligand-receptor binding results in conformational changes, allowing the assembly of a large multi-protein complex known as the Death Initiation Signalling Complex (DISC). This complex leads to the activation of the caspase cascade, with caspase-8 being first activated, followed by caspase-3. Caspase-3 then induces the cellular changes that characterize apoptosis.[7] On the other hand, the intrinsic pathway is initiated within the cell, in response to DNA damage and severe cell stress. These stresses induce the formation of proteins called apoptosomes. Apoptosomes then recruit and activate caspase-9, which in turn promotes the activation of caspase-3, causing apoptosis.[8]

Besides apoptosis, the other mode of cell death is known as necrosis. This refers to cell death caused by external factors such as trauma or infection, resulting in irreversible changes within the

nucleus and cytoplasmic structure, and finally cytolysis (bursting of cells). It is mediated by two main mechanisms; interference with the energy supply of the cell, and direct damage to the cell membrane.[9]

Cell death through apoptosis or necrosis is very different in terms of the morphology and biochemistry. Some of the main differences are given in Table 1.1, and methods to differentiate between the two have been developed. Three methods to distinguish apoptosis will be described.

Table 1.1. Differences between apoptosis and necrosis.[10]

Characteristics	**Apoptosis**	**Necrosis**
Stimuli	Physiological or pathological	Pathological (injury)
Occurrence	Single cells	Group of cells
Cellular organelles		
Cell shape	Shrinkage and formation of apoptotic bodies	Swelling and later disintegration
Membranes	Blebbing	Blebbing prior to lysis
Cytoplasm	Late-stage swelling	Very early swelling
Nucleus	Convolution of nuclear outline and breakdown (karyorrexis)	Disappearance (karyolysis)
Biochemical level		
Gene activation	Present	Absent
Activation of caspases	Present	Absent
Nuclear chromatin	Compaction in uniformly dense mass	Clumping not sharply defined
DNA breakdown	HMW and internucleosomal	Randomized
Phosphatidylserine exposure	Present	Absent

1.3.1 Apoptosis assay based on phosphatidylserine exposure

In normal viable cells, phosphatidylserine (PS), an important phospholipid membrane component of the cell membrane, is held facing the cytoplasmic (inner) side of the cell membrane.

However, during apoptosis, they can be translocated from the inner to the outer leaflet of the plasma membrane, exposing it to the external cellular environment (Figure 1.3).

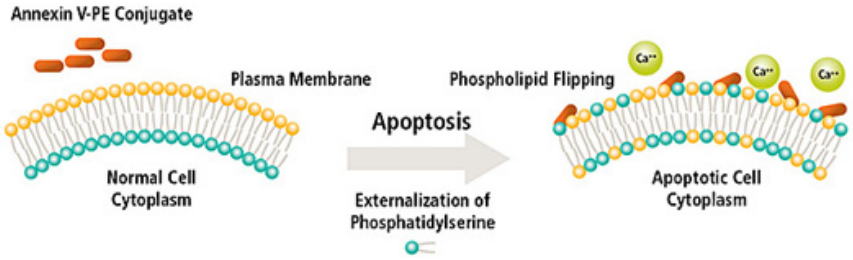

Figure 1.3. Externalization of Phosphatidylserine in apoptotic cells.[11]

The translocation of PS to the outer plasma membrane in apoptotic cells thus allows the labeling of apoptotic cells, by using FITC conjugated Annexin V because FITC Annexin V, has a high affinity for PS, will stain apoptotic cells with green fluorescence. The incorporation of a second dye, propidum iodide (PI) allows the labeling of necrotic cells (red fluorescence), as PI is impermeant to live cells and apoptotic cells. Hence, after staining with FITC annexin V and PI in the binding buffer, apoptotic cells will show green fluorescence (PI negative, FITC positive), necrotic cells will show red and green fluorescence (PI and FITC positive), and live cells will show little or no fluorescence (Figure 1.4).

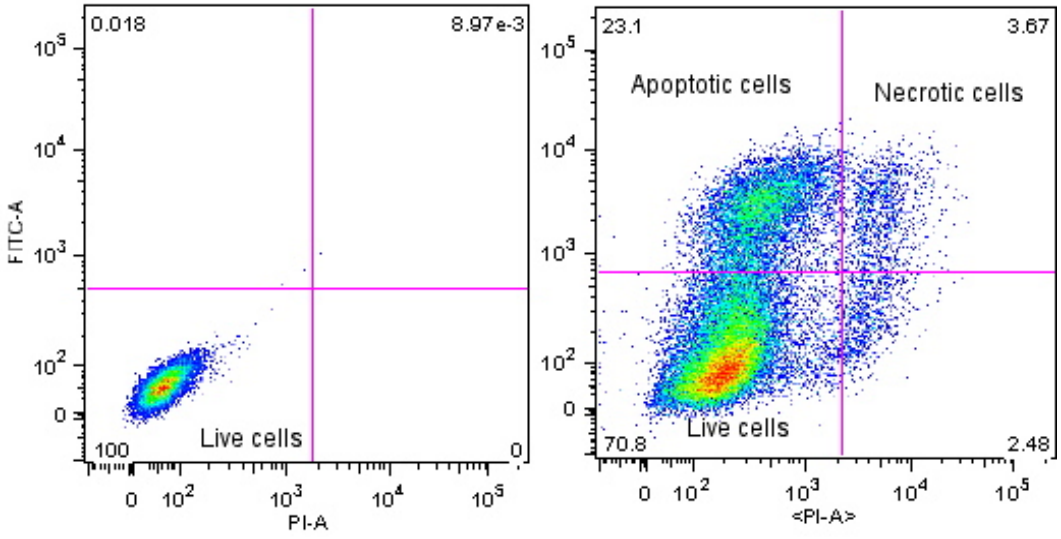

Figure 1.4. Detection of apoptotic MDA-MB-231 cells after staining with Annexin V-FITC and PI. (a) Control, (b) Apoptotic and necrotic cells.

1.3.2 DNA fragmentation in apoptotic cells

An early event in apoptosis is the activation of endonuclease Caspase-Activated DNAse (CAD), an enzyme that cleaves DNA. This causes extensive DNA fragmentation in apoptotic cells.[12] Hence, one can detect apoptotic cells by detecting DNA fragmentation. Determination of the DNA content in cells is usually done by first permeabilizing the cell membrane (using chemical fixing agents like alcohols), followed by staining with DNA binding dyes such as PI, and then analysis using a flow cytometer. Fixation with ethanol is inadequate to preserve the degraded, low molecular weight DNA inside apoptotic cells. As a result, apoptotic cells often end up with deficient DNA content, and are thus recognized by flow cytometry as cells having less DNA. This gives a characteristic sub-G1 peak in the DNA frequency histogram (plot of number of cells against DNA content) (Figure 1.5).[13]

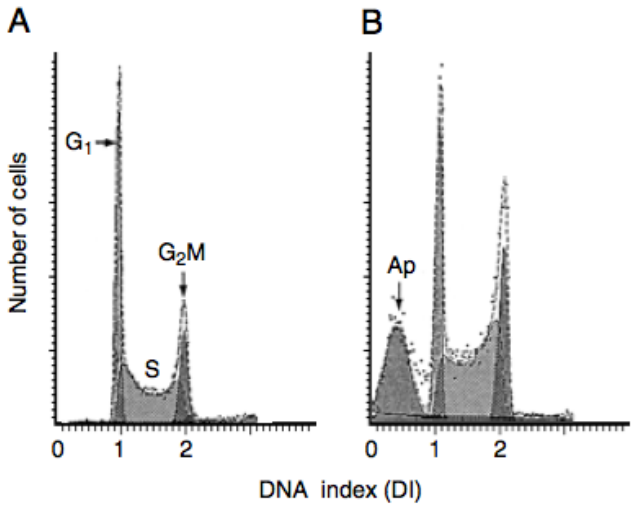

Figure 1.5. DNA histogram of a) live cells, b) apoptotic cells.[14]

1.3.3 Nuclear chromatin condensation in apoptotic cells

Cellular assays often involve techniques, such as, trypsinization and centrifugation, which cause preferential loss of apoptotic cells during sample preparation. One of the best methods to distinguish apoptotic cells is thus based on their morphological characteristic through examination under the microscope. One example is to examine nuclear chromatin condensation in apoptotic cells by staining with DAPI (Figure 1.6).

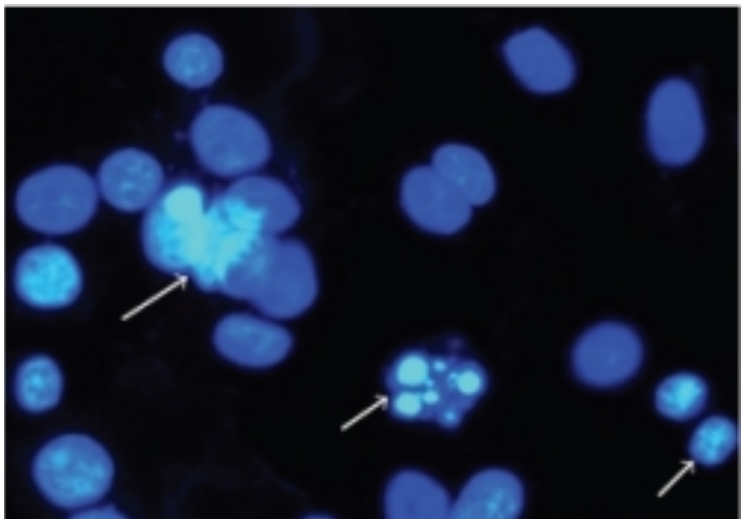

Figure 1.6 Cells stained with DAPI and examined fluorescent micropcopy. Apoptotic cells are indicated in arrows.[15]

The arrows shown in figure 1.6 highlight the nuclear chromatin condensation, a trademark for apoptotic cells, while the rest of the cells (live cells) show intact round nuclei.

1.4 Cellular Senescence

Senescence, which comes from the word *senex* in latin, means "old age" or biological aging. Cellular senescence refers to the phenomenon whereby cells cease to divide. It was first described by Haflick and colleagues who showed that cell cultures, after many cell doublings, lose their ability to divide.[16] These non-dividing cells failed to divide despite the presence of ample space and medium, but they remained viable for many weeks. The discovery of this phenomenon brought on an important hypothesis; the fact that many cancer cells proliferate indefinitely. The senescence response is therefore beneficial as it prevents cancer cells from further dividing, and also prevents metastasis.

Cellular senescence comprises three phenotypes. The first is the inability to progress through the cell cycle, also known as growth arrest. Once arrested, they usually possess a DNA content that is typical of G1 phase arrest, as initiation of DNA replication fails despite the cells remaining metabolically active and even with adequate growth conditions.[17] Secondly, senescent cells are apoptosis resistant. Senescence, like apoptosis, is also a response to cellular stress, but instead of

being engulfed (undergoing apoptosis), they stop growing (senescence). Lastly, senescent cells show altered gene expression, particularly in changes in the cell-cycle inhibitors or activators, such as, the cyclin-dependent kinase inhibitors (CDK1s).[18]

There are several marker-based assays used to identify senescent cells, but none are exclusive to the senescent state. The first is the senescence-associated β-galactosidase (SA-β-gal) assay. It is based on the increase in lysosomal β-galactosidase level in senescent cells. In non-senescent cells, the lysosomal hydrolase β-galactosidase cleaves galactose from glycoproteins at pH 4 – 4.5. However, during senescence, the increase in lysosomal β-galactosidase protein levels and lysosomal size allows for the detection of β-galactosidase activity at the suboptimal pH of 6 during senescence.[19] Lysosomal β-galactosidase activity in senescent cells can thus be detected by performing a cytochemical assay with X-gal, a chromogenic substrate that forms a blue precipitate when cleaved by β-galactosidase, at pH 6. Senescent cells will thus be stained blue, while non-senescent cells will not be stained. (Figure 1.7)

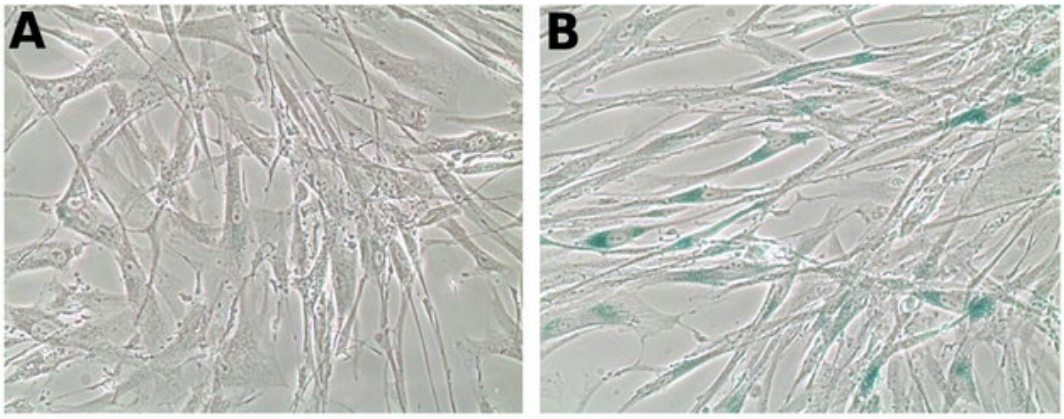

Figure 1.7. (a) Non-senescent cells, (b) Senescent cells.[20]

1.5 Anti-cancer drugs

The main target of most chemotherapeutic drugs is to impair the cell cycle of cancer cells, to prevent them from further division. This can be achieved through various mechanisms of action, such as, damaging DNA replication, preventing mitosis, inducing apoptosis, or senescence. This section describes the mechanisms of action of a few categories of chemotherapeutic drugs.

1.5.1 Alkylating agents

Alkylating agents are the oldest group of anti-cancer drugs that have been in use. They act by forming cross-links on DNA, thus interfering with the action of enzymes involved in DNA replication. The cells are then either unable to divide or apoptosis is triggered. Examples of such agents are the nitrogen mustards, nitrosoureas and the aziridines (Figure 1.8).

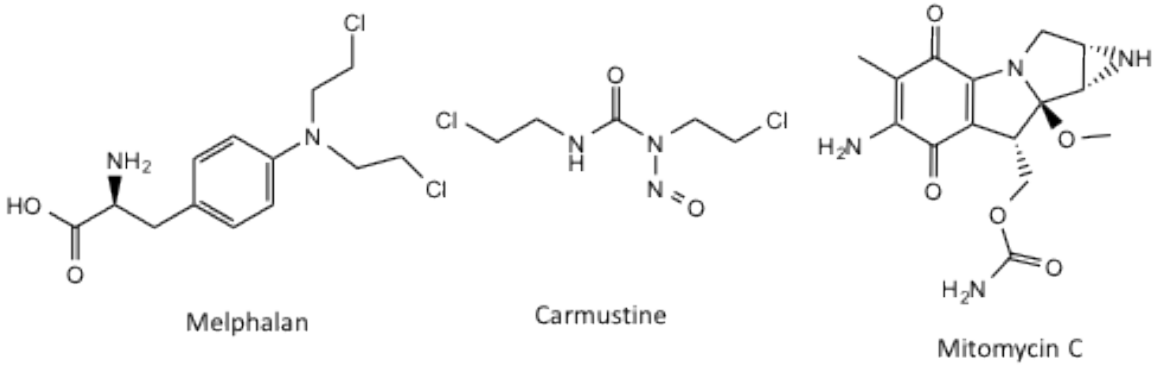

Figure 1.8. Examples of alkylating agents used as chemotherapeutic agents.

Melphalan is an example of a nitrogen mustard alkylating agent. It acts by alkylation of the nucleotide guanine in DNA and thus inhibiting DNA and RNA syntheses.[21] Carmustine is a dialkylating agent that forms interstrand crosslinks in DNA. It also prevents DNA replication as well as DNA transcription.[22] Lastly, mitomycin is a potent bis-alkylating agent (through two N-alkylations) that is used to treat many forms of cancer such as esophageal, anal and breast cancers.[23]

1.5.2 Antimetabolites

Antimetabolites share similar structures to naturally occurring compounds used in nucleic acid (DNA and RNA) synthesis. They compete with the natural metabolite for the active site on an essential enzyme/receptor. Generally, antimetabolites induce cell death at the S phase of the cell cycle, and are known to be cytostatic (inhibits cell growth) instead of cytotoxic (killing the cells). There are three main classes of antimetabolites - folic acid antagonists, and the pyrimidine and purine analogues (Figure 1.9).

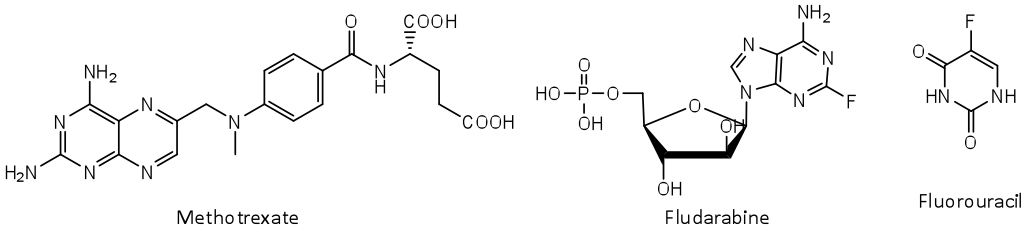

Figure 1.9. Examples of antimetabolites as chemotherapeutic drugs.

The most commonly used folic acid antagonist is methotrexate. It binds to the enzyme dihydrofolate reductase (DHFR) and deactivates it. This prevents methylation and decreases the availability of purine and thymidine bases for DNA and RNA synthesis, hence disrupting the S phase of cell growth.[24] The pyrimidine and the purine analogues act as purine and pyrimidine antagonists, respectively; they are incorporated into DNA during nucleotide synthesis, leading to strand termination, and hence preventing cell division.[25]

1.5.3 Spindle poisons

In contrast to the above which affect DNA synthesis or replication (G1 or S phase of the cell cycle), spindle poisons are stress signal inducers that block mitosis (M phase). Mitosis is the final phase of the cell cycle during which the chromosomes divide into two identical sets. This segregation of the chromosomes between daughter cells requires the help of mitotic spindles, subcellular structures that are composed from the binding of microtubules (polymerized tubulins) with the protein kinetochore.

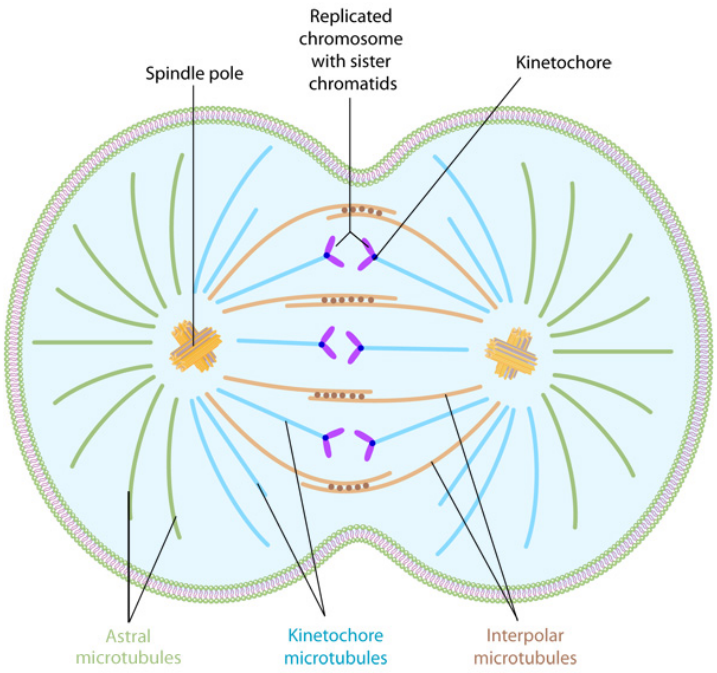

Figure 1.10. Types of microtubules and spindle involved in mitosis.

Spindle poisons disrupt this cell division by inhibiting the kinetochores, preventing it from binding with microtubules. This leads to disruption of the spindle assembly and mitotic arrest. There are generally two types of spindle poisons - the vinca alkaloids which inhibit the polymerization of tubulins into microtubules, resulting in G2/M arrest; and the taxanes which stabilize the microtubule polymer, protecting it from disassembly and thus prolonging activation of the mitotic checkpoint, which then triggers apoptosis or reversion to G-phase without cell division.[26]

1.5.4 Mitochondrial drugs

Although many of the anticancer drugs are designed to disrupt nucleic acid synthesis in the nucleus, compounds which target the mitochondria (the “power plant”) that gives energy to keep cells alive, is a promising new class of anticancer drugs. The idea of mitochondrial drugs or “mitocans” became of interest after the finding that tumors of the same type from individual patients can differ in mutations.[27] The implication of this is that it will be unlikely to overcome cancer by targeting a single gene pathway. In contrast, the mitochondrion is an invariant target present in all tumours. Since then, many classes of mitocans have been developed, ranging from

compounds which target the Bcl-2 family proteins (proteins that control mitochondrial outer membrane permeabilization) to lipophilic cations that target the inner membrane. A schematic illustration depicting the molecular targets of each class of mitocans is shown in Figure 1.11.

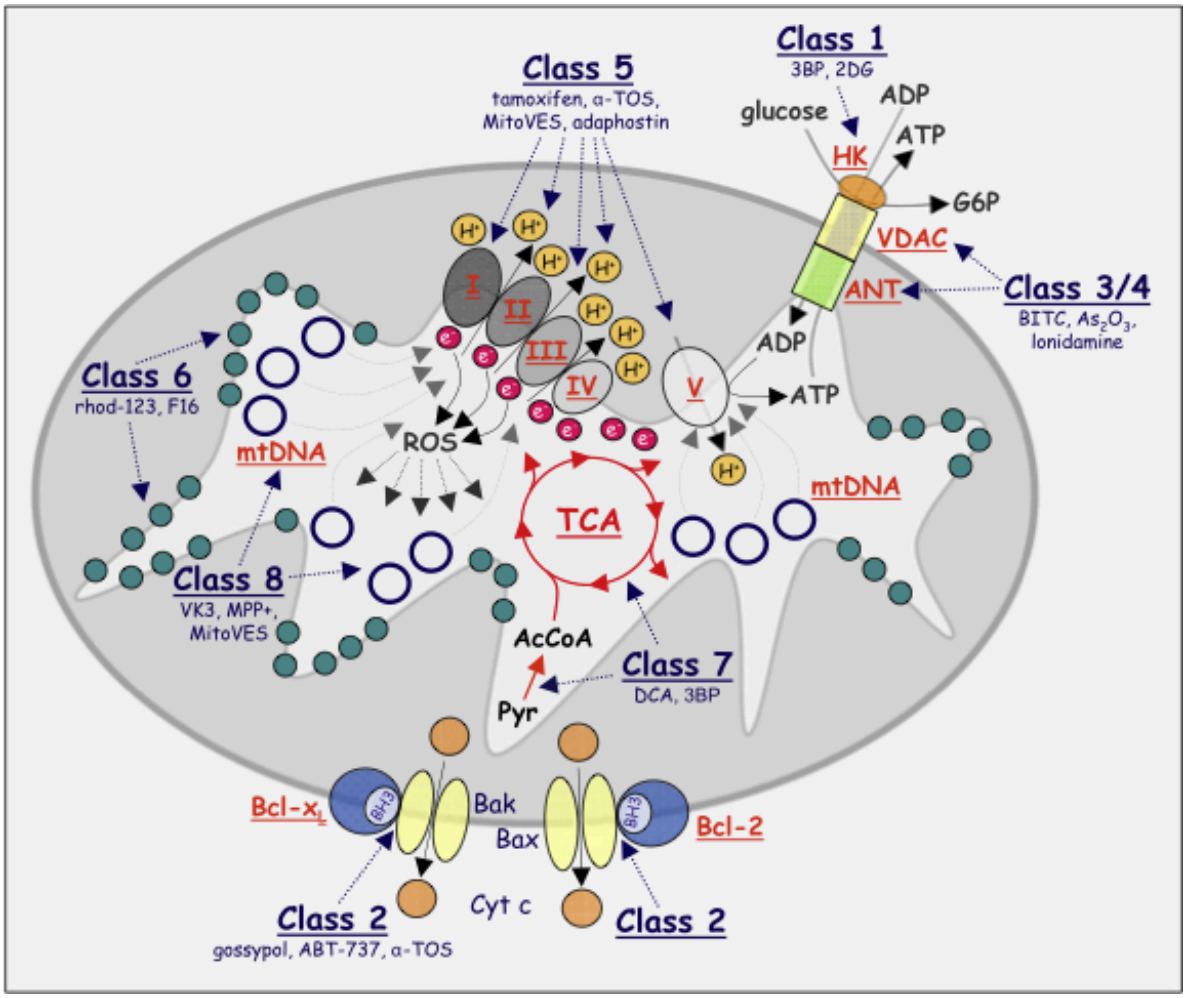

Figure 1.11. Schematic diagram of the molecular targets of each class of mitocans.[28]

1.5.5 Cisplatin

Metal-based drugs are one of the categories of the different anticancer drugs being classified, with cisplatin as one of the first that made it to the market. It is also referred to as the "penicillin of cancer" because it is used to treat a wide variety of cancers, including sarcomas, small cell lung cancer, lymphomas, and cervical cancer.[29] The general mode of action of cisplatin is shown in Figure 1.12.

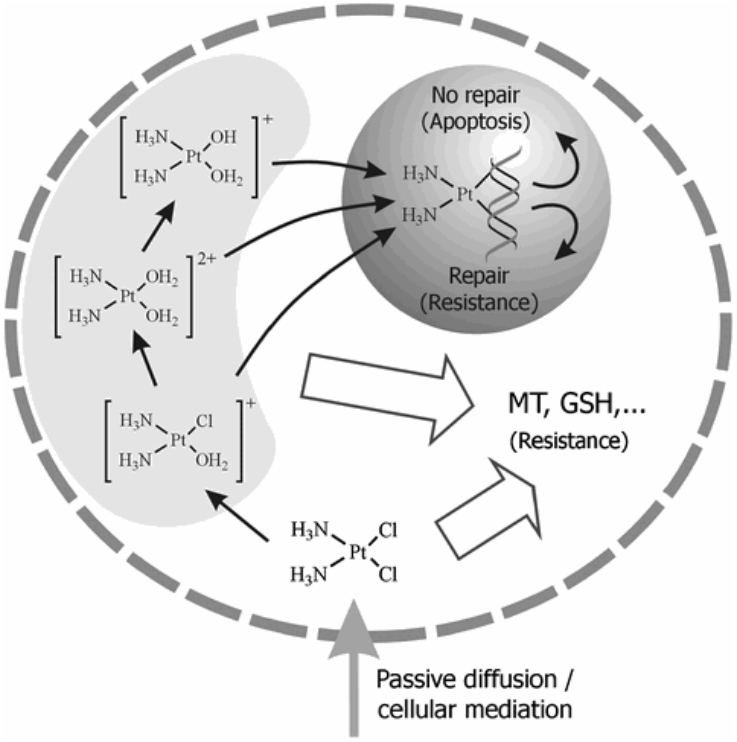

Figure 1.12. General schematic illustration showing the mode of action of cisplatin.

Before cisplatin penetrates through the membrane, either by active transport or passive diffusion, the concentration of chloride (100 mM) is high enough to prevent the loss of chloride ligands. Once in the cytoplasm, the lower chloride concentration (4 mM) facilitates aquation, which activates cisplatin to react with the nucleophilic N-sites of purine bases in DNA to form interstrand crosslinks. These DNA adducts result in a cascade of pathways leading to apoptosis.[30] Due to the high reactivity of the aquated cisplatin, however, it can also react with nucleophilic GSH and cysteine-rich metallothionein, resulting in lower level of the active species and thence some drug resistance.[31]

1.6 Organometallic anti-cancer drugs

The discovery of cisplatin has led to tremendous interest in the development of organometallic compounds as drugs.[32] Organometallic compounds, which consist of at least one metal-carbon bond, offer the advantages of a variety of available interactions (H-bond, coordinative bond, etc), rigidity around the metal and flexibility of the ligands, and redox activity. There are two general approaches to the design of organometallic anticancer drugs - ones which are active by virtue of the metal centre, and those which make use of the metal complex as a structural scaffold for an already-known active molecule.

1.6.1 Titanocenes

Titanocene dichloride, one of the pioneer organometallic anticancer drugs that made it to clinical trials, is representative of the first strategy; its structure is shown in figure 1.13.

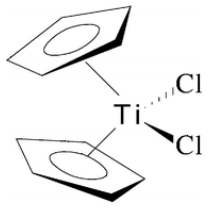

Figure 1.13. Chemical structure of titanocene dichloride.

The Ti-Cl bond undergoes fast hydrolysis, and the hydrolyzed form interacts with DNA.[33] This mode of action is similar to that of cisplatin but, in addition, it was also found that the Ti(IV) ion played a role by binding strongly to human serum transferrin, which helped its delivery into cancer cells.[34]

1.6.2 Organometallic Arene complexes

Organometallic arene complexes have gained interest as anticancer agents over the years.[35] These complexes possess a 'piano-stool' structure as shown:

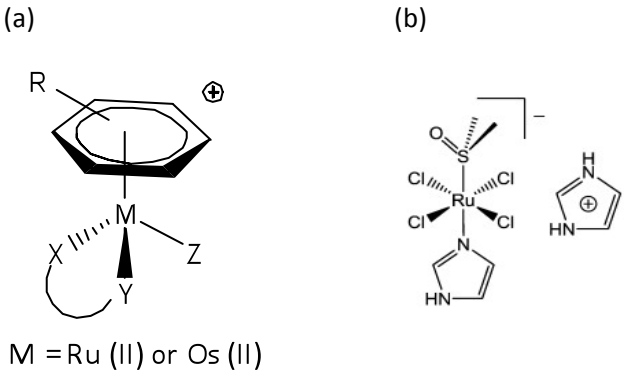

Figure 1.14. (a) General structure of Ru(II) and Os(II) 'piano stool' arene complexes, (b) NAMI-A.

They are potential anticancer agents as their pharmacological properties can be tuned by varying the properties of the arene, the XY chelating ligand, the Z monoionic ligand, and even the metal itself. For example, the monodentate ligand Z can be a labile ligand, thus providing a vacant coordination site for biomolecules.[36] The chelating ligand XY provides additional stability to the whole structure and the capability of tuning the electronic properties of the metal centre. For example, a chelating ligand that consists of electron-withdrawing groups will pull electron density away from the metal centre, making the complex more acidic.[37] Changing the metal makes a difference. For example, by changing the metal in the complex [Ru(η^6-arene)(en)(Cl)] to osmium, the pKa was 1.5 units lower, causing the complex to exist in the less reactive form at physiological pH.[38] One prime example of a Ru-arene complex is NAMI-A, which has already made it to phase II clinical trials (Figure 1.14b). In vitro, NAMI-A was found to be almost non-toxic against the cell lines. However, in vivo, they were found to inhibit lung mestastasis.[39] This is of high practical interest, as the treatment options for mestastases are quite limited. Studies have shown that the Ru metal plays an important role in its selectivity – the complex first exist as a non-toxic Ru (III) complex which was then activated to the active Ru (II) species due to the acidic reducing environment solely at site of the cancerous cells.[40]

1.6.3 Triosmium carbonyl clusters

Leong and co-workers first discovered a series of triosmium carbonyl clusters **1**-**4** (Figure 1.15)

that showed activity against both estrogen receptor positive (ER+) and estrogen receptor negative (ER-) breast cancers (IC_{50} of 6 – 10 μM).[41] That they are active against ER- breast cancer cells is of special interest as the current drug used for the treatment of breast cancer, Tamoxifen, acts as a hormone antagonist and is only active against ER+ breast cancer. Through a number of biochemical assays, it has been shown that the probable mode of action is through the loss of the labile ligands and binding to protein targets. One possible target is the sulfhydryl residues, and this leads to hyperstabilization of the microtubules and the induction of apoptosis.[42]

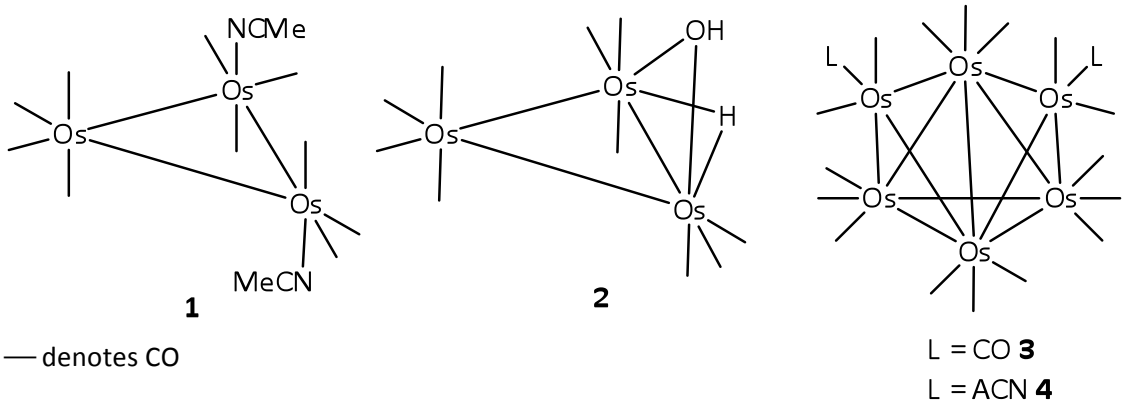

— denotes CO

Figure 1.15. Osmium carbonyl clusters with anti-cancer properties.

There are also a number of other metal clusters with anticancer properties. For example, Rosenberg and co-workers synthesized a series of water-soluble benzoheterocycle triosmium clusters that showed activity against the MCF-7 (ER+) breast cancer cell line, with IC_{50} ranging from 5 to 48 μM.[43] Their activity depended on the charged ligands, which interacted with telomerase. More recently, Reddy and co-workers reported a novel ruthenium-maltol cluster that showed anti-cancer activity (Figure 1.16).[44] The ligand of this complex is hemilabile, as the bond between the ketone oxygen and Ru is weak.

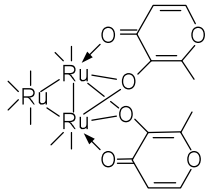

Figure 1.16. Ruthenium-maltol cluster.

1.6.4 Ferrocifens

The strategy used by Jaouen and co-workers involved the second approach, by enhancing the activity of the already-active molecule tamoxifen with a ferrocenyl substituent - these compounds have been named ferrocifens. The two prime ferrocifen series – the hydroxyferrocifen and ferrocidiphenol (Figure 1.17) - exhibited high antiproliferative activity against both ER+ and ER- breast cancer cells (IC_{50} ~ 0.5 μM).[45]

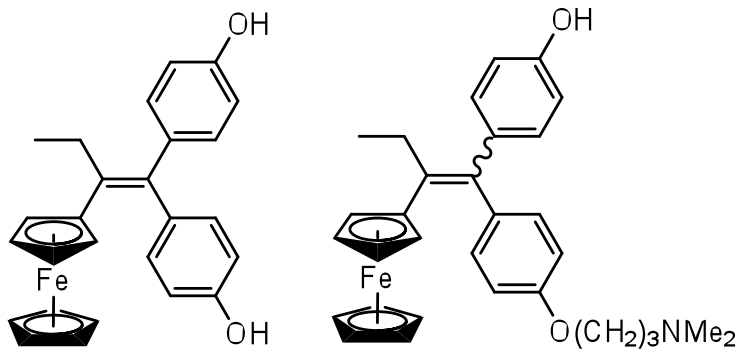

Figure 1.17. Chemical structure of hydroxyferrocifen and ferrocidiphenol.

In a structure-activity relationship (SAR) study, it was found that ferrocifen has a higher lipophilicity constant than estradiol, indicating that it penetrated the cell membrane more easily. Its relative binding affinity (RBA) was less than tamoxifen, meaning that it bind less strongly to the estrogen receptor though it had a stronger antiproliferative effect. These suggested that ferrocifen has a different mode of action from that of tamoxifen. The cytotoxicity of hydroxyferrocifen was later attributed to the generation of reactive quinones via ferrocene-modulated phenol oxidation.[46] This result indicates that the organometallic fragment did not merely enhance the activity of the organic fragment, but that the metal plays a direct role in its antiproliferative activity.

1.6.5 Other metal complexes

A number of other organometallic complexes have also been investigated for cancer therapy. For example, Os(II) arene complexes,[47] and half-sandwich Rh(III) and Ir (III) complexes,[48] have been

examined as possible improvements on the activity of Ru complexes. Besides the osmium derivatives mentioned above, other metal carbonyl complexes studied include those of cobalt,[49] iron,[50] chromium,[51] and manganese.[52] Furthermore, Au NHC complexes have displayed promising activity through the impairment of mitochondrial functions because of their high selectivity towards selenocysteine residues.[53] Reviews on organometallic compounds as potential anticancer agents have been made by Gasser,[54] and Hartinger.[55]

1.7 Aims and Objectives

The aim of the project described in this thesis stems from the developments first described by Leong and Jaouen and their co-workers, each representing the two different general strategies for organometallic compounds as anti-cancer agents. The work of Leong and co-workers suggests that osmium carbonyl clusters with labile ligands can exhibit cytotoxicity. It has also been demonstrated by others that targeting ligands and/or hemilabile ligands can also be useful. It is therefore desirable to explore whether such features can be incorporated into osmium carbonyl clusters. The SAR for the osmium carbonyl clusters also bear further study.

The work of Jaouen and co-workers has shown that one of the factors responsible for the antiproliferative activity of the ferrocifens is the metal. It has already been found that the ruthenocene analogues are inactive against the ER- breast cells,[56] and this has been attributed to the instability of the ruthenocenium cation. It is therefore logical to extend the study to the osmocene analogues. Work by others have shown that osmium complexes are often more active than their ruthenium and iron analogues. For example, Sadler, et. al. have shown that the osmium phenylazopyridine complex is more active than its ruthenium analogue,[57] and Yamazaki, et. al. have reported an osmocenium salt that is more active than the ferrocenium salt towards some tumor cells.[58]

In this project therefore, the aim is to study the SAR and anti-cancer properties of two classes of organometallic compounds of osmium:

(i) Triosmium carbonyl clusters, and

(ii) Tamoxifen analogues.

The development of more potent variants from those already reported is of great interest. A better understanding of the structure-activity relationships and possibly the modes of action, will also be important, especially towards the design of future variants.

References

1 What is cancer. (2015, February 9). Retrieved March 15, 2015, from http://www.cancer.gov/cancertopics/what-is-cancer

2 *World Cancer Report 2014*. World Health Organization. 2014. pp. Chapter 1.1. ISBN 92-832-0429-8.

3 L. J. Veer, H. Dai, M. J. Vljver, Y. D. He, A. A. M. Hart, M. Mao, H. L. Peterse, K. Kooy, M. J. Marton, A. T. Witteveen, G. J. Schreiber, R. M. Kerkhoven, C. Roberts, P. S. Linsley, R. Bernards, S. H. Friend, *Nature*, **2001**, *415*, 530.

4 P.C. John, M. Mews, R. Moore, *Protoplasma*, **2001**, *216*, 119.

5 S. Elmore, *Toxicol Pathol*. **2007**, *35(4)*, 495.

6 B. Favaloro, N. Allocati, V. Graziano, C. Di Ilio, V. De Laurenzi V, *Aging*, **2012**, *4(5)*, 330.

7 S. Fulda, K. M. Debatin, *Oncogene*, **2006**, *25*, 4798; I. M. Ghobrial, T. E. Witzig, A. A. Adjei, *A Cancer Journal for Clinicians*, **2005**, *55*, 178.

8 S. J. Riedl, G. S. Salvesen, *Nature Reviews Molecular Cell Biology*, **2007**, *8*, 405; Y. Tsujimoto, *Genes to Cells*, **1998**, *3*, 697.

9 S. W. G. Tait, D. R. Green, *Nature Reviews Molecular Cell Biology*, **2010**, *11*, 621.

10 B. Zhivotovsky, S. Orrenius, *Cellular Aging and Death: Current Protocols in Cell Biology*, **2001**, 18.1.1

11 Apoptosis. (2015, January 1). Retrieved March 15, 2015, from https://www.bdbiosciences.com/research/apoptosis/analysis/cell_death.jsp

12 J. H. Zhang, M. Xu, *Cell Research*, **2000**, *10*, 205

13 Z. Darzynkiewicz. Flow cytometry: Methods in Cell Biology, **1994**, *41*, 27.

14 M. A. Hotz, J. Gong, F. Traganos, Z. Darzynkiewciz, *Cytometry*, **1994**, *15*, 237.

15 Y. H. Wong, A. K. Habsah, *Evid Based Complement Alternat Med,* **2011**, 293060.

16 Hayflick, L. *Exp. Cell Res.* **1965**, *37*, 614.

17 a) A. DiLeonardo, S. P. Linke, K. Clarkin, G. M. Wahl, *Genes Dev*, **1994**, *8*, 2540; b) U. Herbig, W. A. Jobling, B. P. Chen, D. K. Chen, j. Sedivy, *Mol. Cell*, **2004**, *14*, 501; c) V. V. Orgyzko, T. H. Hirai, V. R. Russanova, D. A. Barbie, B. H. Howard, *Mol. Cell. Biol*, **1996**, *16*, 5210; d) M. Serrano, A. W. Lin, M. E. McCurrach, D. Breach, S. W. Lowe, *Cell*, **1997**, *88*, 593.

18 a) D. X. Mason, T. J. Jackson, A. W. Lin, *Oncogene*, **2004**, *23*, 9238; b) I. P. Trougakos, A. Saridaki, G. Panayotou, E. S. Gonos, *Mech. Ageing Dev,* **2006**, *127*, 88; c) H. Zhang, K. H. Pan, S. N. Cohen, *Proc. Natl Acad. Sci. USA*, **2003**, *100*, 3251

19 D. J. Jurz, S. Decary, Y. Hong, J. D. Erusalimsky, *J. Cell. Sci*, **2000**, *113*, 3613.

20 I. M. Zubiaurre, C. G. Fenton, H. Taman, I. Pettersen, T. Hellevik, R. H. Paulssen, *Journal of Cancer Therapy*, **2013**, *4*, 208

21 B. Samuels, J. D. Bitran, *J. Clin. Oncol*, **1995**, *13*, 1786.

22 V. H. Bono, *Cancer Treat Rep*, **1976**, *60*, 699.

23 A. J. Deans, S. C. West, *Nature Reviews Cancer*, **2011**, *11*, 467.

24 P. T. R. Rajagopalan, Z. Zhang, L. McCourt, M. Dwyer, S. J. Benkovic, G. G. Hammes, *Proceedings of the National Academy of Science*, **2002**, *99*, 13481.

25 W. B. Parker, *Chem. Rev.*, **2009**, *109*, 2880.

26 a) D. R. Matson, P. T. Stukenberg, *Mol. Interv*, **2011**, *11*, 141; b) M.A. Jordan, L. Wilson, *Nat Rev Cancer*, **2004**, *4*, 253.

27 S. Jones, X. Zhang, D. W. Parsons, J. C. Lin, R. J. Leary, P. Angenendt, P. Mankoo, H. Carter, H. Kamiyama, A. Jimeno, S. M. Hong, B. Fu, J. Hartigan, D. R. Smith, M. Hidalgo, S. D. Leach, A. P. Klein, E. M. Jaffe, M. Goggins, A. Maitra, C. Iacobuzio-Donahue, J. R. Eshleman, S. E. Kern, R. H. Hruban, R. Karchin, N. Papadopoulos, G. Parmigiani, B. Vogelstein, V. E. Velculescu, K. W. Kinzler, *Science,* **2008**, *321*, 1801.

28 J. Neuzil, L. Dong, J. Rohlena, J. Truksa, S. J. Ralph, *Mitochondrion*, **2013**, *13*, 199.

29 Cisplatin - The Cancer Medicine. (n.d.). Retrieved March 15, 2015, from http://www.cisplatin.org

30 a) Z.H.Siddik, *Oncogene*, **2003**, *22*, 7265; b) D. Gibson, *Dalton Trans*., **2009**, 10681.

31 M. Kartalou, J. M. Essigmann, *Mutation Research,* **2001**, *478*, 23.

32 R.H. Fish, G. Jaouen, *Organometallics,* **2003**, *22*, 2166

33 P. Kopf-Maier. *J. Struct. Biol*. **1990**, *105*, 35.

34 H. Sun, H. Li, RA. Weir, PJ. Sadler. *Angew. Chem. Int. Ed*. *Engl.* **1998**, *37*, 1577.

35 a) R. E. Morris, R. E. Aird, PdS. Murdoch, H. Chen, J. Cummings, N. D. Hughes, S. Parsons, A. Parkin, G. Boyd, D. I. Jodrell, P. J. Sadler, *J Med Chem*, **2001**, *44*, 3616; b) R. E. Aird, J. Cummings, A. A. Ritchie, M. Muir, R. E. Morries, H. Chen, P. J. Sadler, D. I. Jorell, *Br Cancer*, **2002**, *86*, 1652; c) Y. K. Yan, M. Melchart, A. Habtemariam, P. J. Sadler, *Chem Commun*, **2005**, 4764.

36 A. F. A. Peacock, A. Habtemariam, R. Fernandez, V. Walland, F. P. A. Fabbiani, S. Parsons, R. E. Aird, D. I. Jodrell, P. J. Sadler. *J. Am. Chem. Soc*. **2006**, *128*, 1739.

37 R. Fernandez, M. Melchart, A. Habtermariam, S. Parson, P. J. Sadler, *Inorg Chim Acta*, **2006**, *359*, 3020.

38 A. F. A. Peacock, A. Habtermariam, S. A. Moggach, A. Prescimone, S. Parsons, P. J. Sadler, *Inorg Chem*, **2007**, *46*, 4049.

39 G. Sava, R. Gagliardi, A. Bergamo, E. Alessio, G. Mestroni, *Anticancer Res.* **1999**, *19*, 969.

40 E. Alessio, G. Mestroni, A. Bergamo, G. Sava, *Curr. Top Med Chem,* **2004**, *4*, 1525

41 K.V. Kong, W.K. Leong, S. P. Ng, T. H. Nguyen, L.H.K. Lim. *ChemMedChem.* **2008**, *3*, 1269.

42 K.V. Kong, W.K. Leong, L.H.K. Lim. *J. Organomet. Chem*. **2009**, *694*, 834.

43 D.Colangelo, A. Ghiglia, A. Ghezzi, M. Ravera, E. Rosenberg, F. Spada, D. Osella*. J. Inorg. Biochem.* **2005**, *99*, 505.

44 V.D. Reddy, D. Dayal, D. J. Szalda, S. C. Cosenza, M.V. R. Reddy. *J. Organomet. Chem*. **2012**, *700*, 180.

45 a) S. Top, A. Vessières, C. Cabestaing, I. Laios, G. Leclercq, C. Provot, G. Jaouen, *J. Organomet. Chem*. **2001**, *637*, 500; b) E. A. Hillard, P. Pigeon, A. Vessières, A. Amatore, G. Jaouen, *Dalton Trans*, **2007**, 5073; c) A. Nguyen, A. Vessières, E. A. Hillard, S. Top, P. Pigeon, G. Jaouen, *Chimia.* **2007**, *61*, 716; d) A. Vessières, *J. Organomet. Chem.* **2013**, *734*, 3; e) S. Top, A. Vessières, G. Leclercq, J. Quivy, J. Tang, J. Vaissermann, M. Huché, G. Jaouen, *Chem Eur J*. **2003**, *9*, 5223.

46 a) E. A. Hillard, A. Vessières, L. Thouin, G. Jaouen, C. Amatore, *Angew. Chem. Int. Ed.* **2006**, *45*, 285; b) P. Pigeon, S. Top, O. Zekri, E, A. Hillard, A. Vessières, M. A. Plamont, O. Buriez, E. Labbé, M. Huche, S. Boutamine, C. Amatore, G. Jaouen, *J. Organomet. Chem*. **2009**, *694*, 895; c) J. de J. Cázares-Marinero, E. Labbé, S. Top, O. Buriez, C. Amatore, G. Jaouen, *J. Organomet. Chem*. **2013**, *744*, 92-100; d) J. de J. Cázares-Marinero, O. Buriez, E. Labbé, S. Top, C. Amatore, G. Jaouen, *Organometallics*. **2013**, *32*, 5926-5934; e) D. Hamels, P. M. Dansette, E, A. Hillard, S. Top, A. Vessières, P. Herson, G. Jaouen, D. Mansuy, *Angew. Chem.* **2009**, *121*, 9288; *Angew. Chem. Int. Ed.* **2009**, *48*, 9124.

47 H. Kostrbuonya, J. Florian, O. Novakova, A. F. A. Peacock, P. J. Sadler, V. Bravec, *J. Med Chem*, **2008**, *51*, 3635.

48 a) S. Schaefer, W. S. Sheldrick, *J. Organomet. Chem.* **2007**, *692*, 1300; b) M. A. Scharwitz, I. Ott, Y. Geldmacher, R. Gust, W. S. Sheldrick, *J. Organomet. Chem.* **2008**, *693*, 2299.

49 I. Ott, B. Kircher, R. Dembinski, R. Gust, *Expert Opin. Ther. Pat.* **2008**, *18*, 327.

50 D. Schlawe, A. Majdalani, J. Velcicky, E. Hessler, T. Wieder, A. Prokop, H. G. Schmalz, *Angew. Chem. Int. Ed.* **2004**, *43*, 1731.

51 G. B. Jones, J. E. Matthews, *Bioorg. Med. Chem. Lett*, **1995**, *5*, 93.

52 J. Niesel, A. Pinto, H. W. P. N'Dongo, K. Merz, I. Ott, R. Gust, U. Schatzschneider, *Chem. Commun.* **2008**, 1798.

53 I. Ott, *Coord. Chem. Rev.* **2009**, *253*, 1670.

54 G. Gasser, I. Ott, N. Metzler-Nolte, *J. Med. Chem*, **2011**, *54*, 3.

55 C. G. Hartinger, N. Metzler-Nolte, P. J. Dyson, *Organometallics,* **2012**, *31*, 5677.

56 P. Pigeon, S. Top, A. Vessières, M. Huché, E. Hillard, E. Salomon, G. Jaouen. *J. Med. Chem.* **2005**, *48*, 2814.

57 a) Y. Fu, A. Habtemariam, A. M. Pizarro, S. H. van Rijt, D. J. Healey, P. A. Cooper, S. D. Shnyder, G. J. Clarkson, P. J. Sadler, *J. Med. Chem.* **2010**, *53*, 8192.; b) Y. Fu, A. Habtemariam, A. M. B. H. Basri, D. Braddick, G. J. Clarkson, P. J. Sadler, *Dalton Trans.* **2011**, *40*, 10553

47. Y. Yamazaki, M. Ogawa, T. Shimura, S. Oka, H. Okuno, M. Goto. Jpn. Kokai Tokkyo Koho. 1995, JP 07101972A 19950418.

Chapter 2. Structure-activity relationship studies on triosmium carbonyl clusters

As introduced in chapter 1, organometallic osmium clusters and, in particular, compound **2** has been found to be active against both the MCF-7 and MDA-MB-231 cancer cell lines in vitro via the MTS assay (IC_{50} = 7.2 μM and 4.8 μM respectively).[1]

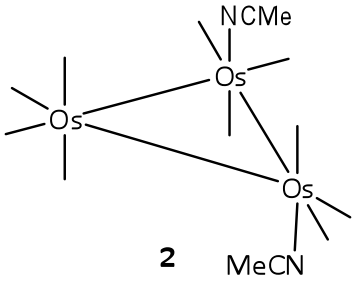

2

Figure 2.1 Triosmium carbonyl cluster **2** that showed anticancer activity.

This was somewhat surprising as these compounds were generally insoluble in water and also did not have very good solubility in DMSO, the solvent used in cytotoxicity assays. The possible effect of solubility on their anti-cancer activity is therefore of interest. It was also suggested in that earlier study that the loss of two labile ligands was required for their cytotoxicity as the mono-substituted analogue $Os_3(CO)_{11}(NCCH_3)$, **1**, did not show any activity against the breast cancer cells. As part of the SAR study, it will be desirable to investigate: (1) the effect of solubility, (2) whether two vacant sites are necessary, and (3) the effect of different ligands, on the anti-cancer activity.

2.1 Effect of solubility

The osmium cluster **1** is less soluble in DMSO compared to the disubstituted derivative **2**. It is therefore uncertain if the lack of activity of **2** is due to solubility problem, or the need for two vacant coordination sites; the acetonitrile ligands are labile and can be readily replaced by stronger ligands or nucleophiles. To investigate the effect of solubility, clusters **1** and **2** were protonated using HBF_4 to give **1'** and **2',** respectively, to increase their solubility (Scheme 2.1).

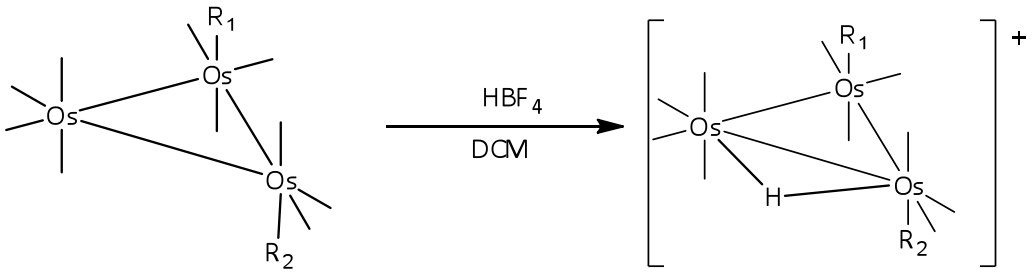

R_1 = CO, R_2 = NCMe **1**
R_1 = NCMe, R_2 = NCMe **2**

R_1 = CO, R_2 = NCMe **1'**
R_1 = NCMe, R_2 = NCMe **2'**

Scheme 2.1 Protonation of triosmium carbonyl clusters **1** and **2**.

Cell viability assays (via the MTS assay) were performed with the MDA-MB-231 (ER-) cell line, and the results are shown in Figure 2.2. The results show that protonation of **2** to **2'** did not lead to any significant improvement in its activity. Conversely, the cytotoxicity of **1** was found to increase significantly upon protonation to **1'**.

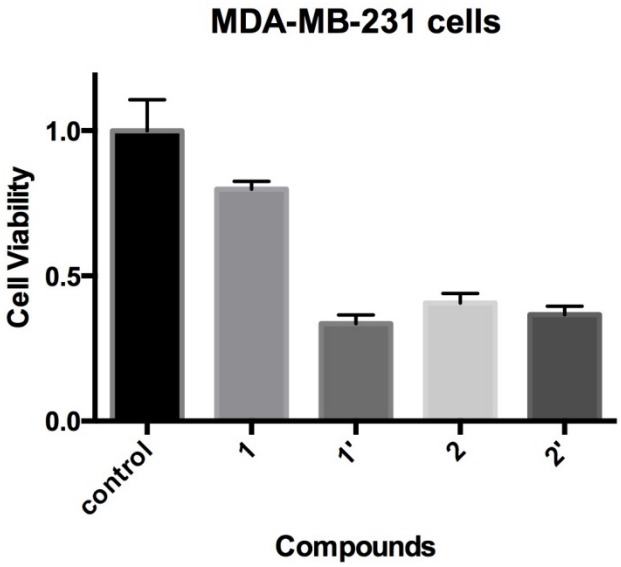

Figure 2.2 MTS assay of osmium clusters **1**, **1'**, **2** and **2'** (20 μM) on MDA-MB-231 breast cancer cells. Control: DMSO (0.2 % v/v).

Lipophilic cations are known to attack the mitonchondria, leading to cell death.[2] In order to rule out the possibility that difference in cytotoxicity between **1** and **1'** may be due to the positive charge on the latter, the osmium carbonyl cluster $Os_3(CO)_{11}(PPh_3)(\mu\text{-}H)^+BF_4^-$ **3'**, a cationic osmium carbonyl cluster containing a non-labile triphenylphosphine ligand, was synthesized and tested for its antiproliferative activity (Figure 2.3). Cluster **3'** does not show any cytotoxicity, thus

indicating that the positive charge does not play a role.

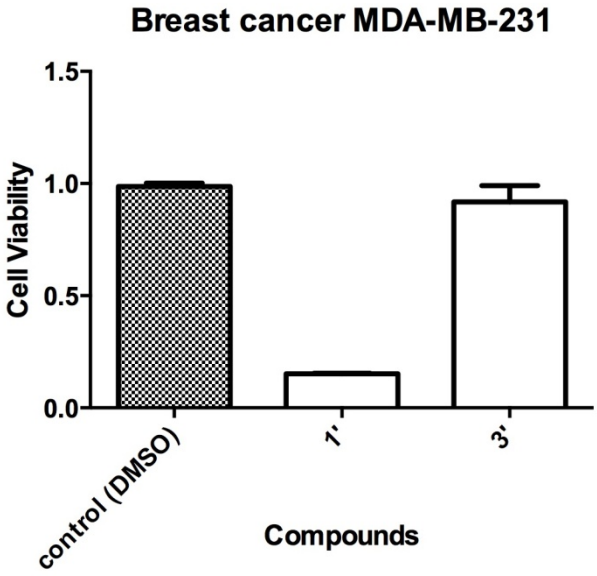

Figure 2.3 MTS assay of osmium clusters **1'** and **3'** (20 μM) on MDA-MB-231 breast cancer cells. Control: DMSO (0.2 % v/v).

These results thus indicate that protonation of the clusters imparted solubility, but an increased solubility alone is insufficient; a labile ligand, one and not two, is also required.

2.2 Effect of vacant sites

To confirm that only one vacant site is required, nitrile substituted triosmium carbonyl clusters, in which the nitrile ligand carries a polar group to increase its solubility, were synthesised (Figure 2.4).

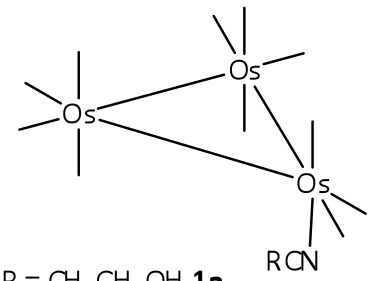

R = CH_2CH_2OH **1a**

R = *p*-C_6H_4OH **1b**

Figure 2.4 Triosmium carbonyl clusters with different polar nitrile ligands.

The syntheses of these clusters cannot be carried out using the method established for $Os_3(CO)_{11}(NCMe)$, which involves heating $Os_3(CO)_{12}$ in excess acetonitrile in the presence of trimethylamine-N-oxide (TMNO), because the nitriles to be used were a solid or a high boiling-

point liquid, which could not be removed easily. An alternative would be to carry out a displacement reaction with the desired nitrile using **1** as the precursor, but distinguishing the product and precursor spectroscopically will be difficult as they showed almost identical patterns for their carbonyl stretches in the IR spectrum. A synthetic route based on a different cluster $Os_3(CO)_{11}(COE)$ **3a** that also contains a labile ligand, as the intermediate was thus developed for the syntheses of **1a** and **1b** (Scheme 2.2).

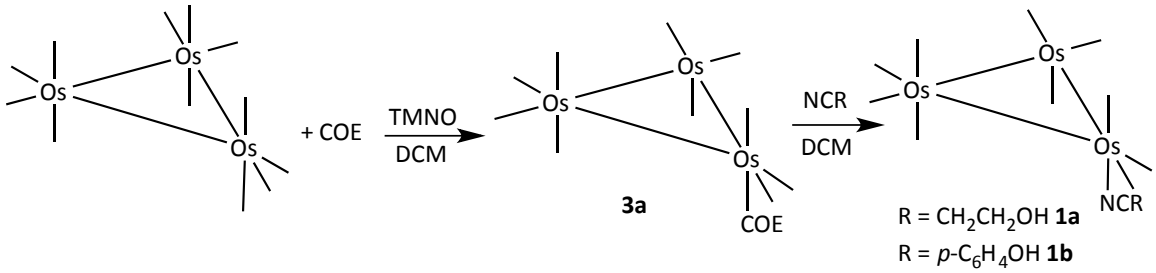

Scheme 2.2 Synthetic route to triosmium carbonyl clusters with nitrile ligands.

The synthesis of **3a** was carried out similarly to the method to synthesize **1**, by heating $Os_3(CO)_{12}$ in DCM in the presence of excess *cis*-cyclooctene (COE) and a slight excess of TMNO. TMNO was used as the decarbonylation agent, to create an empty site for the binding of the COE ligand; while excess COE can be removed under the vacuum. The identity of **3a** was then established via its IR spectrum (Figure 2.5a), which showed a similar pattern for the CO stretches to that of the ethene analogue, $Os_3(CO)_{11}(C_2H_4)$.[3] As the compound has not been reported, its identity was further confirmed by its reaction with PPh_3, to form the known derivative $Os_3(CO)_{11}(PPh_3)$ **3**.[4] Since COE is more labile than ACN, the subsequent addition of the desired nitrile easily replaces the COE ligand, giving **1a** and **1b** respectively. In addition, as the IR spectrum of $Os_3(CO)_{11}(NCR)$ type (Figure 2.5b) is significantly different from that of **3a**, the formation of **1a** and **1b** can be monitored by IR spectroscopy.

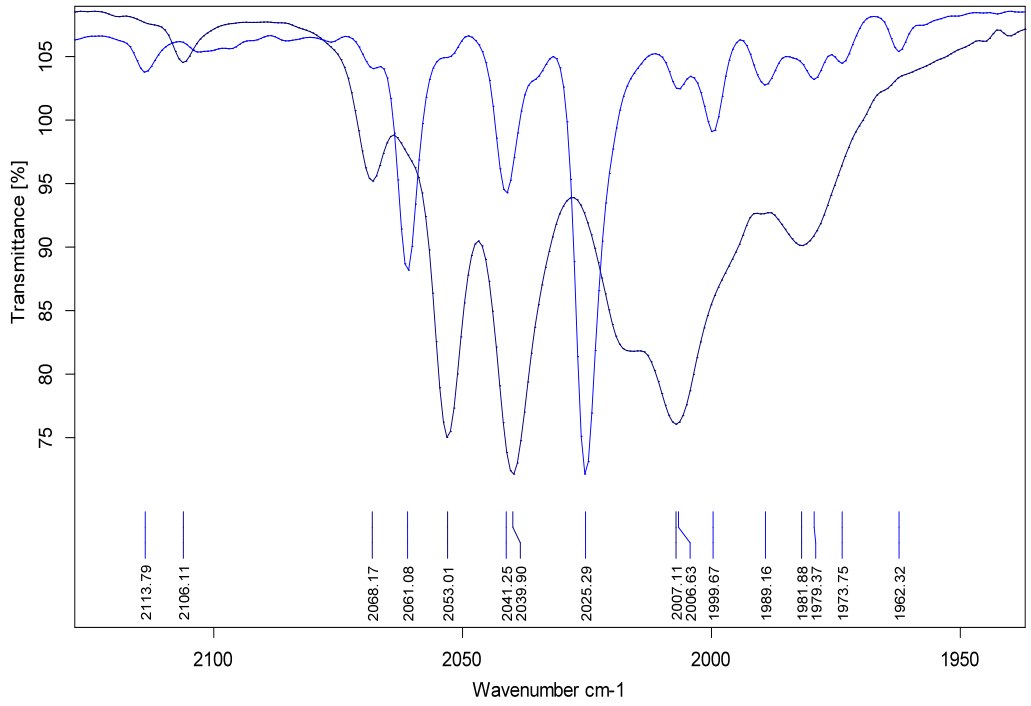

Figure 2.5 a) IR spectrum of $Os_3(CO)_{11}(COE)$ **3a** (blue, in cyclohexane); Lit IR of $Os_3(CO)_{11}(C_2H_4)$ in cyclohexane: 2117 (w), 2064 (s), 2048 (s), 2027 (vs), 2009 (m), 2005 (m), 1995 (m), 1983 (w), 1967 (w).[3] b) IR spectrum of type $Os_3(CO)_{11}(NCR)$ (black, in DCM).

The effect of the vacant sites was also explored with the bis derivatives of **1a** and **1b**, namely, $Os_3(CO)_{10}(NCCH_2CH_2OH)_2$ **2a** and $Os_3(CO)_{10}(NCC_6H_4OH)_2$ **2b**, to see if an additional polar nitrile ligand/vacant site can further improve its activity. The syntheses of **2a** and **2b** are shown in Scheme 2.3.

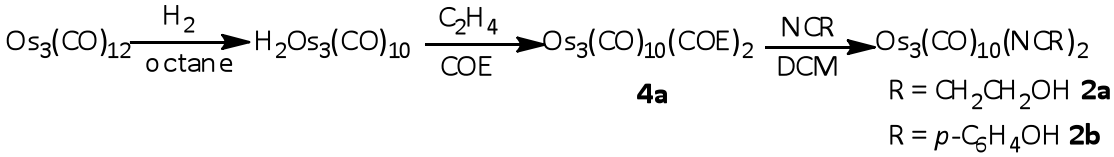

Scheme 2.3 Syntheses of bis(nitrile) triosmium clusters **2a** and **2b**.

The method to synthesize **2a** and **2b** is similar to that for the mono(nitrile) derivatives, i.e., through displacement of the COE ligands in $Os_3(CO)_{10}(COE)_2$ **4a** with the respective nitrile ligands. The difference lies in the synthesis of the precursor 4**a** using the published method from the reaction of $Os_3(CO)_{10}(\mu\text{-}H)_2$ with COE in the presence of ethylene gas,[5] as that for the synthesis of **3a** failed to yield **4a**. The mechanism as inferred from the known reaction of $Os_3(CO)_{10}(\mu\text{-}H)_2$ with alkenes[6], is shown in Scheme 2.4.

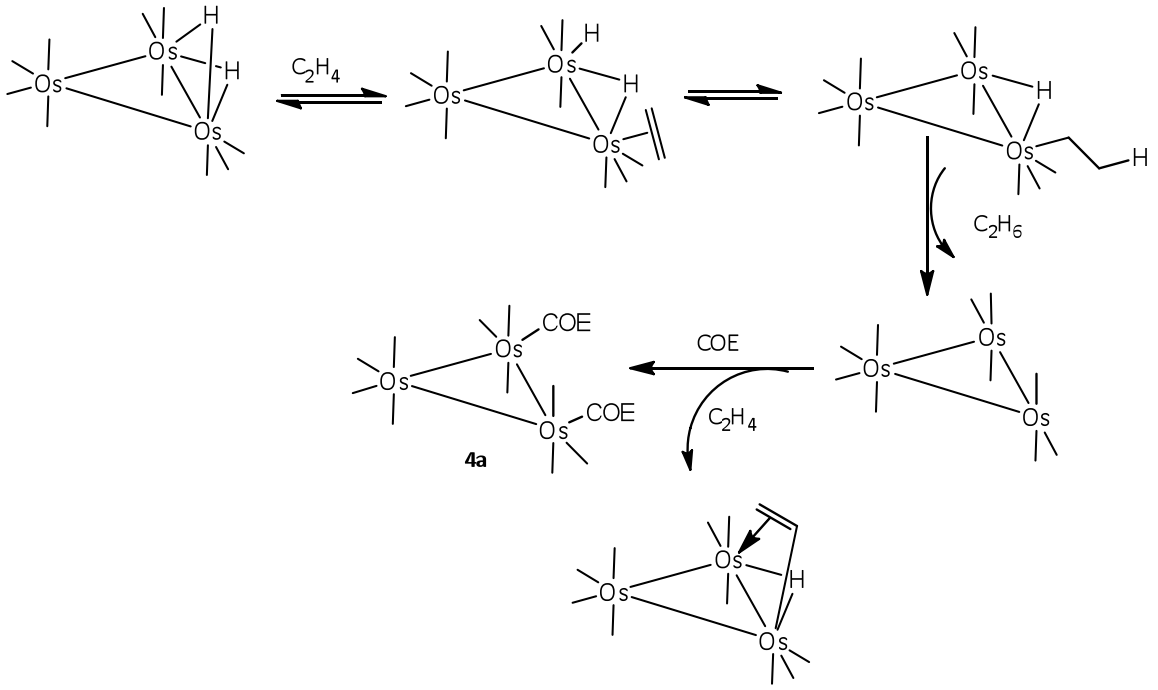

Scheme 2.4 Mechanism for the synthesis of **4a**.

A side product expected from this reaction is $HOs_3(CO)_{10}(CHCH_2)$ from the competition of COE and ethylene for the 'Os_3CO_{10}' species. As **4a** was unstable under standard purification methods such as Thin Layer Chromatography, this side product could not be separated from it and hence, both the bis(nitrile) analogues **2a** and **2b** contained a small amount of $HOs_3(CO)_{10}(CHCH_2)$ which could be detected in their IR spectra (Figure 2.6).

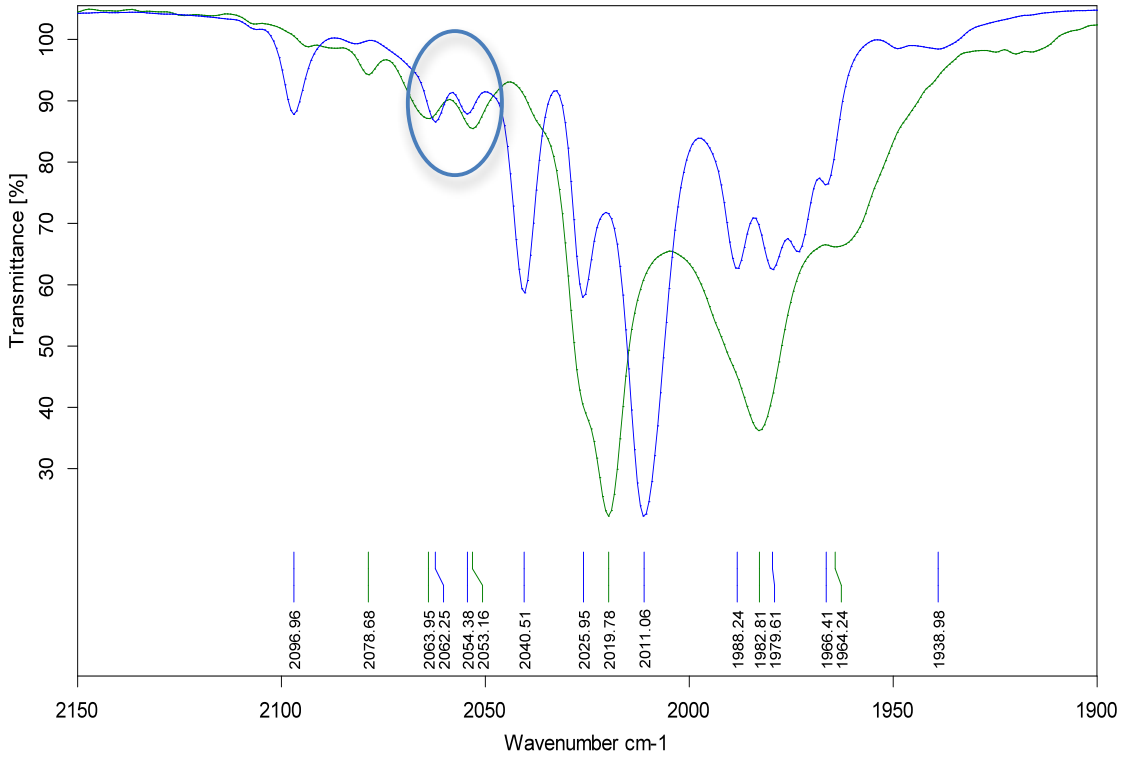

Figure 2.6 IR spectra of $Os_3(CO)_{10}(COE)_2$ (blue) in cyclooctene and $Os_3(CO)_{10}(NCR)_2$ (green) in DCM. The presence of $HOs_3(CO)_{10}(CHCH_2)$ is indicated in circle. Lit IR values of $HOs_3(CO)_{10}(CHCH_2)$ (cyclohexane):[7] ν_{CO} 2110 (w), 2066 (vs), 2058 (s), 2026 (vs), 2018 (s), 2014 (m, sh), 1998 (m), 1989 (w, sh), 1984 (w).

Lastly, **1a** and **1b** were also protonated to give **1a'** and **1b'** (Scheme 2.5) to see if protonation of these clusters further improved the activity.

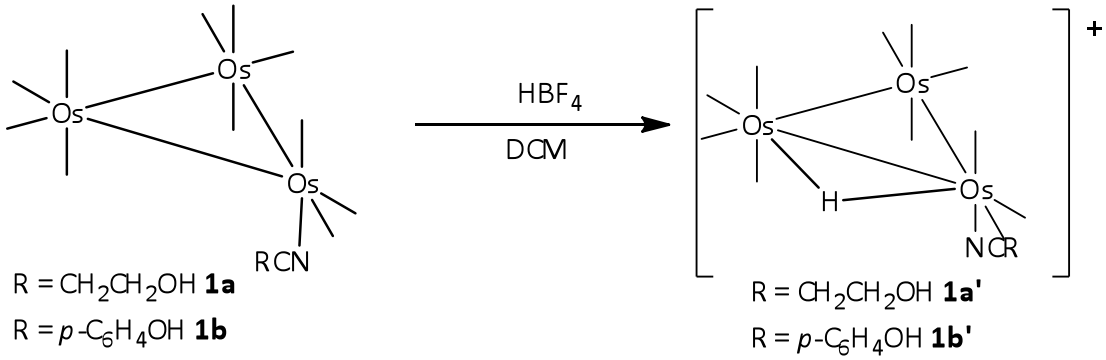

Scheme 2.5 Syntheses of cationic mono(nitrile) osmium clusters **1a'** and **1b'**.

Cell viability assays performed on these synthesized mono(nitrile), cationic mono(nitrile) and bis(nitrile) analogues are shown in Figure 2.7.

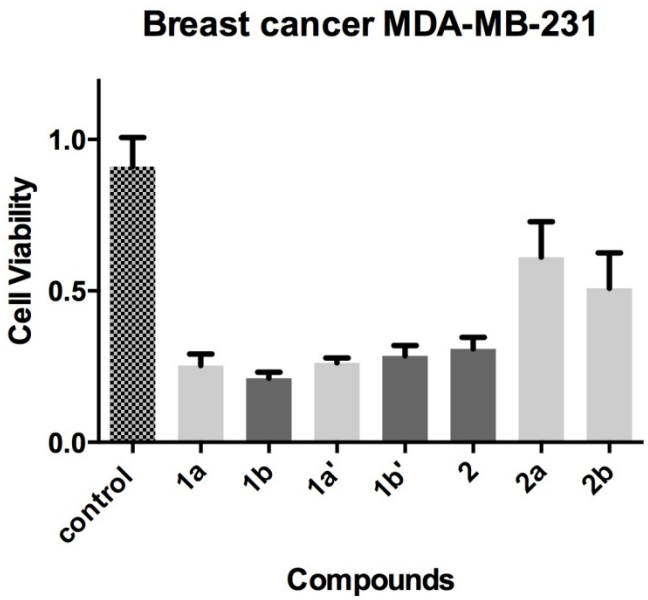

Figure 2.7 Comparison on the antiproliferative activity among the mono(nitrile) derivatized osmium clusters **1a** and **1b**, its cationic derivatives **1a'** and **1b'** and the bis(nitrile) derivatized osmium clusters **2a** and **2b** on MDA-MB-231 breast cancer cells, using **2** as the positive control. Concentration used: 20 μM; control: DMSO (0.2 % v/v).

The mono(nitrile) derivatized osmium clusters were found to be active, confirming that only one vacant site is necessary. On the other hand, the bis(nitrile) derivatives were found to be not as active as compared to the corresponding mono analogues and bis(acetonitrile) osmium cluster **2**. This may be due to the instability of the compounds, as well as the presence of the side product $HOs_3(CO)_{10}(CHCH_2)$ which was found to be inactive. These clusters were therefore not further studied. Lastly, there is no significance difference in activity between **1a** and **1b** with their protonated analogues **1a'** and **1b'**.

2.3 Effect of different ligands

The suggestion that only one vacant site is required made available many more clusters. It was recently reported that the ruthenium-maltol cluster below showed anti-cancer activity against several cancer cell lines (Figure 2.8).[8]

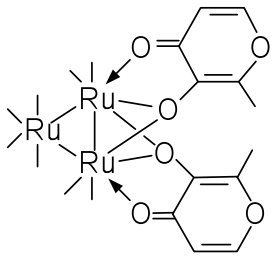

Figure 2.8 Ruthenium-maltol cluster.

The maltolato ligand is hemilabile, as the bond between the ketone oxygen and Ru is weak, thus enabling two vacant sites on the metal centre. This prompted us to look at complex **5** (Figure 2.9), an osmium-maltol complex obtained from the reaction of $Os_3(CO)_{10}(\mu\text{-H})(\mu\text{-OH})$ with maltol, which we reported some time earlier.[9]

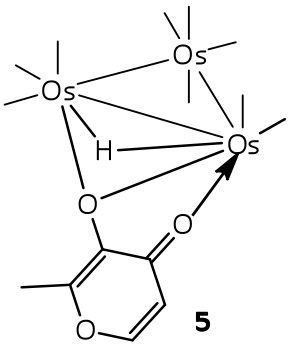

Figure 2.9 Osmium-maltol cluster **5**.

The antiproliferative activity of **5** against MDA-MB-231 breast cancer cells is shown in Figure 2.10. Compound **5** is highly toxic, which may be ascribed to its stability and good solubility. The maltolato ligand may also play a part, as it is known that maltolato-metal complexes, especially those of iron, can generate reactive oxygen species (ROS).[10]

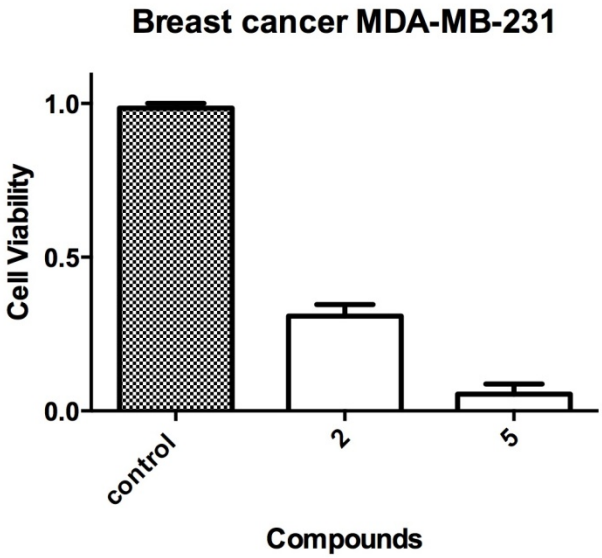

Figure 2.10 MTS assay of osmium-maltol cluster **5** (20 μM) on MDA-MB-231 breast cancer cells. Control: DMSO (0.2 % v/v); positive control: **2** (20 μM)

2.4 Antiproliferative activity against other breast cell lines

The triosmium clusters which showed significant antiproliferative activity in the SAR studies above (Figure 2.11) were also screened against MCF-7, an estrogen receptor positive (ER+) breast cancer cell line, as well as normal breast epithelial cells MCF-10A. The IC_{50} values are shown in Table 2.1. Compound **2**, for which the activity for the three cell lines have previously been established,[1] was used as positive control for comparison.

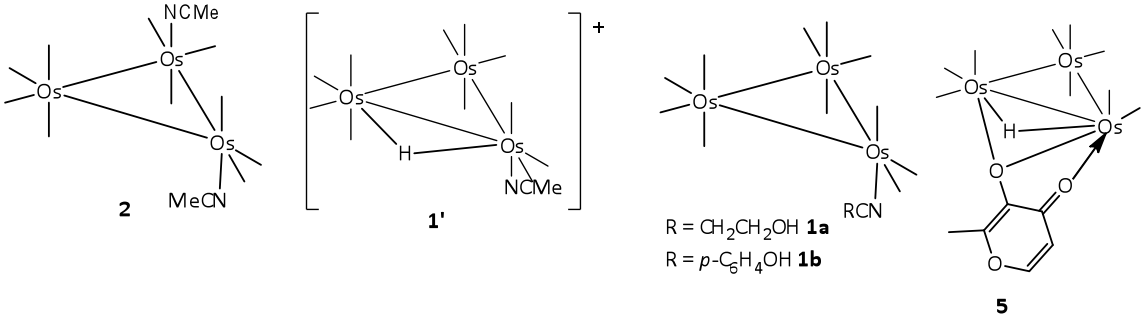

Figure 2.11 Triosmium carbonyl clusters tested for antiproliferative activity on three cell lines, namely, MCF-7, MDA-MB-231 and MCF-10A.

Table 2.1. Inhibition of cell growth (IC_{50}, μM) by triosmium carbonyl clusters, after 24 h, as determined by MTS assay.

Compound	MCF 7	MDA-MB-231	MCF-10 A
2	5.3 ± 0.6	5.1 ± 0.3	18 ± 1
1a	5.3 ±0.4	5.4 ± 0.4	>30
1b	6.1 ± 0.8	5.8 ± 0.1	19 ± 2
1'	5.9 ± 0.5	5.7 ± 0.7	22 ± 1
5	4.8 ± 0.6	5.7 ± 0.3	22 ± 3

Interestingly, all the compounds were found to be more active against MDA-MB-231 and MCF-7 than against MCF-10A, which is consistent with the results obtained previously.[1] This is in contrast to tamoxifen, the drug currently used for the treatment of breast cancer, which is only active against hormone dependent breast cancers.[11] It would therefore appear that these compounds do not have the same mode of action as tamoxifen.

2.5 Osmium cluster-thymidine bioconjugate

The osmium-maltol cluster **5** offers the attractive possibility of derivatization of the maltolato ligand to enhance its efficacy. One possibility is based on the idea of thymidine as a 'Trojan horse'.[12] This stems from the activity of thymidine kinase 1 (TK1), an enzyme responsible for the phosphorylation of thymidine to thymidine monophosphate. The activity of TK1 is elevated especially during the S-phase of the cell cycle, due to the incorporation of thymidine in DNA synthesis, and thus, it has been associated with proliferating cells.[13] The overexpression of TK1 in cancer cells has been confirmed in many forms of cancer, including breast cancer.[14] This overexpression of TK1 in cancer cells may be utilized towards increasing the selectivity for cancer cells via an osmium cluster-thymidine bioconjugate such as **6** (Figure 2.12).

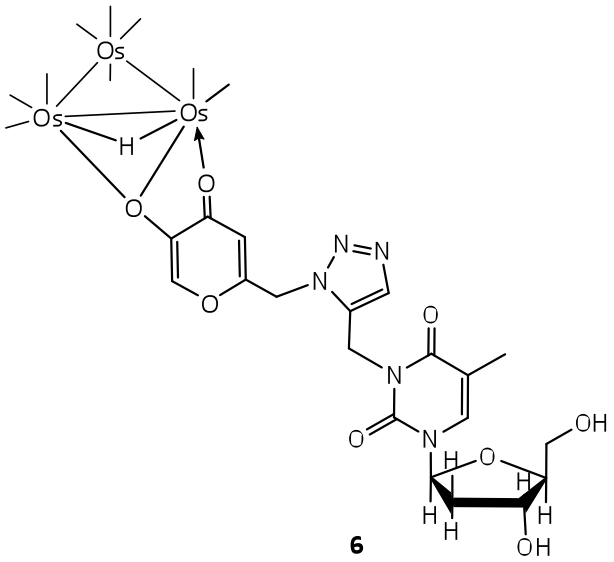

6

Figure 2.12 Osmium cluster-thymidine bioconjugate **6**.

The osmium cluster-thymidine bioconjugate **6** consists of two main fragments. The thymidine fragment can undergo phosphorylation by TK1 and then be trapped intracellularly; the phosphorylated product cannot cross the cell membrane. Since TK1 activity is increased several folds in proliferating cells, there would be a higher amount of **6** trapped intracellularly in cancer cells over normal cells. The osmium cluster fragment is capable of generating a vacant site at the metal centre, thereby allowing it to exhibit its biological activity.

The retrosynthetic analysis for **6** is shown in Scheme 2.6.

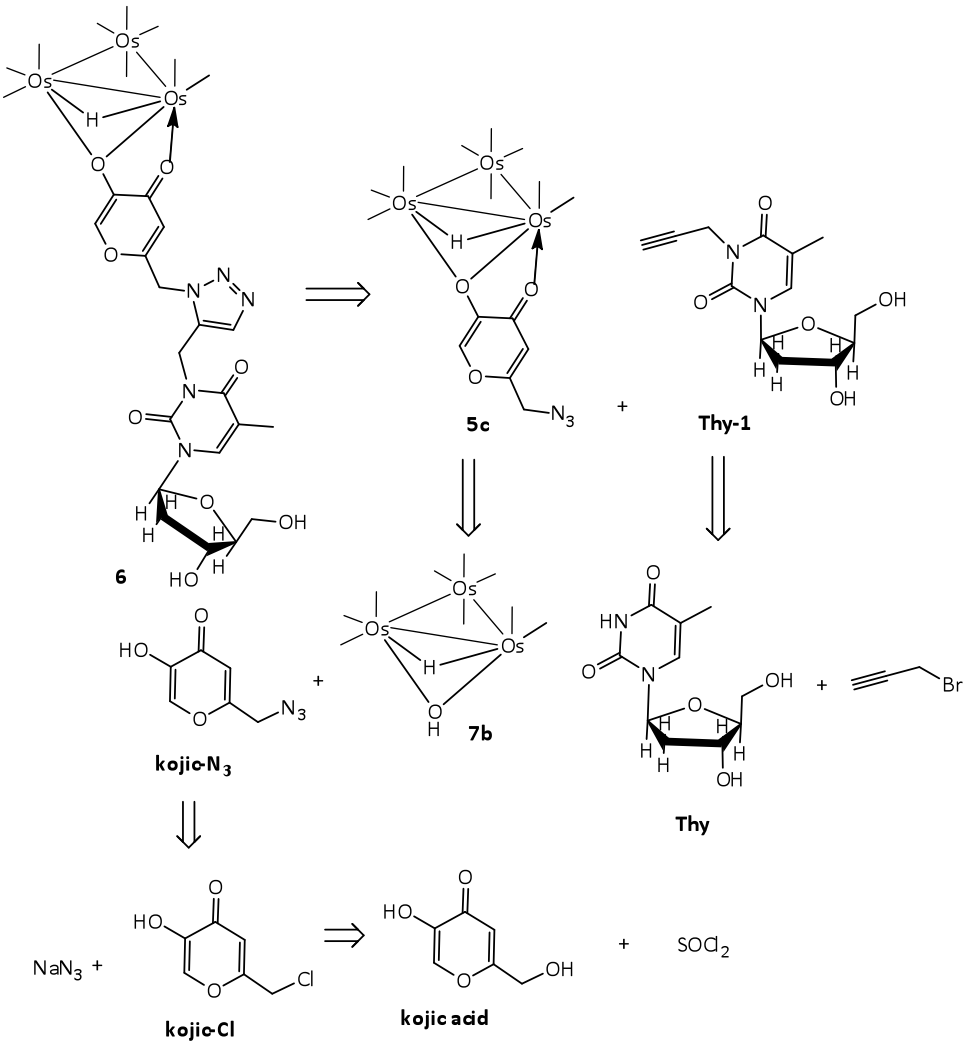

Scheme 2.6. Retrosynthetic route to the synthesis of osmium bioconjugate **6**.

The synthesis makes use of the well-known the azide-alkyne Huisgen cycloaddition, as it is highly selective and proceeds in high yields. The precursor **5c** was chosen as a similar reaction (synthesis of **5**) has already been established.[9] The remaining precursors **7b**,[15] **Thy-1**,[16] and **Kojic-N$_3$**,[17] were prepared according to published procedures. Unfortunately, the reaction between **7b** and **kojic-N$_3$** did not yield **5c**; high temperature (> 70 °C) causes the decomposition of **Kojic-N$_3$** and no reaction occurred at lower temperature. An alternative route to the synthesis of **5c** (Scheme 2.7) was attempted but appeared to have led to decomposition on the last azidation step; the metal hydride resonance disappeared from the ^{1}H NMR spectrum.

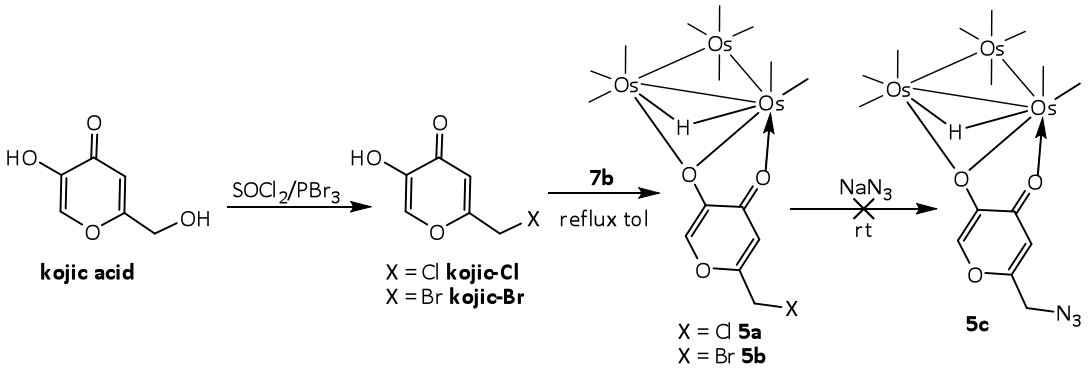

Scheme 2.7 Alternative routes to the synthesis of **5c**.

An alternative route through the precursor **5e** was also explored (Scheme 2.8). This made use of the Steglich esterification reaction using N-dimethylaminopropyl-N'-ethylcarbodiimide (EDC) as the coupling reagent and 4-dimethylaminopyridine (DMAP) as the catalyst.[18] The reaction is relatively mild and can take place at room temperature. Unfortunately, the ^{1}H NMR spectrum of the reaction after 1 h of stirring at room temperature showed the disappearance of the metal hydride resonance at δ -9 ppm, which is characteristic of such pyrone-derivatized osmium clusters. Most of the products could not be eluted on the TLC plate; the ^{1}H NMR spectrum of the major isolable product (approx. 1-2 % yield) shows a hydride resonance at δ -12 ppm and absence of the pyrone ligand.

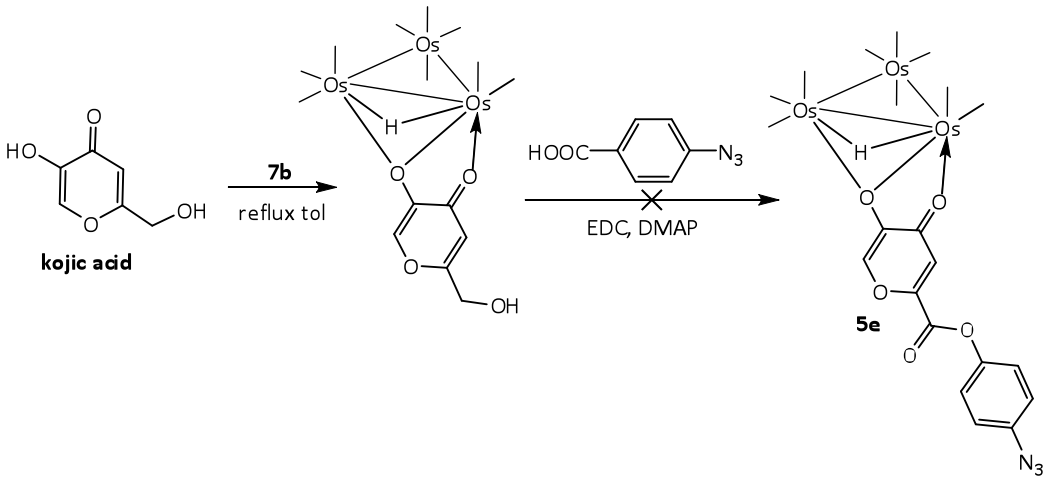

Scheme 2.8 Synthesis of **5e** using the Steglich esterification reaction.

2.6. Conclusion

In this chapter, we have shown that the availability of one vacant site and good solubility are necessary for the triosmium carbonyl clusters to be active against breast cancer cells. In the course of this study, two new classes of osmium clusters, $Os_3(CO)_{11}(NCMe)(\mu\text{-}H)^+$ **1'** and $Os_3(CO)_9(\mu\text{-}H)(\mu\text{-}\gamma\text{-}C_6H_5O_3)$ **5**, which were structurally different from **2**, were also found to be active against cancer cells, and were selective over normal breast epithelial cells; their mechanisms of actions are explored in the next chapter. Attempts at increasing the selectivity through the synthesis of an osmium cluster thymidine bioconjugate have been unsuccessful so far due to difficulties with the synthesis.

2.7. Experimental

Synthetic steps were carried out under an atmosphere of argon using standard Schlenk techniques. ^{1}H NMR spectra were recorded on a Jeol 400 NMR spectrometer as $CDCl_3$ solutions unless otherwise stated; chemical shifts reported were referenced against the residual proton signals of the solvent. IR spectra were recorded on a Bruker ALPHA FTIR spectrometer as DCM solutions unless otherwise stated. The starting material $Os_3(CO)_{12}$ was obtained from Oxkem Ltd; all other chemicals were purchased from other commercial sources and used as supplied. The clusters **1**,[19] **1'**,[20] **2**,[21] **2'**,[20] **3'**,[22], **5**[9], **7b**[15], **kojic-Cl**[17], **kojic-N$_3$**[17], and **Thy-1**[16] were synthesized according to the literature methods.

Experimental cultures of the MCF-7, MDA-MB-231 and MCF-10A cell lines were obtained from American Type Culture Collection (ATCC) and cultured in tissue culture dishes (Nunc Inc., Naperville, IL, USA). For MCF-7 and MDA-MB-231, the cells were maintained in Dulbecco's modified Eagle's medium (DMEM, Grand Island, NY, USA) supplemented with 10% fetal bovine serum (FBS), 1% L-glutamine (GIBCO Laboratories), and 1% penicillin (GIBCO Laboratories) at 37 °C in 5% CO_2 atmosphere. For MCF-10A, they were maintained in DMEM:F12 supplemented with 7.5% FBS, 1 % L-glutamine, 0.4 % gentamicin (GIBCO Laboratories), and growth factors EGF (Invitrogen), insulin (Invitrogen), hydrocortisone (Sigma Aldrich) and cholera toxin (Sigma

Aldrich) at 37 °C in 5% CO_2 atmosphere. Phosphate-buffered saline (PBS) was obtained from GIBCO.

2.7.1 Synthesis of $Os_3(CO)_{11}$(COE), 3a

A sample of $Os_3(CO)_{12}$ (20 mg, 22 µmol) and Me_3NO (2 mg, 26 µmol) were added to dichloromethane (10 mL) and cis-cyclooctene (1 mL) in a reaction vessel equipped with a magnetic stir bar. The reaction mixture was stirred for 2 h at 40 °C under argon bubbling and formation of the product was monitored by IR spectroscopy. The mixture was then filtered through silica gel to remove any unreacted Me_3NO and the solvent was removed under vacuum. Yield: 21.3 mg (98 %).

^{1}H NMR: δ 3.66 – 3.69 (m, 2H, vinylic protons), 2.49 – 2.54 (m, 2H, allylic protons), 1.88 – 1.97 (m, 2H, allylic protons), 1.68 – 1.82 (m, 4H, 4H of C_8H_{14}), 1.43 – 1.53 (m, 4H, 4H of C_8H_{14}).

IR (cyclohexane): ν_{CO} 2114 (w), 2061 (s), 2041 (s), 2025 (vs), 2006 (w), 2000 (m), 1989 (w), 1979 (w), 1974 (w), 1962 (w) cm^{-1}.

IR of $Os_3(CO)_{11}(C_2H_4)$ (cyclohexane):[3] ν_{CO} 2117 (w), 2064 (s), 2048 (s), 2027 (vs), 2009 (m), 2005 (m), 1995 (m), 1983 (w), 1967 (w) cm^{-1}.

2.7.2 Synthesis of $Os_3(CO)_{11}(PPh_3)$ 3

Cluster **3a** (21 mg, 21 µmol) and PPh_3 (5.6 mg, 21 µmol) were dissolved in dichloromethane. The mixture was then stirred for 1 h at room temperature. Formation of the product was monitored by IR spectroscopy. The dichloromethane was removed under vacuum and the crude product was purified by TLC using hexane/dichloromethane (1.75:1, v/v) as eluent. Yield: 15.8 mg (66 %). IR: ν_{CO} 2107 (m), 2055 (s), 2034 (s), 2018 (s), 1988 (m), 1978 (m) cm^{-1}. Lit. values (cyclohexane):[4] ν_{CO} 2108 (m), 2055 (s), 2035 (s), 2019 (s), 2000 (m), 1989 (m), 1978 (m) cm^{-1}.

2.7.3 Synthesis of $Os_3(CO)_{11}(NCCH_2CH_2OH)$ 1a and $Os_3(CO)_{11}(NCC_6H_4OH$-*p*$)$ 1b

An identical procedure to the synthesis of $Os_3(CO)_{11}(PPh_3)$ was followed except that no further purification was carried out. Removal of the solvent afforded a yellow product.

1a: Yield = 18.5 mg (93%). ^{1}H NMR: δ 3.90 – 3.95 (td, 2H, J = 5.5 Hz, C*H*$_2$OH), 3.22 – 3.25 (t, 2H, J = 5.5 Hz, NCCH$_2$, 1.88 (t, J = 5.5 Hz, 1H, CH$_2$O*H*). IR: ν_{CO} 2106 (w), 2067 (m), 2053 (vs), 2040 (vs), 2017 (s, sh), 2008 (vs), 1980 (m) cm^{-1}.

1b: Yield = 18.2 mg (87%). ^{1}H NMR: δ 7.53 – 7.57 (m, 2H, 2H of C$_6$H$_4$), 6.90 – 6.98 (m, 2H, 2H of C$_6$H$_4$), 5.61 (m, OH). IR: ν_{CO} 2106 (w), 2068 (m), 2053 (vs), 2040 (vs), 2017 (s, sh), 2007 (vs), 1982 (m) cm^{-1}. ESI: 998.55 [M+H]$^+$.

2.7.4 Synthesis of Os$_3$(CO)$_{11}$(NCCH$_2$CH$_2$OH)(μ-H)$^+$BF$_4^-$ 1a' and Os$_3$(CO)$_{11}$(NCC$_6$H$_4$OH-*p*)(μ-H)$^+$BF$_4^-$ 1b'

Cluster **1a** (3 mg, 3 μmol) or **1b** (3 mg, 3 μmol) was dissolved in dichloromethane (3 mL) and a solution of HBF$_4$ (51-57 % in diethyl ether, 20 μL) was added. Formation of the product was monitored by IR spectroscopy and the solvent was removed under vacuum. The product was not purified further. Both compounds gave the same IR spectrum.

1a': Yield = 1.8 mg (60%); **1b'**: Yield = 2.0 mg (66 %)

1a' IR: ν_{CO} 2150 (w), 2108 (s), 2087 (vs), 20634(vs), 2037 (m), 2021 (m) cm^{-1}. ESI: 951.52 [M+H]$^+$.

1b' IR: ν_{CO} 2150 (w), 2108 (s), 2087 (vs), 2061 (s), 2040 (m), 2021 (m) cm^{-1}. ESI: 951.52 [M+H]$^+$.

Lit IR of Os$_3$(CO)$_{11}$(NCMe)(μ-H)$^+$BF$_4$:[20] ν_{CO} 2150 (w), 2108 (s), 2087 (s), 2062 (s), 2019 (m), 2007 (vw) cm^{-1}.

2.7.5 Synthesis of Os$_3$(CO)$_{10}$(COE)$_2$, 4a

Os$_3$(CO)$_{10}$(μ-H)$_2$ (50 mg, 0.06 mmol) in cyclooctene (8 mL) solution was first degassed via three cycles of freeze-pump-thaw. The carius tube was then filled with ethylene gas, and the mixture was stirred overnight at room temperature. The formation of the product was monitored by IR spectroscopy. The solvent was then removed under vacuum and the crude product was not purified further. Yield: 50 mg (100 %)

IR (cyclooctene): ν_{CO} 2097 (w), 2062 (vw), 2054 (vw), 2040 (m), 2026 (m), 2011 (s), 1988 (m), 1980 (m), 1973 (m), 1966 (w) cm^{-1}.

Lit IR (cyclooctene): [5] ν_{CO} 2097 (w), 2041 (m), 2027 (m), 2013 (s), 1990 (m), 1981 (m), 1975 (m), 1967 (w), 1950 (vw) cm^{-1}.

2.7.6 Synthesis of $Os_3(CO)_{10}(NCCH_2CH_2OH)$ 2a and $Os_3(CO)_{11}(NCC_6H_4OH$-*p*) 2b

$Os_3(CO)_{10}(COE)_2$ **4a** (10 mg, 9 μmol) and 3-hydroxypropionitrile (1.7 mg, 24 μmol) or 4-hydroxybenzonitrile (2.9 mg, 24 μmol) were dissolved in dichloromethane. The mixture was stirred at room temperature and the reaction was monitored by IR spectroscopy. The solvent was then removed under vacuum and the crude product was not purified further. Both compounds gave the same IR spectrum.

2a: Yield: 4.8 mg (96 %); **2b**: Yield: 4.9 mg (98 %). IR: ν_{CO} 2079 (w), 2068 (w), 2053 (w), 2025 (sh), 2021 (vs), 1983 (m), 1960 (w) cm^{-1}. Lit IR of $Os_3(CO)_{10}(NCMe)_2$:[21] ν_{CO} 2079 (w), 2025 (sh), 2021 (vs), 1983 (m), 1960 (w) cm^{-1}.

2.7.7 Synthesis of Kojic-Br

Kojic acid (200 mg, 1.4 mmol) was suspended in PBr_3 (1.8 mL, 19.3 mmol) in a Schlenk tube at 40 °C and left to react for 12 h. Water was slowly added to the reaction mixture while cooled in an ice bath to destroy the unreacted PBr_3 and the product was extracted with ethyl acetate and vacuum dried to give a white solid. The formation of **Kojic-Br** was confirmed by comparing with the NMR spectrum of starting material Kojic acid.

Yield: 50 %

^{1}H NMR: δ 4.20 (s, 2H, C*H*$_2$Br), 6.53 (s, 1H), 7.87 (s, 1H).

^{1}H NMR of kojic acid: δ 4.53 (s, 2H, C*H*$_2$Br), 6.57 (s, 1H), 7.83 (s, 1H).

2.7.8 Synthesis of 5a

$Os_3(CO)_{10}(\mu–H)(\mu–OH)$ **7b** (100 mg, 0.12 mmol) was added to the chloro derivative of kojic acid **kojic-Cl** (93 mg, 0.58 mmol) in toluene under argon and left to reflux at 110 °C for 30 h. The reaction mixture was vacuum dried and purified using TLC (hexane/CH_2Cl_2, 3:2, *v/v*). The 3rd band gave unreacted $Os_3(CO)_{10}(\mu–H)(\mu–OH)$ as a yellow solid (17.6 mg) and the 2nd band gave $Os_3(CO)_9(\mu–H)(\mu$-γ-Kojic–Cl) as a yellow solid (27.6 mg).

^{1}H NMR: δ -9.11 (s, 1H, μ-H), 4.43 (s, 2H, C*H*$_2$Cl), 6.85 (s, 1H, α-H), 8.10 (s, 1H, β-H).

IR: ν_{CO} 2103 (w), 2061 (s), 2018 (vs), 2002 (m), 1927 (w) cm^{-1}.

2.7.9 Synthesis of 5b

$Os_3(CO)_{10}(\mu–H)(\mu–OH)$ **7b** (100 mg, 0.12 mmol) was added to the bromo derivative of kojic acid **kojic-Br** (100 mg, 0.49 mmol) in toluene under argon and left to reflux at 110 °C for 30 h. The reaction mixture was vacuum dried and purified using TLC (hexane/CH_2Cl_2, 3:2, *v/v*). The 3rd band gave unreacted $Os_3(CO)_{10}(\mu–H)(\mu–OH)$ as a yellow solid (56 mg) and the 2nd band gave $Os_3(CO)_9(\mu–H)(\mu$-γ-Kojic–Br) as a yellow oil (5 mg).

^{1}H NMR: δ -9.13 (s, 1H, μ-H), 6.80 (s, 1H, α-H), 8.09 (s, 1H, β-H). The C*H*$_2$ signal was obscured by the plasticizer impurities.

IR: ν_{CO} 2103 (w), 2061 (s), 2017 (vs), 2000 (m), 1927 (w) cm^{-1}.

2.7.10 Synthesis of 5c

$Os_3(CO)_{10}(\mu–H)(\mu–OH)$ **7b** (100 mg, 0.12 mmol) was added to azide derivative of kojic acid **kojic-N_3** (93 mg, 0.58 mmol) in toluene under argon and left to reflux at 110 °C overnight. The reaction mixture became brown due to the decomposition of **Kojic-N_3** at high temperature, and no reaction was observed via IR spectroscopy. The reaction was repeated at 70 °C, no reaction was also observed despite **Kojic-N_3** not decomposed.

2.7.11 Synthesis of 5d

$Os_3(CO)_{10}(\mu–H)(\mu–OH)$ **7b** (30 mg, 0.04 mmol) was added to kojic acid (22 mg, 0.15 mmol) in toluene under argon and left to reflux at 110 °C for 30 h. The reaction mixture was vacuum dried and purified using TLC (hexane/ethyl acetate, 2:1, *v/v*). The 1st band gave unreacted $Os_3(CO)_{10}(\mu–H)(\mu–OH)$ as a yellow solid (11 mg) and the 2nd band gave $Os_3(CO)_9(\mu–H)(\mu$-γ-Kojic–OH) as a yellow solid (10 mg).

^{1}H NMR: δ -9.15 (s, 1H, μ-H), 4.64 (s, 2H, C*H*$_2$OH), 6.90 (s, 1H, α-H), 8.05 (s, 1H, β-H).

IR: ν_{CO} 2103 (w), 2061 (s), 2018 (vs), 2000 (m), 1926 (w) cm^{-1}.

2.7.12 Synthesis of 5e

To $Os_3(CO)_9(\mu–H)(\mu$-γ-Kojic–OH) **5e** (52 mg, 54 μmol) and azidobenzoic acid (0.2 M in tert-butyl methyl ether (269 μL, 54 μmol) in DCM (5 ml), 1-(3-Dimethyaminopropyl)-3-ethylcarbodiimide hydrochloride (11 mg, 57 μmol) and 4-(dimethylamino)pyridine (6.57 mg, 54 μmol) was added. It

was allowed to stir for 1 h at room temperature. The reaction mixture was then washed with water (2 x 10 ml), and the DCM extracts evacuated to dryness. Crude NMR shows no conversion to the target compound. The crude product was purified using TLC (hexane/ethyl acetate, 3:2, *v/v*), and the major yellow band was isolated (1 mg, 2 % yield). The identity of this yellow band was not identified.

2.7.13 Proliferation assay

The osmium carbonyl clusters were first dissolved in sterile dimethylsulfoxide (DMSO) to make 10 mM stock solutions. They were then diluted with serum-free medium, with final concentrations used for treatment in the range of 0.1 µM to 200 µM. The cells were then treated with the indicated concentrations of osmium carbonyl clusters in triplicates and incubated for 24 h, after which, Cell Titer 96_ Aqueous One Cell Proliferation Assay (Promega) (20 µL) was added to each well. This was then left to incubate at 37 °C in 5% CO_2 for 2 h. The absorbance at 490 nm was then measured and the cell proliferation relative to the control sample was calculated. The curves were then generated using a sigmoidal dose response (variable slope) equation using the GraphPad Prism 5 software.

2.8. References

1 a) K.V. Kong, W.K. Leong, S. P. Ng, T. H. Nguyen, L.H.K. Lim. *ChemMedChem.* **2008**, *3*, 1269; b) K.V. Kong, W.K. Leong, L.H.K. Lim. *J. Organomet. Chem*. **2009**, *694*, 834.

2 a) G. Cheng, J. Zielonka, B. P. Dranka, D. McAllister, A. G. Mackinnon Jr, J. Joseph, B. Kalyanaraman, *Cancer Res*. **2012**, *72*, 2634; b) D. Dindo, F. Dahm, Z. Szulc, A. Bielawska, L. M. Obeid, Y. A. Hamun, R. Graf, P. A. Clavien, *Mol Cancer Ther*. **2006**, *5*, 1520; c) J. S. Modica-Napolitano, J. R. Aprille, *Advanced Drug Delivery Reviews*. **2001**, *49*, 63.

3 B. F. G. Johnson, J. Lewis, D. A. Pippard, *J. Chem. Soc., Dalton Trans.* **1981**, 407.

4 a) J. Evans, G. S. McNulty, *J. Chem. Soc., Dalton Trans.* **1984**, 79; b) B. F. G. Johnson, J. Lewis, D. A. Pippard, *J. Chem. Soc., Dalton Trans.* **1981**, 407.

5 M. Tachikawa, J. R. Shapley, *J. Organomet. Chem*, **1977**, *124*, C19.

6 J. B. Keister, J. R. Shapley, *J. Am. Chem. Soc,* **1976**, *98*, 1056.

7 J. B. Keister, J. R. Shapley, *J. Organomet. Chem.* **1975***, 85*, C29.

8 V.D. Reddy, D. Dayal, D. J. Szalda, S. C. Cosenza, M.V. R. Reddy. *J. Organomet. Chem*. **2012**, *700*, 180.

9 Q. Lin, W. K. Leong, *Organometallics* **2003**, *22*, 3639.

10 a) M. Hironishi, R. Kordek, R. Yanagihara, RM. Garuto, *Neurodegeneration*. **1996**, *5*, 325; b) K. Murakami, K. Ishida, K. Watakabe, R. Tsubouchi, M. Haneda, M. Yoshino, *Biometals*. **2006**, *19*, 253; c) K. Murakami, K. Ishida, K. Watakabe, R. Tsubouchi, M. Naruse, M. Yoshino, *Toxicol Lett*, **2006**, *161*, 102; d) S, Amatori, G. Ambrois, M. Fanelli, M. Formica, V. Fusi, L. Giorgi, E. Macedi, M. Micheloni, P. Paoli, R. Pontellini, P. Rossi, *J. Org. Chem*. **2012**, *77*, 2207; e) S. Amatori, I. Bagaloni, E. Macedi, M. Formica, L. Giorgi, V. Fusi, M. Fanelli, *Br. J. Cancer*. **2010**, *103*, 239.

11 A. Vessieres, C. Corbet, J. M. Heldt, N. Lories, N. Jouy, I. Laios, G. Leclercq, G. Jaouen, R-A. Toillon, *J. Inorganic. Biochemistry*, **2010**, *104*, 503; S. Top, A. Vessieres, G. Leclercq, J. Quivy, J. Tang, J. Vaissermann, M. Huche, G. Jaouen, *Chem. Eur. J.* **2003**, *9*, 5223.

12 G. P. H. Dietz, M. Bahr, *Mol. Cell. Neurosci*, **2004**, *27*, 85; S. B. Christensen, D. M. Skytte, S. R. Denmeade, C. Dionne, J. V. Moller, P. Nissen, J. T. Issacs, *Anti-Cancer Agents in Medicinal Chemistry,* **2009**, *9*, 277; G. Collet, C. Grillon, M. Nadim, C. Kieda, *Gene*, **2013**, *525*, 208.

13 a) M. M. Alegre, R. A. Robison, K. L. O'Neill, *Cancer and Clinical Oncology*, **2013**, *2,* 159; b) Q. He, S. Skog, B. Tribukait, *Cell Prolif*, **1991**, *24*, 3; c) M. Hengstchlager, M. Pfeilstocker, E. Wawra, *Advances in Experimental Medicine and Biology*, **1998**, *431*, 455

14 a) M. M. Alegre, R. A. Robison, K. L. O'Neill, *J Oncol*, **2012**, 575647; b) N. Li, H. Yang, W. Pan, W. Diao, B. Tang, *Chem. Commun*, **2014**, *50*, 7473

15 D.Roberto, E. Lucenti, C. Roveda, R. Ugo, *Organometallics*, **1997**, *16*, 5974.

16Y. Byun, J. Yan, A. Al-Madhoun, J. Johnsamuel, W. Yang, R. Barth, S. Eriksson, W. Yjarks, *J. Med. Chem.,* **2005**, *48*, 1188.

17 S. M. Meier, M. Novak, W. Kandioller, M. A. Jakupec, V. B. Arion, N. Metzler-Nolte, B. K. Keppler, C. G. Hartinger, *Chem. Eur. J.* **2013**, *19*, 9297

18 B. Neises, W. Steglich, *Angew. Chem. Int. Ed*. **1978**, *17*, 522.

19 J. Y. Jung, B. S. Newton, M. L. Tonkin, C. B. Powell, G. L. Powell, *J. Organomet. Chem.* **2009**, *694*, 3526.

20 C. E. Anson, E. J. Ditzel, M. Fajardo, H. D. Holden, B. F. G. Johnson, J. Lewis, J. Puga, P. R. Raithby, *J. Chem. Soc. Dalton Trans.* **1984**, 2723.

21 J. Y. Jung, D. K. Kempe, L. J. Loh, S. E. Shoultz, G. L. Powell, *J. Organomet. Chem.* **2012**, *700*, 219.

22 A. J. Deeming, S. D. Mtunzi, S. E. Kabir, M. B. Hursthouse, K. M. A. Malik, N. P. C. Walker, *J. Chem. Soc., Dalton Trans*. **1987**, 1869.

Chapter 3. Mode of action studies on osmium carbonyl clusters

Structure-activity-relationship studies on the triosmium carbonyl clusters in chapter two revealed two important criteria for its antiproliferative activity – good solubility and one vacant site. Of all the compounds tested, $Os_3(CO)_{11}(NCMe)(\mu\text{-}H)^+BF_4^-$ **1'** and $Os_3(CO)_9(\mu\text{-}H)(\mu\text{-}\gamma\text{-}C_6H_5O_3)$ **5** were found to be the most active against breast cancer cells MDA-MB-231, with IC_{50} values of 7 μM and 3 μM, respectively. It has been established that the mode of action of $Os_3(CO)_{10}(NCMe)_2$ **2** is through the induction of apoptosis, most probably by its binding to intracellular sulfhydryl and carboxylate residues.[1] However, it was found that **1'** does not react readily with nucleophiles,[2] and there are also no reported reactivity studies on **5**. Therefore, it will be important to establish if **1'** and **5** caused cell death via the induction of apoptosis, as well as to investigate their chemical reactivity and hence their likely mode of action.

3.1 Mode of action – induction of apoptosis

Three assays were performed on **1'**, *viz*., Annexin V-FITC /PI staining, nuclear staining using DAPI, and DNA fragmentation using PI staining, to determine if it induces apoptosis.

3.1.1 Annexin V-FITC and PI staining

As has been introduced in chapter 1, this assay labels apoptotic cells with Annexin-V FITC stain, while necrotic cells stain both FITC and PI, and live cells show little or no fluorescence.[3] The results of the staining after 15 h of incubation of MDA-MB-231 cancer cells with **1'** is shown in Figures 3.1; ~50 % of the cells were found to be dead, with ~80 % of them apoptotic.

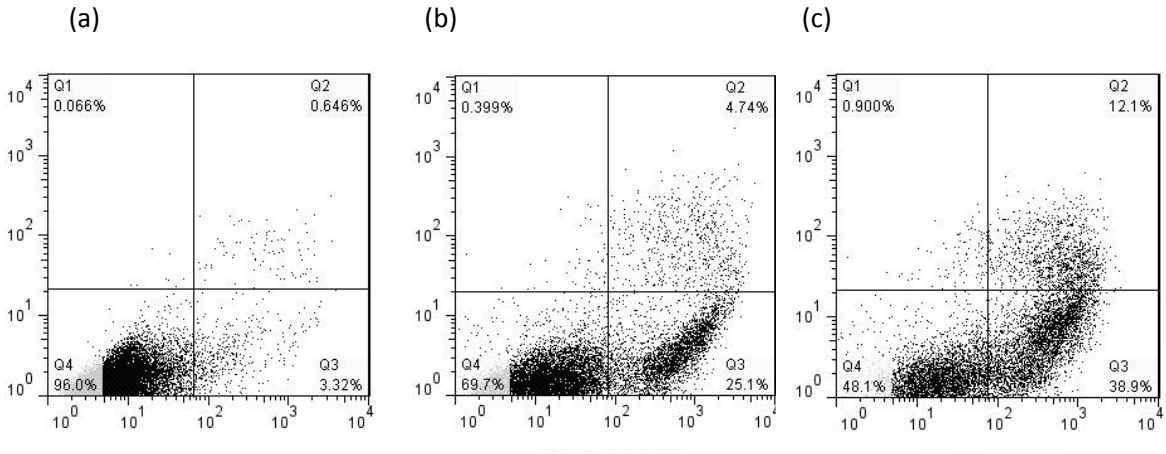

Figure 3.1 MDA-MB-231 cells stained with Annexin V-FITC and PI after 15 h incubation with a) vehicle only (control), b) 10 μM of **2** (positive control), c) 10 μM of **1'**. X-axis refers to Annexin V-FITC and Y-axis refers to PI. Q2: necrotic cells (stained with both annexin V-FITC and PI); Q3: apoptotic cells (stained with Annexin V-FITC only); Q4: live cells (no stain).

The same assay was also performed for **5** on the MDA-MB-231 cell line, giving similar results (Appendix 3.1).

3.1.2 DNA fragmentation using PI

In this assay, apoptotic cells can be recognized by the characteristic sub-G1 peak in the DNA histogram. Indeed, the DNA histograms of MDA-MB-231 breast cancer cells incubated with **1**' (Figure 3.2) showed the characteristic sub-G1 peak, indicating that they are apoptotic cells.

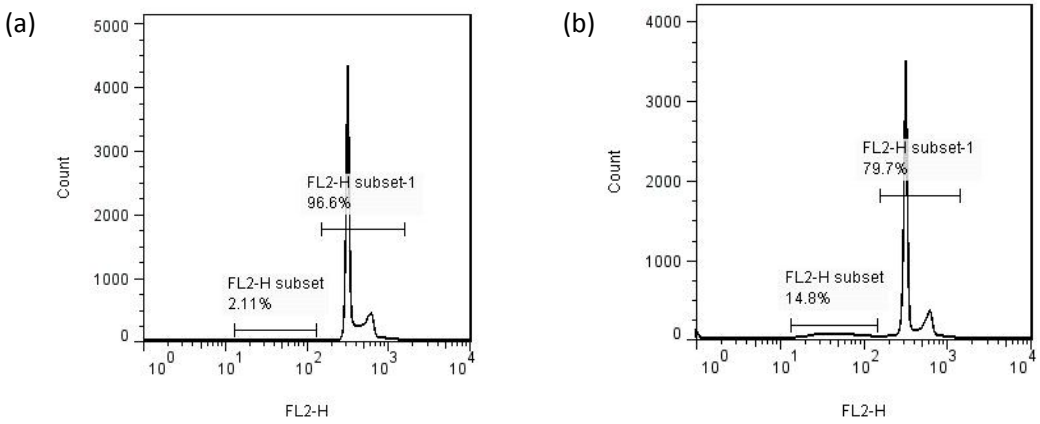

Figure 3.2 DNA histogram of (a) live cells (control), (b) cells incubated with 10 μM of **1'.**

The same assay was also performed for **5** on the MDA-MB-231 cell line, giving similar results (Appendix 3.2).

3.1.3 Nuclear chromatin condensation in apoptotic cells

The last apoptosis assay performed was to examine the nuclear chromatin condensation in apoptotic cells by fluorescent microscopy. MDA-MB-231 cells that were incubated with **1'** were fixed, stained with DAPI, and examined under the fluorescent microscope. Cells indicated in arrow are the condensed nuclear chromatin in apoptotic cells; control cells have round intact nuclei (Figure 3.3).

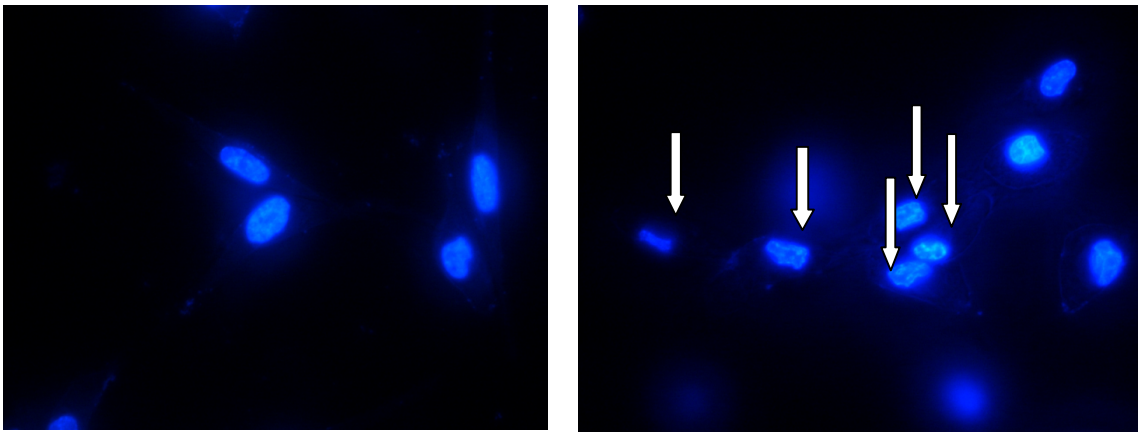

Figure 3.3 Fluorescence image (60 X) of MDA-MB-231 cells stained with DAPI; left: control and right: after incubation with 5 μM of **1'** for 3 h.

3.2 Mode of action – establishing the target

A useful concept that helps in the assessment of the nature and stability of metal-ligand interactions is Pearson's Hard-Soft Acid-Base (HSAB) concept.[4] A metal complex can be regarded as comprising a Lewis acid (the metal centre) surrounded by a number of Lewis bases (the ligands). Both Lewis acids and bases can be classified as either soft or hard, depending on whether they are more or less polarizable. The HSAB concept states that hard Lewis acids will tend to bind more strongly with hard rather than soft Lewis bases, and vice versa. The metal centres in a transition metal carbonyl cluster are soft Lewis acids and hence, they tend to bind strongly with soft Lewis bases such as CO and phosphines, which also tend to be less labile. Hard Lewis bases such as ethers,

alcohols, and nitriles, form weak bonds with clusters and are thus more labile.[5] One classic example of a carbonyl cluster containing labile ligands is the triosmium carbonyl cluster $Os_3(CO)_{10}(NCMe)_2$ **2**, which has been widely used as a precursor for the synthesis of a wide range of substituted organometallic complexes through the displacement of the two weakly-bound acetonitrile ligands with nucleophiles ranging from the phosphines,[6] to thiols,[7] and carboxylic acids, etc.[8] The mechanism of action for the cytotoxicity of **2** was also attributed to its binding to intracellular sulfhydryl and or/carboxylate residues, which is consistent with the known reactivity pattern of **2**.[1] This requires two vacant binding sites on the cluster core, as illustrated in Figure 3.4.

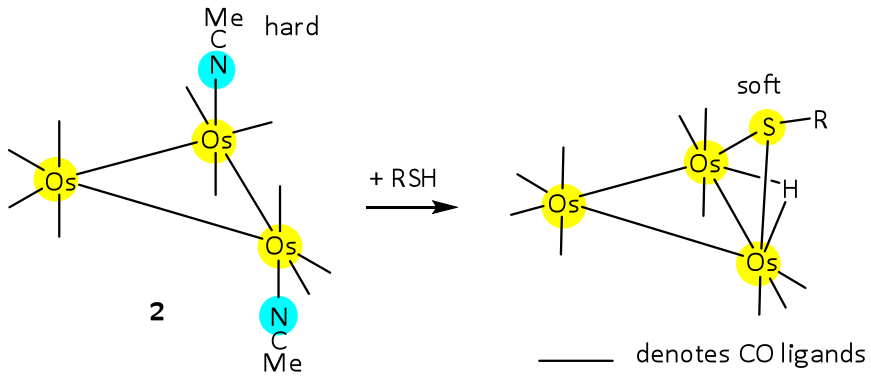

Figure 3.4 Reaction of **2** with thiols.

The two triosmium carbonyl clusters **1'** and **5** are, however, structurally very different from **2**. Compound **1'** is a cationic cluster, and although it contains an acetonitrile ligand, that cannot be displaced easily. Compound **5** can, in principle, produce a vacant site by the de-coordination of the ketone functionality, but there are no studies on how easily such nucleophilic displacement can occur. Nevertheless, given the foregoing, it is likely that the biological targets of both **1'** and **5** were sulfhydryl and or/carboxylate residues, and so their chemical reactivity with thiols and carboxylic acids were first examined before embarking on an assessment of their biological reactivity.

3.2.1 Chemical reactivity of 1'

Reaction with thiols

Compound **1'** did not react with ethanethiol even after stirring overnight, in contrast with **2** which reacted readily. In biological systems, however, histidine residues can abstract a proton from cysteine thereby turning it into a stronger nucleophile. Imidazole (pKa of its conjugated acid = 7) was used to mimic histidine (pKa = 6.5). It was indeed found that **1'** reacted with ethanethiol in the presence of imidazole, after a few hours of stirring, to give $Os_3(CO)_{10}(\mu\text{-}H)(\mu\text{-}SCH_2CH_3)$, **7a**. The identity of **7a** was established on the basis of its IR pattern in the CO vibration region, and the presence of a hydride resonance at ~-17 ppm (Appendices A3.4 and A3.5, respectively), both characteristic of $Os_3(CO)_{10}(\mu\text{-}H)(\mu\text{-}SR)$ clusters.[7] Monitoring of the reaction via IR spectroscopy also showed that an intermediate species **X** was formed, which transformed to **7a** eventually (Figure 3.5a). Subtraction of the spectra (figures 3.5a and 3.5b) gave the spectrum of **X** shown in Figure 3.5c, which has been identified as $Os_3(CO)_{11}$(imidazole) **1d** (see later section).

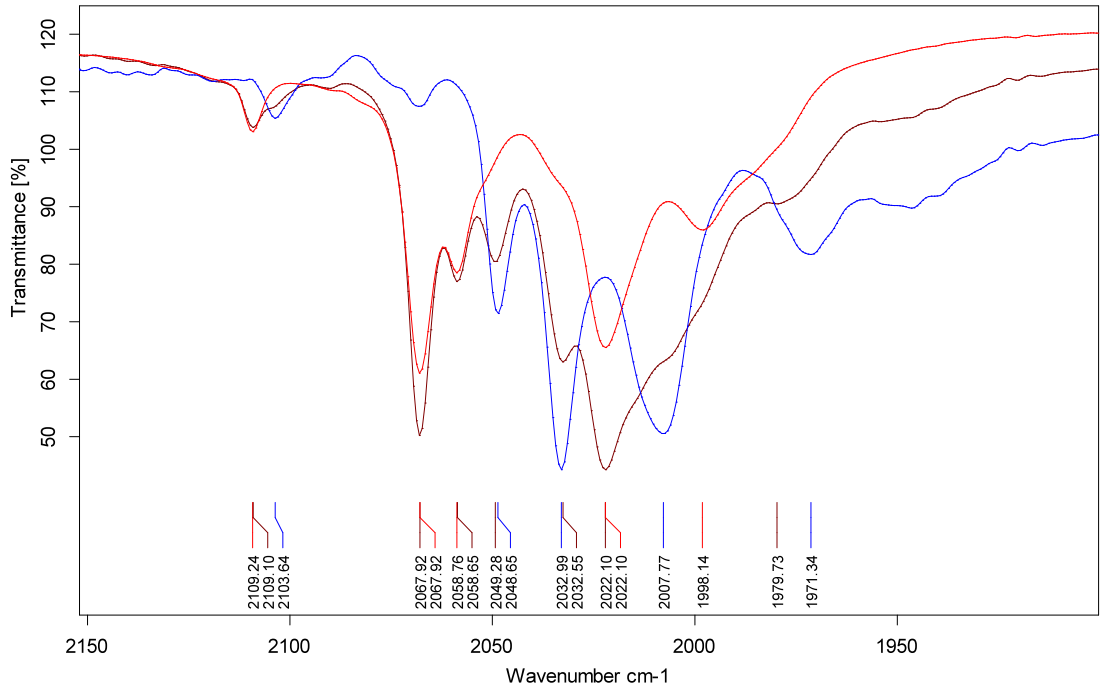

Figure 3.5 IR spectra of (a) reaction of **1'** with imidazole and ethanethiol, containing intermediate **X** (brown), (b) **7** (red), and (c) intermediate **X** (blue).

This result suggests that **1'** was deprotonated, and reaction with excess imidazole gave **1d**. This was confirmed by the sequential addition of imidazole to **1'** in acetonitrile, which led to deprotonation of **1'** to form cluster **1** (Figure 3.6), followed by ethanethiol which converted it to **7a** (Figure 3.7). The role of imidazole is thus the deprotonation of the cationic cluster **1'** rather than the thiol. It has been verified that **7a** could be formed from the reaction of **1** with ethanethiol (Experimental 3.4.4), and the necessity of a thiolate for the reaction was ruled out in a similar experiment with imidazole replaced by pyridine. As pyridine (pKa of its conjugate acid = 5.25) is a weaker base than ethanethiolate (pKa of ethanethiol= 10.6), it will not deprotonate the thiol. Upon the addition of pyridine, the pyridine analogue of **1**, viz., $Os_3(CO)_{11}(py)$, **1c**, was formed (Figure 3.8b); the formation of **1c** instead of **1** was again due to the excess pyridine present. This was followed by the formation of **7a** upon the addition of ethanethiol (Figure 3.8c).

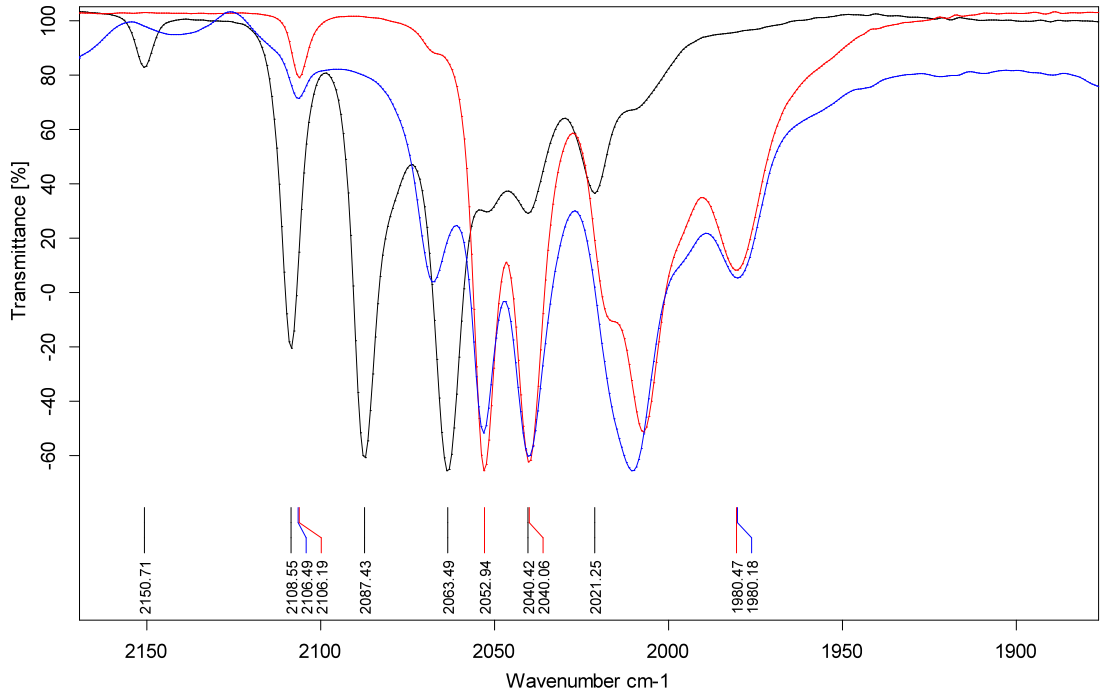

Figure 3.6. IR spectra of (a) **1'** (black), (b) **1'** in the presence of imidazole (blue), (c) **1** (red).

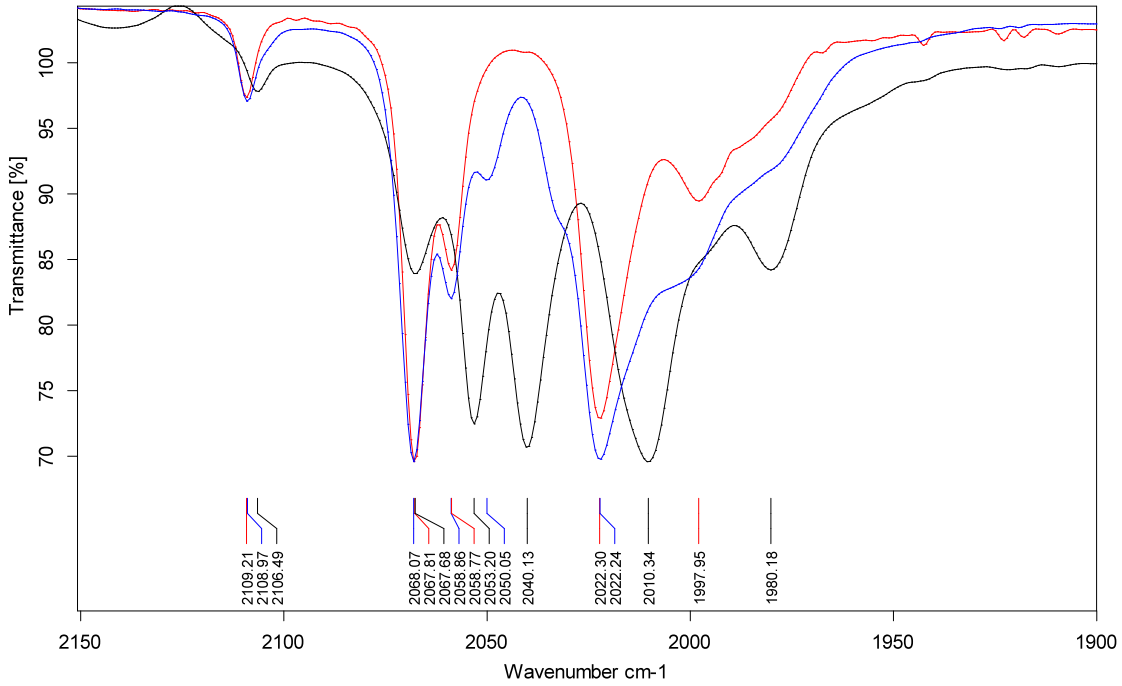

Figure 3.7. IR spectra of (a) **1'** in the presence of imidazole (black), (b) after addition of ethanethiol (blue), (c) pure sample of **7a** obtained after TLC separation (red).

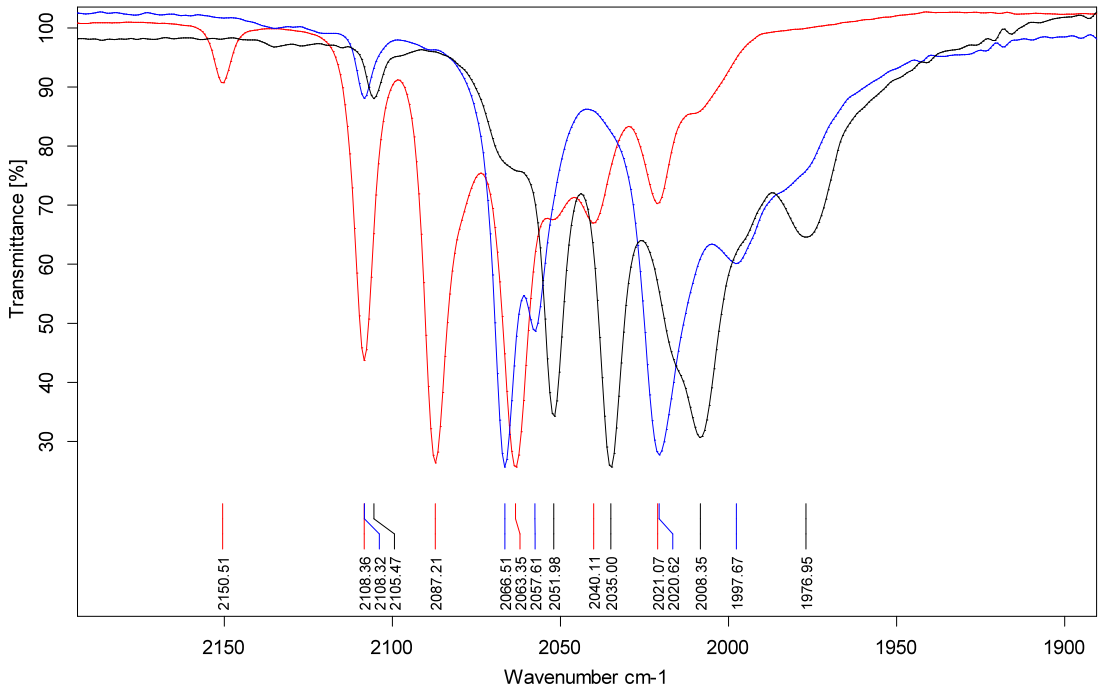

Figure 3.8. IR spectra of (a) **1'** (red), (b) **1'** in the presence of pyridine (black), and (c) after addition of ethanethiol (blue). The identity of **1c** (black spectrum) was established by comparison with literature values.[9]

The above results thus show that, in the presence of a base, **1'** can be deprotonated to the neutral form **1**. This is the active form which can react with thiol to form the thiolate cluster **7a** (Scheme 3.1).

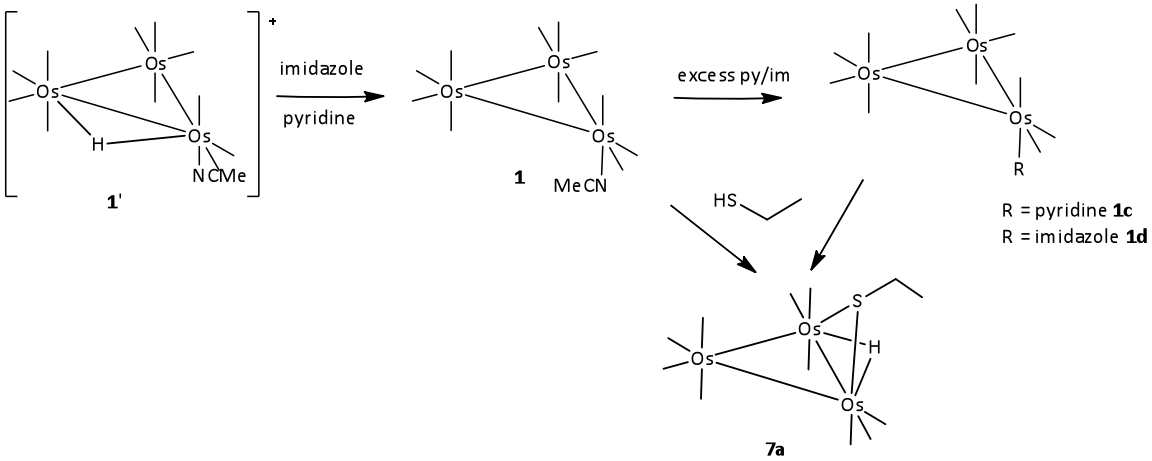

Scheme 3.1. Deprotonation of **1'** by imidazole or pyridine, and subsequent reaction of **1** or **1c**/**1d** (in excess of pyridine or imidazole) with ethanethiol to form **7a**.

Reaction with carboxylic acids

Cluster **1'** also failed to react with ethanoic acid, but in the presence of imidazole, it afforded a product identified as $Os_3(CO)_{11}$(imidazole), **1d** (Scheme 3.2). The identity of **1d** was established on the basis of the similarity of the pattern for the CO vibrations in its IR spectrum (Appendix A3.6) to that of **1**, indicating that they have a similar number and disposition of CO ligands, and a shift in the imidazole resonances in its ^{1}H NMR spectrum (Appendix A3.7). The results here also confirmed the identity of compound **X** in the earlier section to be **1d** as they have identical IR spectrum (Appendix A3.8). Presumably, **1'** was deprotonated as in the case above, but the formation of **1d** was favoured over the formation of the carboxylate osmium cluster $Os_3(CO)_{10}(\mu\text{-H})(\mu\text{-COOCH}_3)$, **9** (Figure 3.9), as verified from the competitive reaction between an equimolar mixture of RCOOH and imidazole to a solution of **1** (Experimental 3.4.6).

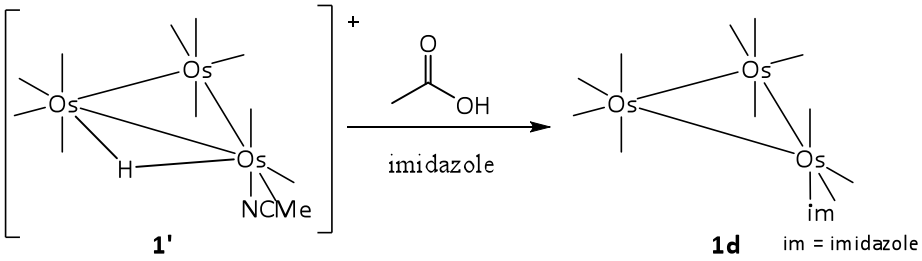

Scheme 3.2 Reaction of **1'** with acetic acid in the presence of imidazole.

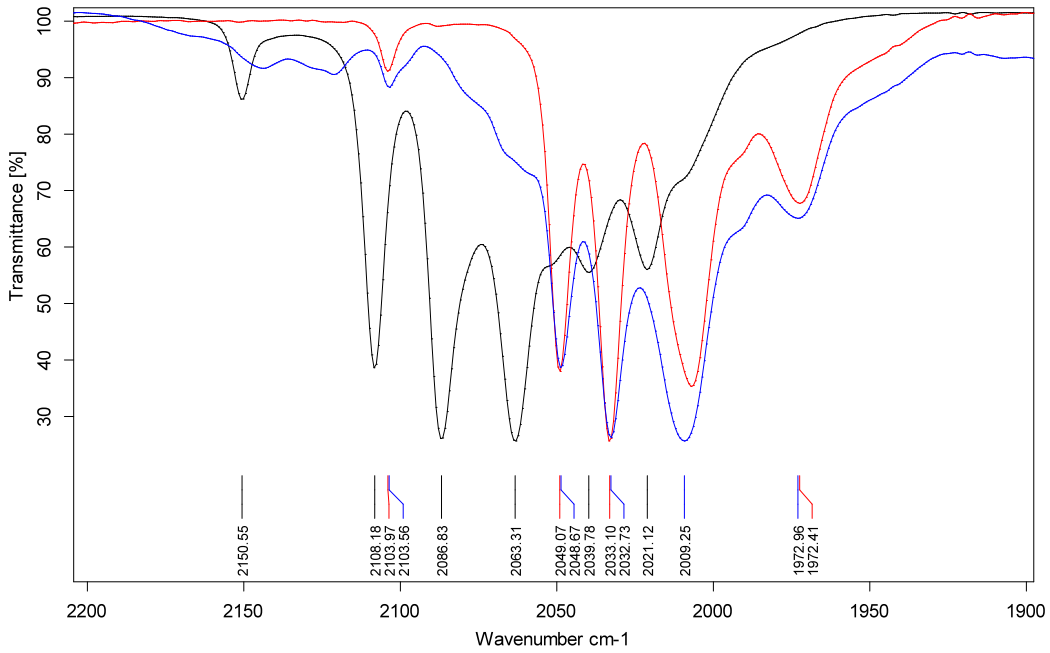

Figure 3.9 IR spectra of (a) **1'** (black), (b) **1'** in the presence of imidazole (blue), (c) **1d** after TLC purification (red).

3.2.2 Interaction of 1' with MDA-MB-231 breast cancer cells

The results above suggest that the likely biological target of **1'** is the sulfhydryl residues. An attempt to verify this was made through the acquisition of the NMR spectrum of MDA-MB-231 breast cancer cells which have been incubated with 40 μM of **1'** (Figure 3.10); thiolate and carboxylate osmium carbonyl clusters $Os_3(CO)_{10}(\mu\text{-H})(\mu\text{-SR})$ and $Os_3(CO)_{10}(\mu\text{-H})(\mu\text{-COOR})$, exhibit characteristic hydride resonances in the NMR spectrum at about -17 ppm and -10 ppm, respectively.[7,8]

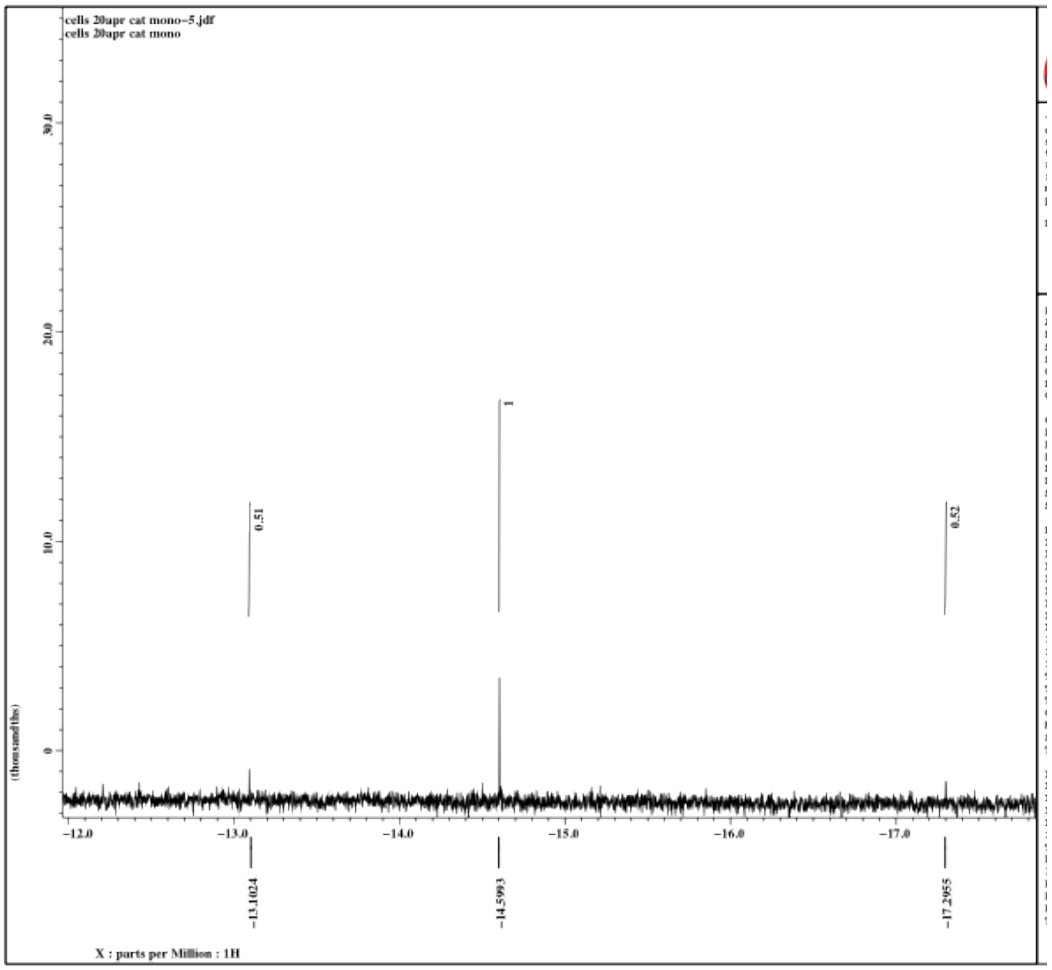

Figure 3.10 NMR spectrum of MDA-MB-231 breast cancer cells incubated with 40 μM of **1'**. Only the metal hydride region is shown.

Three hydride signals were observed, at δ -13.1, -14.6 and -17.3, which can be assigned to $Os_3(CO)_{10}(\mu\text{-H})(\mu\text{-OR})$, $Os_3(CO)_{10}(\mu\text{-H})(\mu\text{-Cl})$ and $Os_3(CO)_{10}(\mu\text{-H})(\mu\text{-SR})$ clusters in 1:2:1 ratio, respectively (Figure 3.11).[10] The most abundant species present is $Os_3(CO)_{10}(\mu\text{-H})(\mu\text{-Cl})$; it results from the reaction with chloride ions. Although its presence may suggest that mitochondria ion channels are a possible target due to the known abundance of chloride ions in the mitochondria,[11] it may also be an artifact left over from the work-up; stirring a sample of **1'** in cell culture media/PBS overnight afforded this cluster (Appendix A3.9).

The presence of clusters of the type $Os_3(CO)_{10}(\mu\text{-H})(\mu\text{-OR})$ and $Os_3(CO)_{10}(\mu\text{-H})(\mu\text{-SR})$ suggests that hydroxyl and sulfhydryl residues, such as threonine and cysteine, are possible targets. There appears, therefore, to be potential new targets for **1'** as the $Os_3(CO)_{10}(\mu\text{-H})(\mu\text{-OR})$ clusters were not observed for **2**. This is surprising as the propensity of these functionalities to bond to osmium is in the order SH > COOH > OH.[12] Competitive studies of **1'** with phenol or methanol in the presence of imidazole also gave **1d** as the only product (Experimental 3.4.7), confirming that alcohol cannot displace the acetonitrile ligand. Hydroxyl residues as the possible target, therefore, has to be re-examined in the future. That the carboxylate osmium cluster $Os_3(CO)_{10}(\mu\text{-H})(\mu\text{-COOR})$ (with a hydride signal at -10 ppm), which was found on incubating MDA-MB-231 cells with **2**, was not observed here is in agreement with the reactivity studies.

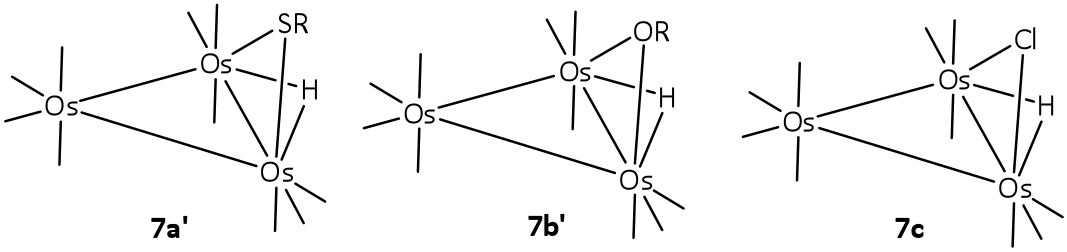

Figure 3.11 Diagrammatic representation of $Os_3(CO)_{10}(\mu\text{-H})(\mu\text{-SR})$ **7a'**, $Os_3(CO)_{10}(\mu\text{-H})(\mu\text{-OR})$ **7b'** and $Os_3(CO)_{10}(\mu\text{-H})(\mu\text{-Cl})$ **7c**.

3.2.3 Chemical reactivity of 5

The reactivity of **5** with ethanethiol is summarised below (Scheme 3.3).

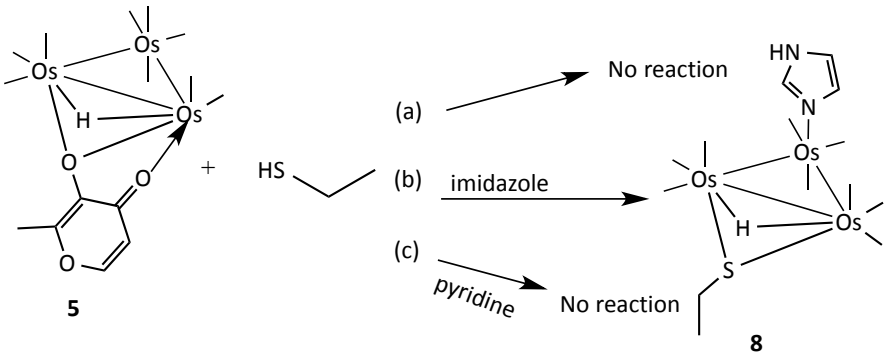

Scheme 3.3 Reaction of **5** with ethanethiol in (a) absence of imidazole, (b) presence of imidazole and (c) presence of pyridine.

While no reaction occurred in the absence of imidazole, a new compound **8** was formed in its presence (Figure 3.12). Compound **8** has been characterized by NMR spectroscopy, as well as by a single crystal X-ray crystallographic study (Appendix A3.11 and A3.12 respectively); the ORTEP plot showing its molecular structure is shown in Figure 3.13.

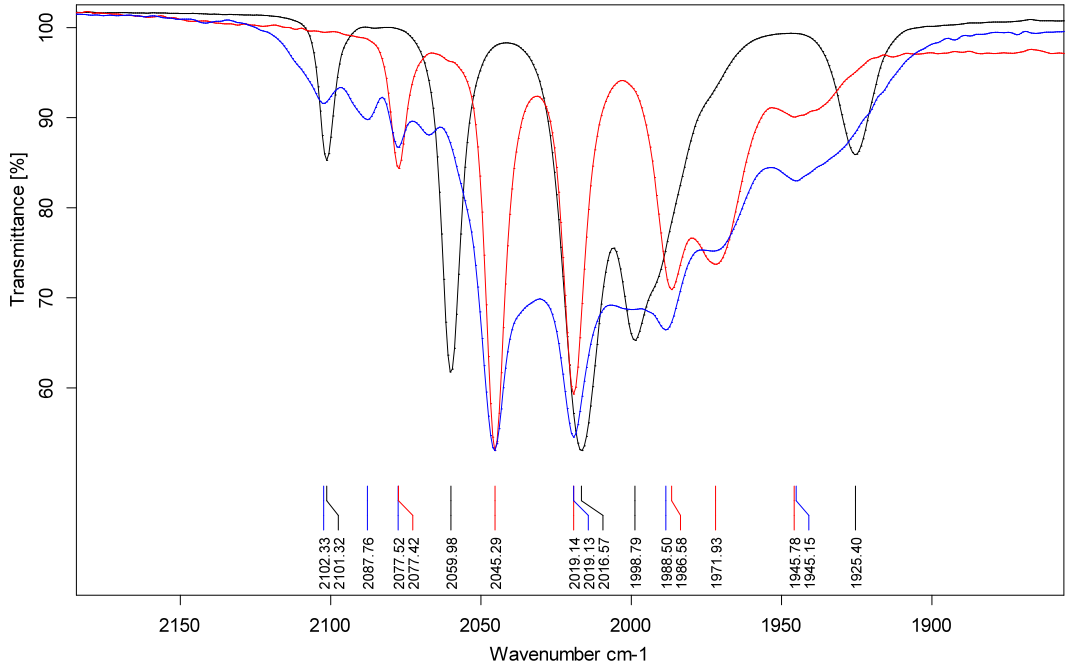

Figure 3.12. IR spectra of (a) **5** (black), (b) **5** in the presence of imidazole (blue), (c) **8** after purification by TLC (red).

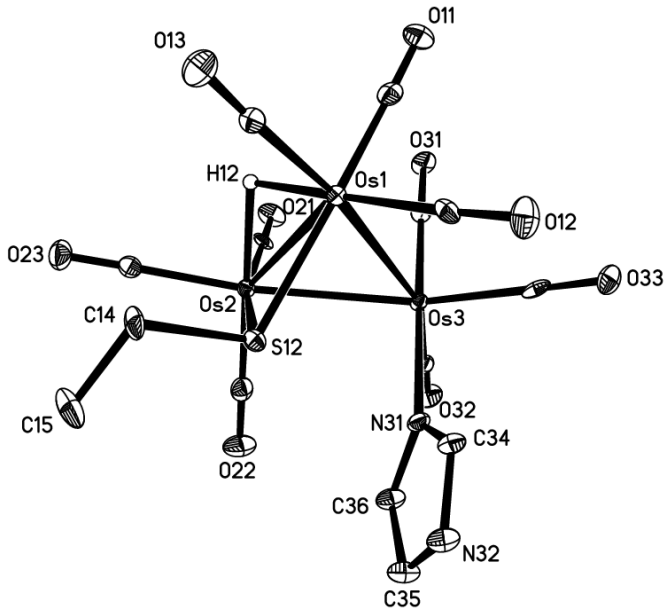

Figure 3.13 ORTEP diagram of **8**. Hydrogen atoms were removed (except hydride) for clarity. Selected bond parameters (Å): Os-Os = 2.8489 (3) – 2.8641(3), Os-C = 1.882(5) – 1.935(5), Os-N = 2.181(4), Os(1)-S(12) = 2.4164 (12), Os(2)-S(12) = 2.4095(12).

The reaction did not proceed when imidazole was replaced with pyridine (Scheme 3.5c). This indicated that the role of imidazole was deprotonation of the thiol to a thiolate. That the maltolato ligand was displaced may also lend support to our earlier hypothesis (chapter 2) that the cytotoxicity of **5** could be partly attributed to displacement of the maltolato ligand which can react with metal ions in the body to form ROS species.[13] However, more studies have to be undertaken to confirm this hypothesis.

In contrast to **1'**, cluster **5** failed to react with ethanoic acid both in the absence and presence of imidazole.

3.2.4 Interaction of 5 with MDA-MB-231 breast cancer cells

The NMR spectrum of MDA-MB-231 breast cancer cells incubated with 40 μM of **5** is shown in Figure 3.14.

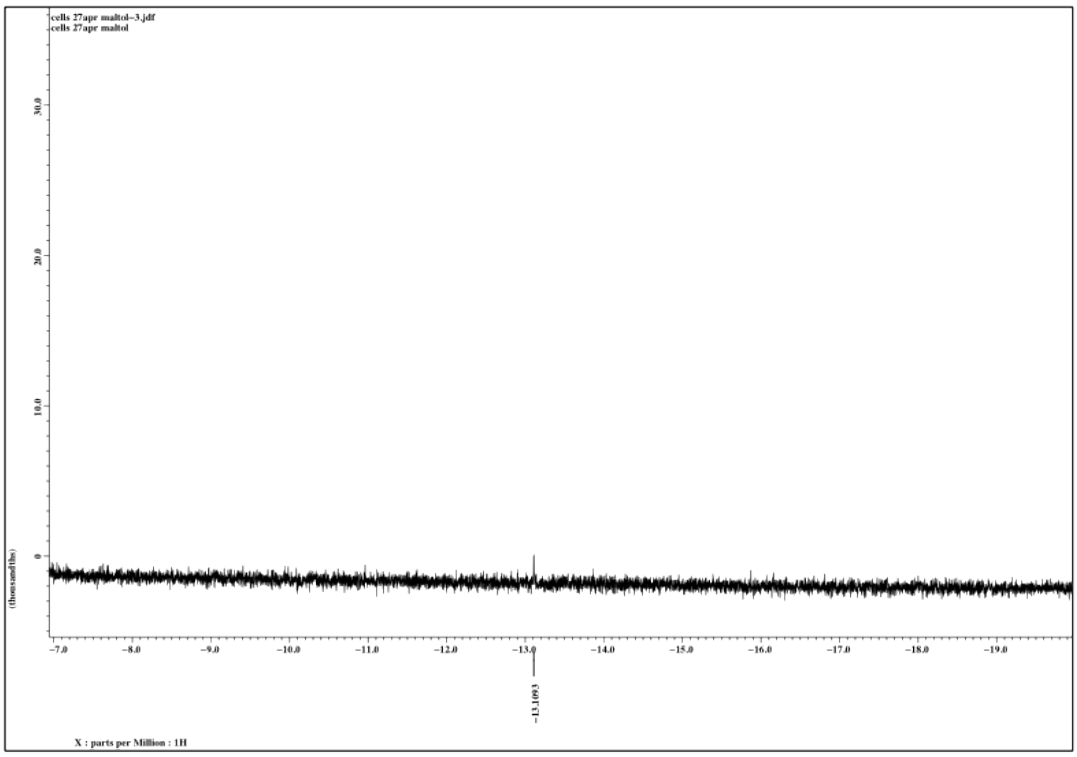

Figure 3.14 NMR spectrum of MDA-MB-231 breast cancer cells incubated with 40 μM of **5**. The spectrum focused on the hydride region only.

Only one hydride signal at -13.1 ppm was observed for the interaction of MDA-MB-231 cells with **5**, indicative of clusters of the type $Os_3(CO)_{10}(\mu\text{-H})(\mu\text{-OR})$. It has been verified that **5** failed to react with phenol even in the presence of imidazole (Experimental 3.4.11). While the chemical reactivity studies above showed that sulfhydryl residues might be possible target, such osmium clusters were not found here. Despite several attempts, a spectrum with a better signal-to-noise ratio could not be obtained; it is therefore unclear at this point if the targets are the hydroxyl or sulfhydryl residues, given the low sensitivity of the NMR technique.

3.3 Concluding remarks

In this chapter, we have established that the osmium carbonyl clusters **1'** and **5** induced apoptosis, similar to the previously reported cluster **2**. The key step to trigger their reactivity is, however, found to be different; **1'** requires deprotonation, while **5** requires a stronger nucleophile.

Their likely targets of action were also found to be different from **2** – carboxylate residues were eliminated as the action target and a new possible target, hydroxyl residues, were recognized which requires further investigation.

3.4 Experimental

Reactivity studies were carried out in air and at 37 °C to mimic biological system. ^{1}H NMR spectra were recorded on a Jeol 400 NMR spectrometer as $CDCl_3$ solutions unless otherwise stated; chemical shifts reported were referenced against the residual proton signals of the solvent. IR spectra were recorded on a Bruker ALPHA FTIR spectrometer as DCM solutions unless otherwise stated. The starting material $Os_3(CO)_{12}$ was obtained from Oxkem Ltd; all other chemicals were purchased from other commercial sources and used as supplied.

Experimental cultures of MDA-MB-231 cell line was obtained from American Type Culture Collection (ATCC) and cultured in tissue culture dishes (Nunc Inc., Naperville, IL, USA). The cells were maintained in Dulbecco's modified Eagle's medium (DMEM, Grand Island, NY, USA) supplemented with 10% fetal bovine serum (FBS), 1% L-glutamine (GIBCO Laboratories), and 1% penicillin (GIBCO Laboratories) at 37 °C in 5% CO_2 atmosphere. Phosphate-buffered saline (PBS) was obtained from GIBCO.

3.4.1 Reaction of 1' with ethanethiol and imidazole

To the solution of **1'** (20 mg, 0.022 mmol) in DCM (5 mL), ethanethiol (2.6mg, 0.022 mmol) was added. It was allowed to stir at 37 °C for 1 h; the IR spectrum showed that no reaction has occurred. Imidazole (2.3 mg, 0.022 mmol) was then added and the reaction was monitored by IR spectroscopy. The reaction mixture was then evacuated to dryness and purified by TLC using DCM:Hex (3:2, v/v) as the eluant.

IR: ν_{CO} 2109 (w), 2067 (vs), 2058 (s), 2022 (vs), 1998 (m) cm $^{-1}$.

^{1}H NMR δ: 2.39 (q, 2H, CH_2, J = 7.32 Hz), 1.28 (t, 3H, CH_3, J = 7.32 Hz), -17.42 (s, 1H, Os*H*Os)

3.4.2 Reaction of 1' with imidazole, followed by the addition of ethanethiol

To the solution of **1'** (10 mg, 0.011 mmol) in ACN (5 mL), imidazole (1.5 mg, 0.022 mmol) was added and it was allowed to stir at 37 °C. Reaction was monitored by IR spectroscopy, and **1** was observed after 1h. Ethanethiol (2.6mg, 0.022 mmol) was then added, and the reaction was again monitored by IR spectroscopy.

IR of **1**: ν_{CO} 2106 (w), 2066 (m), 2052 (vs), 2040 (vs), 2008 (br, vs), 1980 (m)

Lit IR of **1**: ν_{CO} 2106 (w), 2052 (vs), 2040 (vs), 2021(m, sh) 2008 (vs), 1980 (m).[9]

IR: ν_{CO} 2109 (w), 2067 (vs), 2058 (s), 2022 (vs), 1998 (m) cm^{-1}.

3.4.3 Reaction of 1' with pyridine, followed by the addition of ethanethiol

To the solution of **1'** (10 mg, 0.011 mmol) in acetone (5 mL), pyridine (2.3 mg, 0.03 mmol) was added and it was allowed to stir at 37 °C. Reaction was monitored by IR spectroscopy, and **1c** was observed by IR spectroscopy. Ethanethiol (2.6mg, 0.022 mmol) was then added, and the reaction was again monitored by IR spectroscopy.

IR of **1c**: ν_{CO} 2104 (m), 2063 (vs), 2052 (vs), 2017 (vs), 2009 (s, sh), 1991 (s), 1967 (m), 1942 (w)

Lit IR of **1c**: ν_{CO} 2104 (m), 2063 (vs), 2052 (vs), 2017 (vs), 2009 (s, sh), 1991 (s), 1967 (m), 1942 (w).[9]

IR: ν_{CO} 2109 (w), 2067 (vs), 2058 (s), 2022 (vs), 1998 (m) cm^{-1}.

3.4.4 Reaction of 1 with ethanethiol

To the solution of **1** (20 mg, 0.022 mmol) in DCM (5 mL), ethanethiol (2.6mg, 0.022 mmol) was added and it was allowed to stir at 37 °C for 1 h. The reaction mixture was then evacuated to dryness and purified by Thin Layer Chromatography using DCM:Hex (3:2, v/v) as the eluant.

IR: $_{CO}$ 2109 (w), 2067 (vs), 2058 (s), 2022 (vs), 1998 (m) cm^{-1}.

^{1}H NMR δ: 2.39 (q, 2H, CH_2, J = 7.32 Hz), 1.28 (t, 3H, CH_3, J = 7.32 Hz), -17.42 (s, 1H, Os*H*Os)

3.4.5 Reaction of 1' with ethanoic acid

To the solution of **1'** (15 mg, 0.016 mmol) in acetone (2 ml), ethanoic acid (1.9 mg, 0.032 mmol) was added, and it was allowed to stir at 37 °C. The reaction was monitored by IR spectroscopy. After 24

h, no reaction was observed, and imidazole (2.18 mg, 0.032 mmol) was added. The reaction was again monitored by IR spectroscopy. The reaction mixture was then evacuated to dryness and purified by Thin Layer Chromatography using DCM:Hex (3:2, v/v) as the eluant.

IR: ν_{CO} 2104 (w), 2049 (s), 2033 (s), 2007 (s), 1972 (m)

^{1}H NMR δ: 7.75 (s, 1H), 7.12 (s, 1H), 6.91 (s, 1H)

3.4.6 Reaction of 1 with ethanoic acid and imidazole

To the solution of **1** (15 mg, 0.016 mmol) in DCM (2 ml), ethanoic acid (1 mg, 0.017 mmol) and imidazole (1.2 mg, 0.017 mmol) was added, and it was allowed to stir at 37 °C. The reaction was monitored by IR spectroscopy. The IR spectrum only shows the formation of **1d**.

IR: ν_{CO} 2104 (w), 2049 (s), 2033 (s), 2007 (s), 1972 (m)

3.4.7 Reaction of 1' with phenol and imidazole

To the solution of **1'** (15 mg, 0.016 mmol) in acetone (2 ml), phenol (3.1 mg, 0.032 mmol) and imidazole (2.2 mg, 0.032 mmol) was added, and it was allowed to stir at 37 °C. The reaction was monitored by IR spectroscopy. The IR spectrum only shows the formation of **1d** even after stirring overnight.

IR: ν_{CO} 2104 (w), 2049 (s), 2033 (s), 2007 (s), 1972 (m)

3.4.8 Reaction of 5 with ethanethiol and imidazole

To the solution of **5** (34 mg, 0.036 mmol) in DCM (5 mL), ethanethiol (2.7 mg, 0.043 mmol) was added and it was allowed to stir at 37 °C overnight; no reaction occurred. Imidazole (2.9 mg, 0.043 mmol) was then added and the reaction was allowed to continue overnight. The reaction mixture was then evacuated to dryness and purified by TLC using DCM:Hex (3:2, v/v) as the eluant.

IR: ν_{CO} 2077 (w), 2045 (vs), 2019 (s), 1987 (m), 1972 (m), 1947 (vw)

^{1}H NMR (d_6-acetone) δ: 8.00 (s, 1H, im), 7.21 (s, 1H, im), 7.19 (s, 1H, im), 2.34 (q, 2H, 7.36 Hz, SCH_2CH_3), 0.99 (t, 3H, 7.36 Hz, SCH_2CH_3), -16.3 (s, 1H, Os*H*Os).

3.4.9 Reaction of 5 with ethanethiol and pyridine

To the solution of **5** (6.8 mg, 0.007 mmol) in DCM (5 mL), pyridine (1.1 mg, 0.014 mmol) was added and it was allowed to stir at 37 °C overnight; no reaction occurred. Ethanethiol (0.87 mg, 0.014 mmol) was then added and the reaction was allowed to continue overnight; no reaction was observed by IR spectroscopy.

3.4.10 Reaction of 5 with ethanoic acid

To the solution of **5** (10 mg, 0.011 mmol) in DCM (5 mL), ethanoic acid (1.3 mg, 0.022 mmol) was added and it was allowed to stir at 37 °C overnight; no reaction occurred. Imidazole (1.5 mg, 0.022 mmol) was then added and the reaction was allowed to continue overnight; no reaction was observed by IR spectroscopy.

3.4.11 Reaction of 5 with phenol

To the solution of **5** (10 mg, 0.011 mmol) in DCM (5 mL), phenol (1.3 mg, 0.022 mmol) was added and it was allowed to stir at 37 °C overnight; no reaction occurred. Imidazole (1.5 mg, 0.022 mmol) was then added and the reaction was allowed to continue overnight; no reaction was observed by IR spectroscopy.

3.4.12 NMR spectroscopy of cells treated with 1' or 5

MDA-MB-231 cells were first grown in ten 100-mm^2 dishes with DMEM supplemented with fetal bovine serum (10%), L-glutamine (1%) and penicillin (1%) until confluence. They were then serum starved for 15 h, before treatment with **1'** or **5** (40 μM, in DMEM without FBS) for 4 h and 2 h respectively, to induce apoptosis, as monitored through the microscope. The treated cells were then trypsinized and centrifuged (200 *g*, 5 min) to obtain a pellet. The pellet was washed with PBS (3X, 10 ml, 200 *g*, 5 min) and re-suspended in acetone (10 ml). The cells were then lysed by sonication in a water bath for 30 – 60 min. The acetone portion was evacuated to dryness, and ^{1}H NMR spectroscopy was then carried out in *d*-acetone.

3.4.13 Annexin V FITC and PI staining for flow cytometry

MDA-MB-231 cells were plated in T25' flasks at the same initial density, and allowed to adhere and grow for 24 h. They were then serum starved for 24 h before treatment with **1'** and **5** (10 μM and 3 μM respectively). The cells were harvested after the incubation period (15 h) and washed in cold PBS (5 mL). The washed cells were centrifuged to obtain a pellet, the supernatant discarded, and the pelleted cells were washed twice with PBS (2 x 5 mL) before re-suspension in 1X Annexin-Binding Buffer (Invitrogen). FITC annexin V (5 μL) and PI (1 μL) stains were then added and the stained cells were analyzed using the flow cytometer (BD FACSCalibur for **1'** and Fortessa X20 for **5**).

3.4.14 DNA fragmentation using PI

MDA-MB-231 cells were plated in T25' flasks at the same initial density, and allowed to adhere and grow for 24 h. They were then serum starved for 24 h before treatment with treatment with **1'** and **5** (10 μM and 4 μM respectively) for 15 h. After treatment, the cells were fixed with 70% ethanol (2 mL, -20 °C, overnight). They were then centrifuged (200 x g, 5 min), suspended in PBS (0.8 ml) and centrifuged again (300 x g, 5 min). The cell pellet was then suspended in PBS (0.25 mL), DNA extraction buffer (0.5 mL) added and then incubated for 5 min at room temperature to facilitate the extraction of low molecular weight DNA. The cells were then centrifuged, PI solution containing DNA free RNase (0.4 mL) added, and incubated at room temperature in the dark for 30 min. The stained cells were then analyzed using a flow cytometer (BD FACSCalibur for **1'** and Fortessa X20 for **5**).

3.4.15 Nuclear staining with DAPI

MDA-MB-231 cells were plated in single-well plates (Ibidi) at the same initial density, and allowed to adhere and grow for 24 h. They were then serum starved for 24 h before treatment with 5 μM of **1'** for 3 h. After treatment, the cells were fixed with 3.7% formalin (RT, 1h), washed with PBS (2 mL), stained with 4,6-diamidino-2-phenylindole (DAPI, 1μg/mL in PBS, 5 min at 37 °C), washed, and then photographed using a confocal microscope equipped with a UV light filter (Nikon D Eclipse C1).

3.4.16 X-ray crystal determination

Yellow needles were grown by slow cooling of a DCM/ hexane solution at 4 °C. The crystals chosen were mounted on a quartz fiber. X-ray diffraction data were collected on a Bruker X8 APEX Single-Crystal X-ray Diffractometer at 103(2) K, using Mo Kα radiation, with the SMART program.[14] Reflections data was processed and corrected for Lorentz and polarization effects with SAINT,[15] and for absorption effects with SADABS.[16] The structure was solved by direct methods, and subsequent difference maps were used for locating the rest of the non-hydrogen atoms to complete the structure. Hydrogen atoms were placed in calculated positions and refined with a riding model. In the final model, all non-hydrogen atoms were given anisotropic displacement parameters. Appropriate restraints were placed on all disordered parts. Structural solution and refinement were carried out using the SHELXTL suite of programs.[17]

3.5 References

1 a) K.V. Kong, W.K. Leong, S. P. Ng, T. H. Nguyen, L.H.K. Lim. *ChemMedChem.* **2008**, *3*, 1269; b) K.V. Kong, W.K. Leong, L.H.K. Lim. *J. Organomet. Chem*. **2009**, *694*, 834.

2 Z. Lam, *personal communication*.

3 I. C. Vermes, C. Haanen, J. Reutelingsperger*. Immunol. Methods.* **2000**, *243*, 167.

4 J. O. Edwards, R. G. Pearson, *J. Am. Chem. Soc,* **1963**, *84*, 16.

5 S. P. Tunik, *Russian Chemical Bulletin, International Edition,* **2004**, *53*, 2657.

6 a) R. Persson, M. J. Stchedroff, R. Gobetto, C. J. Carrano, M. G. Richmond, M. Monari, E. Nordlander, *Eur. J. Inorg. Chem.* **2013**, *13*, 2447; b) H. G. Ang, S. G. Ang, Q. Zhang, *J. Chem. Soc., Dalton Trans.* **1996**, 2778.

7 a) S. M. Lee, *Journal of Cluster Science,* **1996**, *7*, 435; b) N. K. Kiriakidou-Kazemifar, E. Kretzschmar, H. Carlsson, M. Monari, S. Selva, E. Nordlander, *J. Organomet. Chem.* **2001**, *623*, 191; c) M. Monari, R. Pfeiffer, U. Rudsander, E. Nordlander, *Inorganica Chimica Acta*, **1996**, *247*, 131; d) C. Li, W. K. Leong, *J. Organomet. Chem.* **2008**, *693*, 1292.

8 a) A. J. Amoroso, B. F. G. Johnson, J. Lewis, C-K. Li, M. C. Ramirez de Arellano, P. R. Raithby, G. P. Shields, W-T. Wong, *Inorganica Chimica Acta*, **2006**, *359*, 3589; b) R. Ganguly, W. K. Leong, *Organometallics,* **2011**, *30*, 3966; c) E. W. Ainscough, A. M. Brodie, R. K. Richard, B. A. Coombridge, J. M. Waters, *J. Organomet. Chem.* **1998**, *556*, 197.

9 B.F.G. Johnson, J. Lewis, D. A. Pippard, *J. Chem.Soc., Dalton Trans.* **1981**, 407.

10 (a) E.W. Ainscough, A.M. Brodie, R. K. Coll, A. J. A. Mair, J. M. Waters, *J. Organomet Chem*. **1996**, *509*, 259. (b) C. E. Anson, E. J. Ditzel, M. Fajardo, H. D. Holden, B. F. G. Johnson, J. Lewis, J. Puga, P. R. Raithby, *J. Chem. Soc., Dalton Trans*. **1984**, 2723.

11 a) Y. Okada, E. Maeno, T. Shimizu, K. Manabe, S. Mori, T. Nabekura, *Plugers Arch*, **2004***, 448*, 287; b) G. Heimlich, JA. Cidlowski*, J. Biol. Chem.* **2006**, *281*, 2232; c) Y. Okada, T. Shimizu, E. Maeno, S. Tanabe, X. Wang, N. Takahashi, *J. Membr. Biol.* **2006**, *209*, 21.

12 S. M. Lee, K. K. Cheung, W. T. Wong, *J. Cluster Sci.* **1996**, *7*, 435.

13 a) M. Hironishi, R. Kordek, R. Yanagihara, RM. Garuto, *Neurodegeneration*. **1996**, *5*, 325; b) K. Murakami, K. Ishida, K. Watakabe, R. Tsubouchi, M. Haneda, M. Yoshino, *Biometals*. **2006**, *19*, 253; c) K. Murakami, K. Ishida, K. Watakabe, R. Tsubouchi, M. Naruse, M. Yoshino, *Toxicol Lett*, **2006**, *161*, 102; d) S, Amatori, G. Ambrois, M. Fanelli, M. Formica, V. Fusi, L. Giorgi, E. Macedi, M. Micheloni, P. Paoli, R. Pontellini, P. Rossi, *J. Org. Chem*. **2012**, *77*, 2207; e) S. Amatori, I. Bagaloni, E. Macedi, M. Formica, L. Giorgi, V. Fusi, M. Fanelli, *Br. J. Cancer*. **2010**, *103*, 239.

14 SMART, version 5.628 ed., Bruker AXS Inc., Madison, WI, **2001**.

15 SAINT+, version 6.22a ed., Bruker AXS Inc., Madison, WI, **2001**.

16 G. M. Sheldrick, SADABS, **1996**.

17 SHELXTL, version 5.1 ed., Bruker AXS Inc., Madison, WI, **1997**.

Chapter 4. Osmium-based Tamoxifens

As mentioned in chapter 1, there are two main strategies in the design of organometallic anticancer drugs - ones which are active by virtue of the metal centre, and those which make use of the metal complex as a structural scaffold for a molecule moiety that is known to be active. A prime example of the second approach is the work of Jaouen and co-workers; they enhanced the activity of the known anti-cancer drug tamoxifen with a ferrocenyl substituent - these compounds have been named ferrocifens.

Three important analogues of the ferrocifen series – the ferrociphenol **10a**, ferrocidiphenol **10b** and hydroxyferrocifen **10c** - are shown in Figure 4.1.

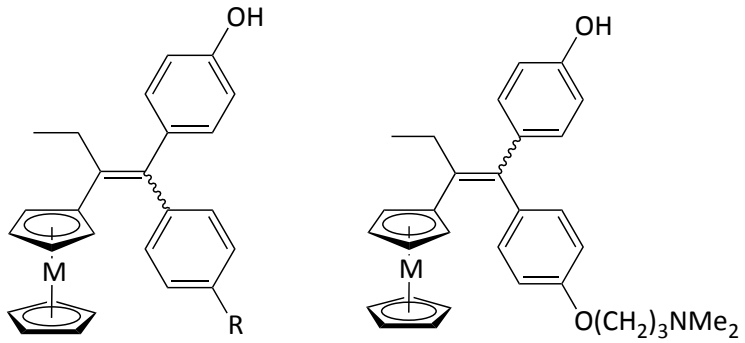

M = Fe, R = H, **10a**
M = Fe, R = OH, **10b**
M = Ru, R = H, **11a**
M = Ru, R = OH, **11b**
M = Os, R = H, **12a**
M = Os, R = OH, **12b**

M = Fe, **10c**
M = Ru, **11c**
M = Os, **12c**

Figure 4.1 Chemical structures of the metallocifens.

The ferrocifens exhibit high antiproliferative activity against both ER+ and ER- breast cancer cells (IC_{50} ~ 0.5 – 1 μM) while Tamoxifen is not active against the ER- breast cancer cells.[1,2,3,4,5] While the tamoxifen act as an antagonist onto the estrogen receptor (anti-hormone effect), the ferrocifens were found to possess an additional cytotoxic effect – the generation of reactive quinones via ferrocene-modulated phenol oxidation, causing ROS production.[6,7,8,9,10] It has already been found that the ruthenium analogues of the hydroxyferrocifen **11c**, did not show any antiproliferative

effects on MDA-MB-231, an ER- breast cancer cell line, at 1 µM concentration.[11] On the other hand, the diphenol ruthenium derivative **11b** showed a proliferative effect on MCF-7 cells at the same concentration.[12] This result indicates that the metal plays an important role in the activity of these complexes. Therefore, it would be interesting to extend the investigations to the osmium analogues. The osmium analogues of the three ferrocifens **10a**, **10b** and **10c**, named osmociphenol **12a**, osmocidiphenol **12b** and hydroxyosmocifen **12c**, respectively, were thus synthesized (Figure 4.1).

4.1 Syntheses of osmium based tamoxifens (osmocifens)

The synthetic routes to the osmocifens **12a**-**c** are shown in Scheme 4.1.

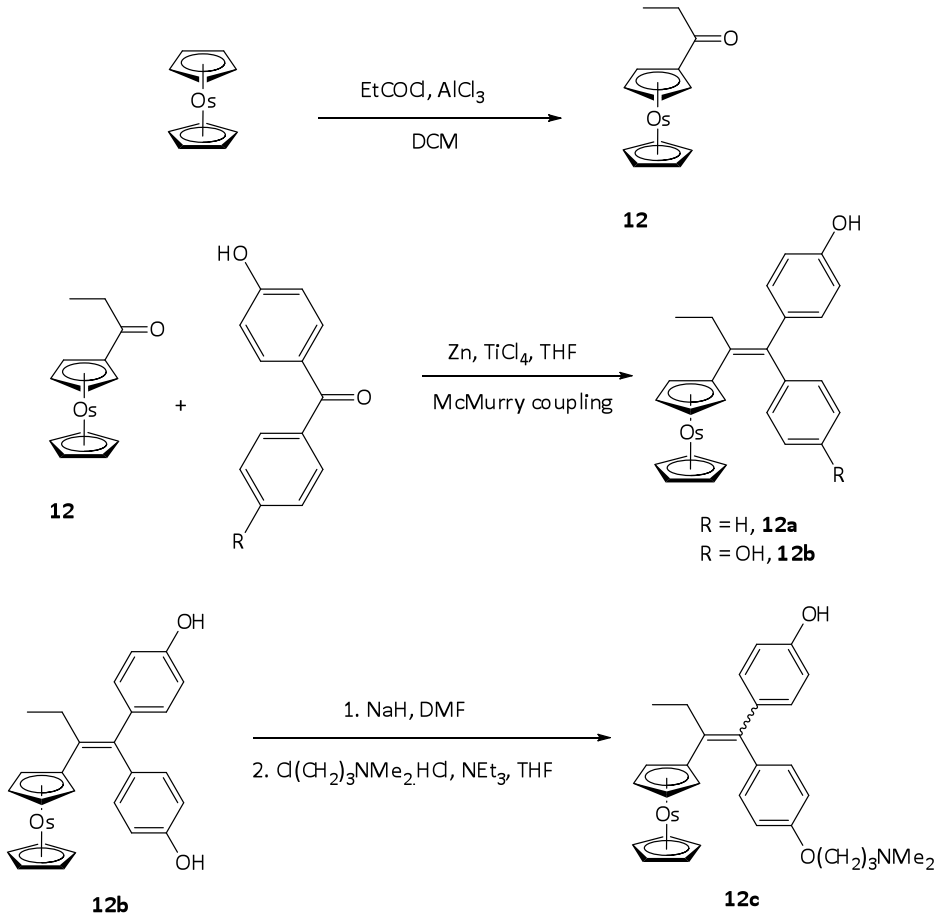

Scheme 4.1. Syntheses of osmocifens **12a** to **12c**.

The first step involved the Friedel-Crafts acylation of osmocene to yield propionyl osmocene **12**. It was found that the ease of acylation decreased down the triad, i.e., acylation using phosphoric acid sufficed for ferrocene, ruthenocene required a strong acylating agent such as $AlCl_3$ at room

temperature, and osmocene required heating with $AlCl_3$. Nevertheless, despite it being less reactive, double acylation could also occur for osmocene. Hence, the reaction time was kept short, as any unreacted osmocene could be readily recovered. The isolated yield of **12** was in the range of 40 – 50%, with almost all of the unreacted osmocene recovered after purification by column chromatography.

The next step was a McMurry coupling (reaction of two carbonyls to form a new double bond) of **12** with 4-hydroxybenzophenone or 4,4'-dihydroxybenzophenone, to give **12a** and **12b**, respectively, in ~73% yields for both compounds. Since **12** could also self-couple, an excess (1.5 equivalents) of the organic carbonyl was used in order to reduce the homo-coupling of **12**. Alkylation of **12b** with chloroethyldimethylamine afforded **12c** in 36% yield; the reaction was similarly halted once formation of the dialkylated product was observed, and any unreacted **12b** was recovered by column chromatography.

All of the compounds **12a-c** have been characterized spectroscopically and analytically, including X-ray crystallographic studies for **12a** and **12b**. The ORTEP diagrams for **12a** and **12b**, together with selected bond parameters, are given in figures 4.2 and 4.3, respectively.

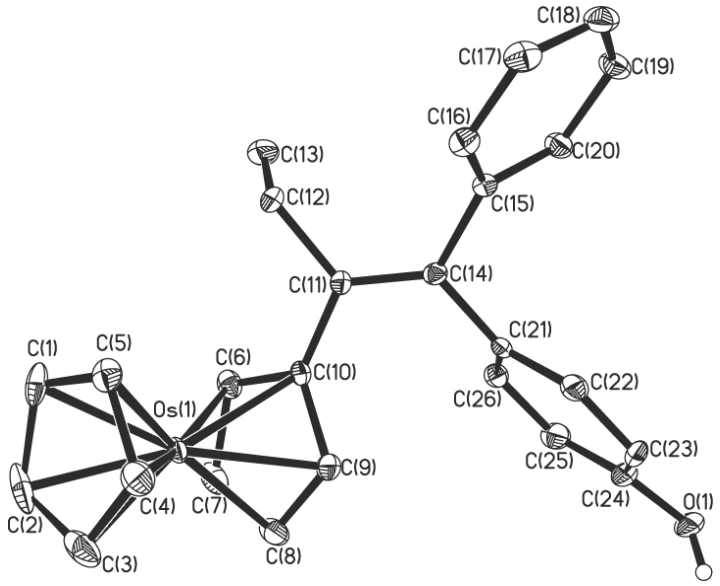

Figure 4.2. ORTEP plot of **12a**. Only one stereoisomer shown. Hydrogen atoms have been omitted for clarity (except for OH).

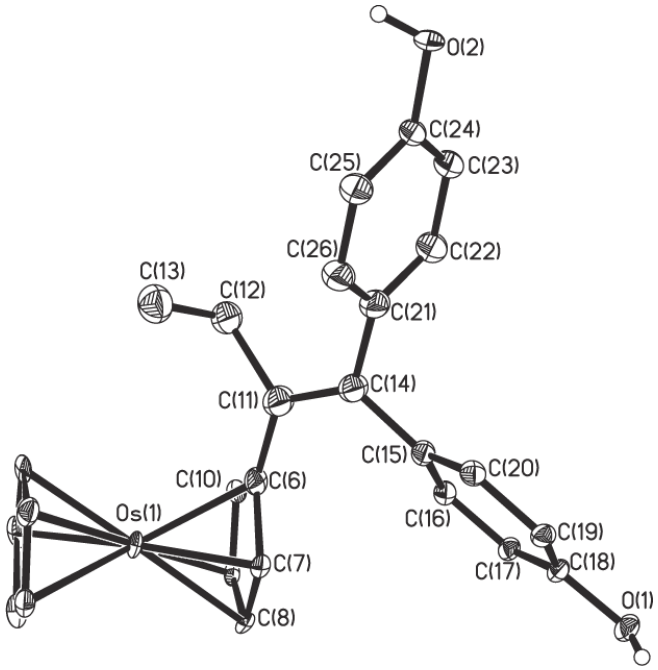

Figure 4.3. ORTEP plot of **12b**. Hydrogen atoms have been omitted for clarity (except for OH).

As in the case of the ruthenocenes,[11] the osmocenes **12a** and **12c** also existed in solutions as rapidly interconverting, 50/50 mixtures of the E and Z isomers. With **12a**, this was also manifested in the solid-state, as disorder of the OH group over both phenyl rings. No attempts were made to separate the E and Z isomers for the subsequent bioassays.

4.2 Antiproliferative activities of the metallocifens 10a – 12c.

To determine if the metal played a role in the antiproliferative activity of the ferrocifens, cell viability assays against the ER+ breast cancer MCF-7 cells and ER- breast cancer MDA-MB-231 cells were conducted on the three series of group 8 metallocifens **10a** – **12c**. Their IC_{50} values are shown in Table 4.1.

In contrast to the ferrocifens **10a-c**, which were all active against both the breast cancer cell lines, only the hydroxymetallocifen analogues of ruthenium and osmium (**11c** and **12c**, respectively) were active on both cell lines; the order of activity was **10c** > **11c** ≈ **12c**. On the other hand, the phenol and diphenol analogues of Ru and Os, *viz.*, **11b**, **11c**, **12b** and **12c**, were less active (IC_{50} values

~30 μM). Overall, the antiproliferative activity of all compounds were higher on MDA-MB-231 cells than on MCF-7 cells. This can be explained by a moderate estrogenic effect of the compounds on estrogen dependent MCF-7 breast cancer cells at low concentrations,[3,7] and is supported by the observation that the phenol derivatives of ruthenium and osmium exhibited proliferative effects at low concentrations, similar to estradiol (E2) (Figure 4.4).

Table 4.1. IC_{50} values of the metallocifens against the breast cancer cells (MDA-MB-231 and MCF-7)

Compound	R_1	R_2	IC_{50} (μM)	
			MDA-MB-231	MCF-7
10a (Fe)	H	OH	1.13 ± 0.07 [a]	2.4 ± 0.1
10b (Fe)	OH	OH	0.64 ± 0.06 [b], 0.60 ± 0.01 [d]	0.7 [c], 0.8 ± 0.20 [d]
10c (Fe)	OH	$O(CH_2)_3NMe_2$	0.5 [g]	0.8 ± 0.20
11a (Ru)	H	OH	29.7 ± 0.8	≈ 30
11b (Ru)	OH	OH	27 ± 1	≈ 30
11c (Ru)	OH	$O(CH_2)_3NMe_2$	1.99 ± 0.03	2.4 ± 0.2
12a (Os)	H	OH	33 ± 1	>30
12b (Os)	OH	OH	29 ± 2	>30
12c (Os)	OH	$O(CH_2)_3NMe_2$	2.7 ± 0.3	2.90 ± 0.05

[a] data from ref [2]. [b] data from ref [13]. [c] data from ref [12]. [d] IC_{50} obtained in this study.

Such an estrogenic interaction is an on-off effect, and increasing the concentration (from 1 μM to 10 μM) does not give any significant change in the cell viability, but at a very high concentration

of 30 µM, this estrogenic property is displaced and the compounds become cytotoxic. Due to this competition between estrogenic and cytotoxic effects, the IC_{50} values of the Ru and Os analogues on MCF-7 cannot be accurately determined, but it may be inferred from Figure 4.4 that they are in the 30 – 40 µM range, and that the antiproliferative effects of the two analogues are almost the same. The hydroxymetallocifens **11c** and **12c** are, on the other hand, highly cytotoxic (IC_{50} of 2.36 µM and 2.90 µM, respectively) to the MCF-7 cells.

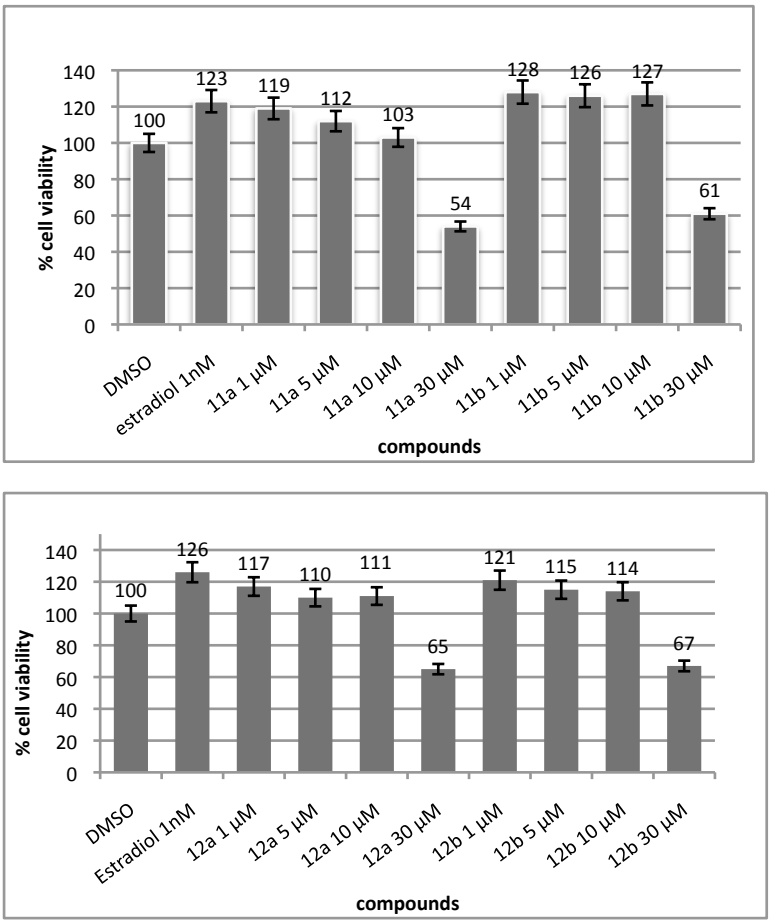

Figure 4.4. Effect of 1 – 30 µM of the monophenol and diphenol complexes of (top) Ru, and (bottom) Os, on the growth of MCF -7 cells after 5 days of incubation.

The fact that there is a big difference in activity among the different metal diphenol analogues (**10b** being active, while **11b** and **12b** were inactive) indicates that the metal plays a strong role in its antiproliferative activity. It has been shown earlier that the ferrociphenols act through the prevention of cell division or senescence instead of apoptosis.[14] Senescence-associated β-

galactosidase (SA-β-gal) assessment were thus performed on the rest of the metallocifens to test whether the osmium and ruthenium analogues induces senescence as well at two concentrations (IC_{50} concentration and 4 μM), and the results are shown in Figure 4.5.

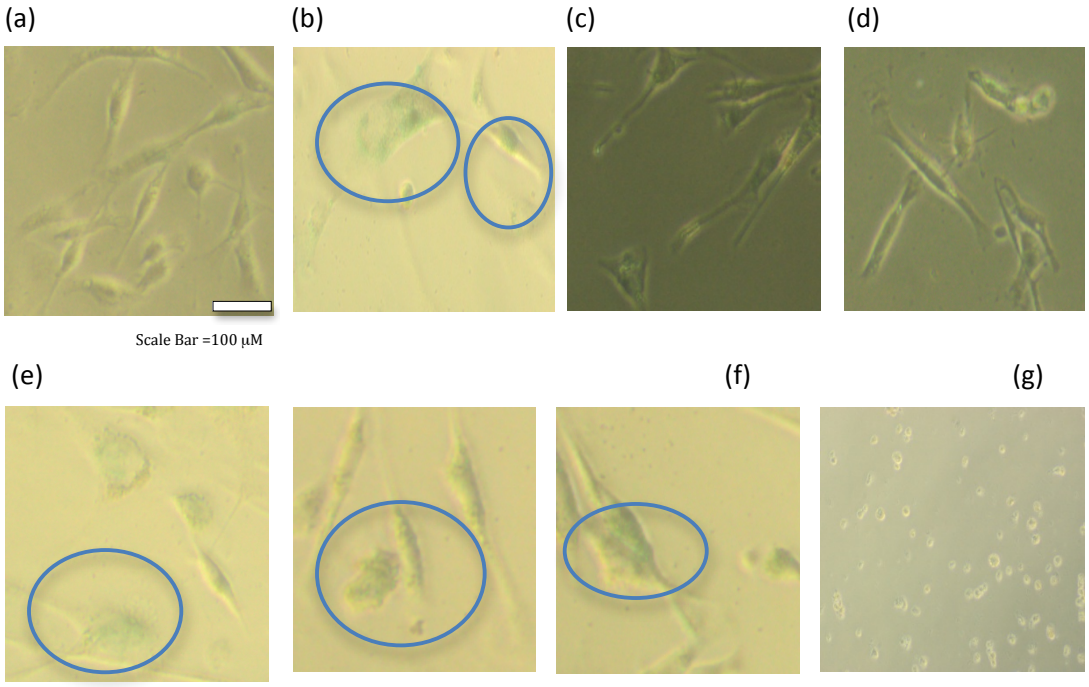

Figure 4.5. MDA-MB-231 cells stained with X-gal incubated with (a) DMSO (control), (b) **10b** (0.5 μM), (c) **11b** (4 μM) (d) **12b** (4 μM), (e) **10c** (0.5 μM), (f) **11c** (2 μM), (g) **12c** (3 μM), (h) **11c** (4 μM). Examples of senescent cells are circled in blue.

The SA-β-gal assay is based on the increase in lysosomal β-galactosidase level in senescent cells. It is a cytochemical assay in which X-gal, a chromogenic substrate, is cleaved by β-galactosidase to form a blue precipitate. Figure 4.5 indicates while **10b** induces senescence (stained blue), **11b** and **12b** do not show senescence associated β-galactosidase staining up to 4 μM and this is in agreement with their antiproliferative activity. Surprisingly, while the metallocifens series **10c**-**12c** showed senescence at low concentration of 1 μM, cells do not stain blue when incubated at higher concentration of 4 μM, but became rounded in shape (Figure 4.5h). This behaviour has also been observed previously for **10c**[15,16] and on hydroxytamoxifen, but at a higher concentration of 5-10

μM. This infers that the cytotoxicity of the tamoxifen analogues of **10-12c** comes from two effects, the effect of the amine chain like that of hydroxytamoxifen and the effect of the metallocene. However, the effect of the metallocene appears to be much stronger for the Fe than the Ru and Os, as inferred from their IC_{50} values (0.6 μM for **10c**, 1.99 μM for **11c** and 2.7 μM for **12c**). Finally, this also indicates that the phenol analogues and the amine chain analogues might have different mechanisms of action.

4.3 Investigating the difference in antiproliferative activity among the three metallocifens

The difference in activity among the different metallocifens strongly indicates that the metal plays an important role in its activity. Their physical properties, as well as chemical reactivity, were therefore investigated in order to gain a better understanding of the difference in antiproliferative activity among the three metallocifens analogues.

4.3.1 Physical properties - structural differences

Selected structural parameters of **12a**, **12b** and those of the ferrocenyl analogue **10c** reported earlier,[5] are tabulated in Table 4.2.

Table 4.2. Selected bond distances and angles of osmocifens 12a, 12b and ferrocifen 10c

Parameter	**10c** (Fe)[5]	**12a** (Os)	**12b** (Os)
M-C_{cp} (Å)	2.04	2.18-2.20	2.17-2.22
C1-C2 (Å)	1.36	1.35	1.33
C1-C2-C4 (°)	125	125	123
C1-C2-C6 (°)	121	122	123
C3-C1-C2 (°)	119	123	127
C5-C1-C2 (°)	126	121	123

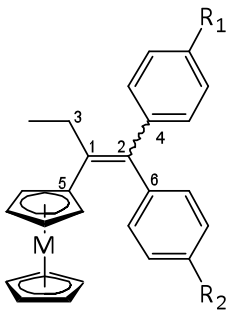

M = Fe, R_1 = OH, R_2 = $O(CH_2)_3NMe_2$, **10c**
M = Os, R_1 = H, R_2 = OH, **12a**
M = Os, R_1 = OH, R_2 = OH **12b**

The three complexes are similar in structure; there is no significant difference in the length of the alkenic C=C bond (1.35, 1.33 and 1.36 Å for **12a**, **12b** and **10c**, respectively, compared with 1.33

Å in tamoxifen), and they have similar angles (121 – 125°) between that double bond and the phenyl substituents (Table 4.2). There are, however, slight differences in bond parameters associated with the metallocenyls. For instance, the Cp-C=C (C5-C1-C2) and Et-C=C (C3-C1-C2) angles show trends consistent with the increase in atomic size from Fe to Os; the former decreases from 126° in **10c** to 121° and 123° for **12a** and **12b**, respectively, while the latter increases from 119° in **10c** to 123° and 127° for **12a** and **12b**, respectively. Similarly, the average metallocenyl ring carbon to metal distances are 2.04 and 2.20 Å, for Fe and Os, respectively. These lead to less steric interaction between the metallocenyl and the adjacent phenol in the osmocifens.

4.3.2 Physical properties – lipophilicity.

Lipophilicity (Log P), a measure of the difference in solubility of the compound in two immiscible solvents – 1-octanol and water – is often used to estimate 'drug likeness'. A 'good drug' has to be sufficiently water soluble to be transported in aqueous media like blood and intracellular fluid, yet lipophilic enough to penetrate the cell membrane. Based on Lipinski's Rule of 5, the ideal log P value should be less than 5.[17] The lipophilicities of the metallocifens **10a** to **12c** were determined, and shown in Table 4.3.

Table 4.3. Log $P_{o/w}$ values of the metallocifens 10a – 12c.

Compound	R_1	R_2	LogPo/w
10a (Fe)	H	OH	6.0 (Z), 6.3 (E) [a]
10b (Fe)	OH	OH	5.0 [b]
10c (Fe)	OH	$O(CH_2)_3NMe_2$	4.3 (Z), 4.5 (E) [c]
11a (Ru)	H	OH	6.6
11b (Ru)	OH	OH	5.4
11c (Ru)	OH	$O(CH_2)_3NMe_2$	4.8
12a (Os)	H	OH	6.3
12b	OH	OH	5.2

(Os)			
12c (Os)	OH	$O(CH_2)_3NMe_2$	4.3

[a] data from ref [2]. [b] data from ref [12]. [c] data from ref [5].

All of the compounds are more lipophilic (log $P_{o/w}$ values range of 4.3 - 6.6) than estradiol (log $P_{o/w}$ = 3.2), indicating that they can permeate the cell membrane better. However, only the hydroxymetallocifen analogues satisfy the Lipinski's Rule of 5. The lipophilicity decreases in the order: metallophenol > metallodiphenol > hydroxymetallocifen, which is the trend expected with the presence of an extra OH group and an amine chain, respectively. Addition of the metallocene significantly increases its lipophilicity (log $P_{o/w}$ of hydroxytamoxifen = 3.2 (Z)) and thus cell membrane permeability. However, within each series, there is no significant difference among the three metals, i.e., the different metal analogues have similar cell membrane permeability.

The above suggests that the metallocifens did not have significant differences in terms of their size and how well they enter the cells. Therefore, the difference in their activities has to do with their chemical reactivities. Their chemical properties were therefore investigated in the following sub sections.

4.3.3 Chemical reactivities – Redox properties

That the ferrocifens were active against the ER- breast cancer cells while tamoxifen was not, led to investigations on the role of the ferrocenyl group, in particular, its redox properties. It was then recognized that their cytotoxicities could be attributed to the generation of reactive quinone methides (QMs) via ferrocene-modulated phenol oxidation, and this pathway has been confirmed for several compounds in the phenol series.[18,19,20] The formation of these quinone methides can be monitored electrochemically (in the presence of a base to initiate proton abstraction after electrochemical oxidation) using cyclic voltammetry. In compounds with low or no cytotoxic effects in vitro, the cyclic voltammograms (CVs) showed little or no change. For the biologically active compounds, however, three major changes were observed: The loss of chemical reversibility, an increase in current for the first oxidation wave, and a new second oxidation wave. An example is

shown in Figure 4.6, and the mechanism which has been proposed to account for this is shown in Scheme 4.2. The mechanism was supported by cyclic voltammetry experiments as well as by an electrochemical synthesis and isolation of the quinone methide which was characterized by ^{1}H and ^{13}C NMR experiments. [27]

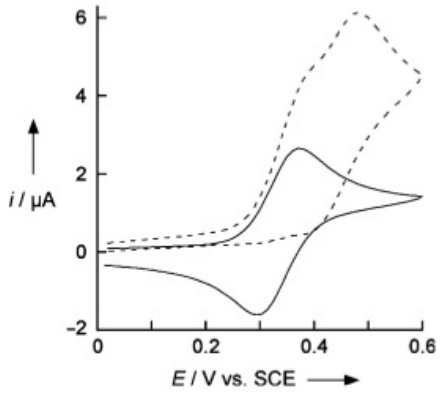

Figure 4.6 Cyclic voltammograms of **10b** (2 mM) in Bu_4NBF_4 (0.1 M, MeOH) in absence (solid line) and presence (dashed line) of pyridine in a 1:6 volume ratio. Scan rate 0.5 V/s. Pt electrode (0.5 mm diameter).[6]

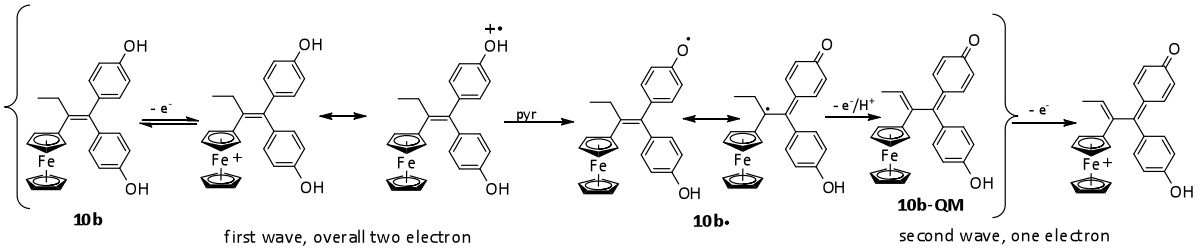

Scheme 4.2 Proposed mechanism for the formation of quinone methides electrochemically from ferrocenyl phenols.

The first oxidation wave is due to the first Fc/Fc^{+} couple, with delocalization of the electron into the phenol. This acidifies the phenolic proton, which is easily abstracted by pyridine. The resulting phenoxy radical species **10b•** is then oxidized at the same oxidation potential, thus giving a two-electron oxidation wave. Another proton abstraction following this second oxidation gives the quinone methide structure **10b-QM**. The third oxidation (second wave) is of **10b-QM**.

Redox properties of ruthenocene (background)

Many cyclic voltammetry studies have been carried out on ruthenocene, and it has been found to possess a two-electron, irreversible cyclic voltammogram.[21,22,23] Studies have shown that this was due to nucleophilic attack by the electrolyte anion (BF_4^-) or the solvent (acetonitrile) onto the strongly electrophilic ruthenocenium(III), to regain its 18-electron configuration, and could be prevented with the use of a bulky electrolyte/non coordinating solvent system.[24,25] This was also the case for compound **11a**.[26] Geiger and co-workers later showed that in a dry, non-donor solvent, and in the absence of nucleophiles, despite showing a reversible voltammogram, this highly reactive ruthenocenium ion actually did not reduce back to ruthenocene(II), but was in equilibrium with its dimer $[Ru_2Cp_4]^{2+}$.[25] It was also found that ruthenocenyl diphenyl (**Rc-diPh**), an analogue of **11a** but without any OH group, showed an chemically irreversible two-electron oxidation wave upon the addition of pyridine, which was speculated to be due to the oxidation of $(Cp_2Ru\text{-}Py)^+$ into $(Cp_2Ru\text{-}Py)^{2+}$ at the similar potential (Figure 4.7).[26]

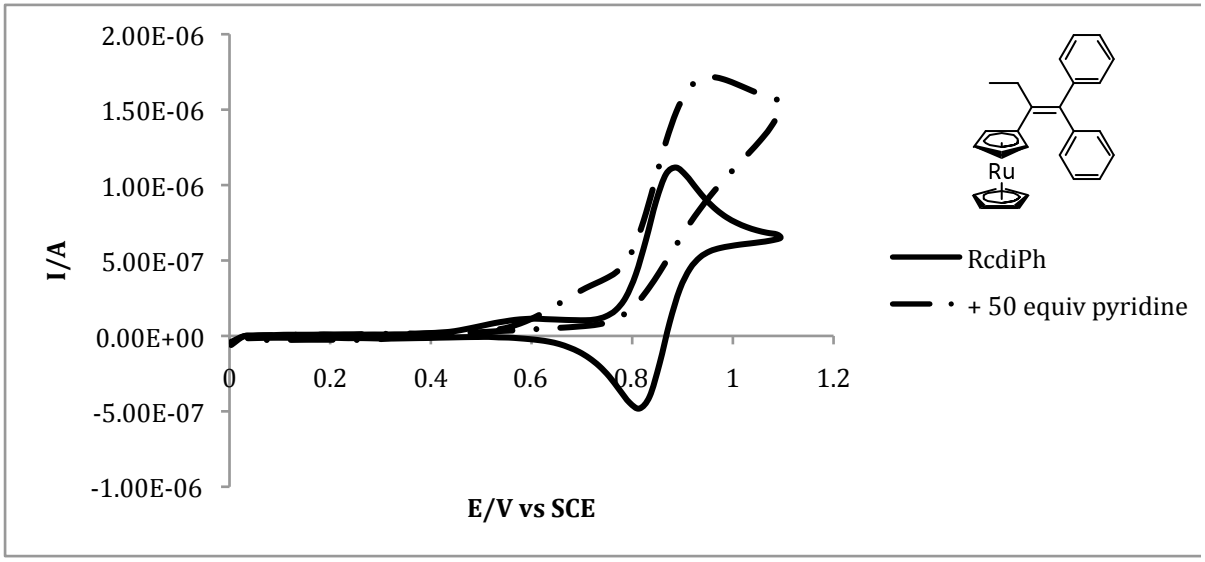

Figure 4.7 CV of **RcdiPh** (2 mM, solid line), and in the presence of 100 mM pyridine (dashed line). Conditions: DCM/[TBA][TFAB] (0.08 M); Pt electrode, 0.5 mm in diameter, scan rate 100 mV/s.

Redox properties of ruthenocifens

The redox properties of the ruthenocifens were investigated using ruthenociphenol **11a** using the bulky electrolyte/non-coordinating solvent system; its cyclic voltammogram of **11a** is shown in Figure 4.8.

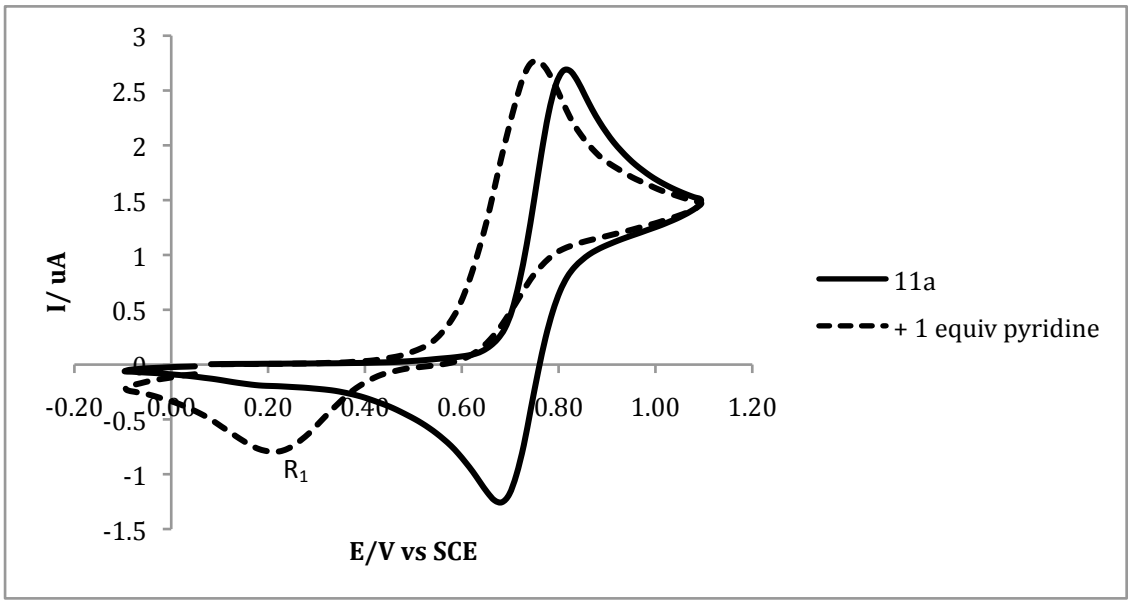

Figure 4.8 a) CV of **11a** (2 mM, solid line) and b) in the presence of 2 mM pyridine (dashed line). Conditions: DCM/[TBA][TFAB] (0.08 M); Pt electrode, 0.5 mm in diameter, scan rate 200 mV/s.

The cyclic votammogram of **11a** was reversible (Figure 4.8a), but became irreversible at high scan rates (> 5V/s, appendix A4.20). This is consistent with the dimerization that has been observed with ruthenocene.[25] That this is not due to isomerisation may be ruled out as both ferrocifens and ruthenocifens exist as E and Z isomers in solution, but for the ferrocifens where dimerization did not occur, the CV remained reversible even at high scan rates. The dimerization, although inevitable, could be reduced with the addition of a base, which could interact with the tamoxifen ligand in **11a+** to induce a pathway similar to that in the ferrociphenols and thus pulling back the dimerization equilibrium. The oxidation of **11a** became fully chemical irreversible upon addition of just one equivalent of pyridine (Figure 4.8b). That the oxidation wave intensity did not double indicated that nucleophilic attack of pyridine on **11a+** did not occur. That the oxidation wave was shifted towards a

less positive value could, by analogy with the ferrociphenol derivatives,[27] be ascribed to deprotonation of the hydroxyl group by pyridine to form the radical species **11a•** (Scheme 4.3).

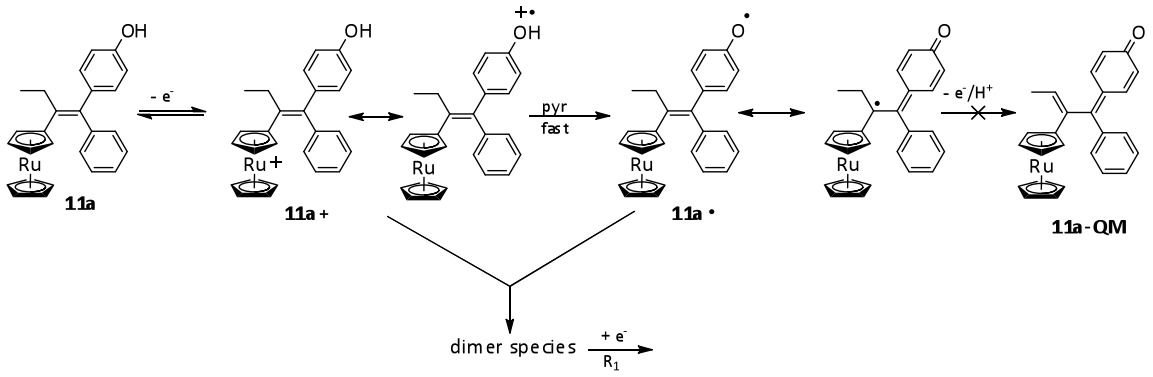

Scheme 4.3 Possible oxidation sequence for **11a**.

The absence of a doubling of the oxidation peak intensity also implied that the second oxidation to the quinone methide **11a-QM** did not occur. This suggests the occurrence of an unexpected follow-up process for **11a•**, which is speculated to be the reaction of **11a•** with **11a+**, producing a dimeric species that reduces at wave R_1 (Figure 4.8b). Dimerization of the radical with **11a+** is proposed instead of self-dimerization as: (i) it is consistent with the probable cationic species observed for ferrocifens in the same potential region,[27] and for $(Rc)_2^{2+}$,[25] and (ii) the high reactivity of the species towards pyridine suggests the presence of an acidic (phenolic) proton.

At a higher pyridine concentration (10 equivalents), a new oxidation wave O_1 (~ 1.1 V) was observed (Figure 4.9a). That this oxidation wave was due to the quinone methide was ruled out by the observation that the oxidation wave of an authentic sample of **11a-QM** did not occur at that oxidation potential (Figure 4.9b, dashed line). The oxidation wave of **11a-QM** in the presence of pyridine (Figure 4.9c, dotted dashed line), however, did correspond to the unknown oxidation wave O_1. This shows that **11a-QM** is relatively unstable, and the O_1 wave may come from the reaction of the oxidized **11a-QM+** with pyridine. This is in contrast with the ferrocifens; the ferrocenyl quinone methide **10a-QM** is stable under CV conditions, regardless of the presence or absence of a base.

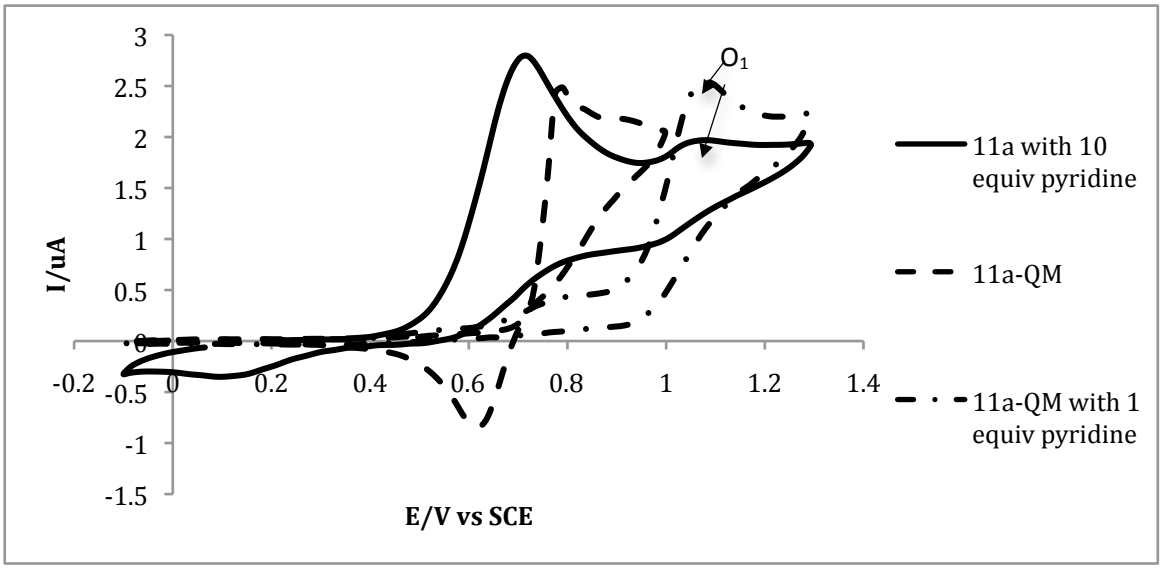

Figure 4.9 a) CV of **11a** (2 mM) in the presence of 20 mM pyridine (solid line), b) CV of **11a-QM** (2 mM) (dashed line) and c) CV of **11a-QM** (2 mM) in the presence of 2 mM pyridine (dotted dashed line). Conditions: study performed in DCM/[TBA][TFAB] (0.08 M); Pt electrode, 0.5 mm in diameter, scan rate 200 mV/s.

The above cyclic voltammetry experiments show that **11a** does not follow the same oxidation sequence as the ferrocifens. Although side reactions such as dimerization, which can disrupt the investigations, are to be noted, it is clear that the corresponding quinone methide is either not formed, or is unstable under the electrochemical conditions.

Redox properties of osmocifens

The redox properties of the osmocifens were investigated using osmociphenol **12a** (Figure 4.10). To prevent any nucleophilic attack of the supporting electrolyte/solvent onto the osmium centre, the [TBA][TFAB]/DCM electrolyte system was used; the base used was also changed to the non-nucleophilic base *2,6*-lutidine. Geiger et al have earlier shown that osmocene did not dimerize and, therefore, dimerization reactions can be ruled out in this case.[25] The cyclic voltammogram of **12a**

showed an chemical irreversible oxidation wave, in contrast to those for the ferrocifen and ruthenocifen derivatives, which showed reversible waves under the same conditions. Presumably, the more electronegative osmium increased the acidity of the phenol group so that **12a+** spontaneously deprotonated to **12a•** through the π-conjugated system (Scheme 4.4). This is supported by two observations: (i) the cyclic voltammogram of osmocene remained fully reversible after addition of phenol (Appendix A4.21), indicating the necessity of the conjugated system and (ii) a reversible CV was observed at high scan rates (250V/s), indicating that the deprotonation process can be blocked at such a fast timescale (Appendix A4.22).

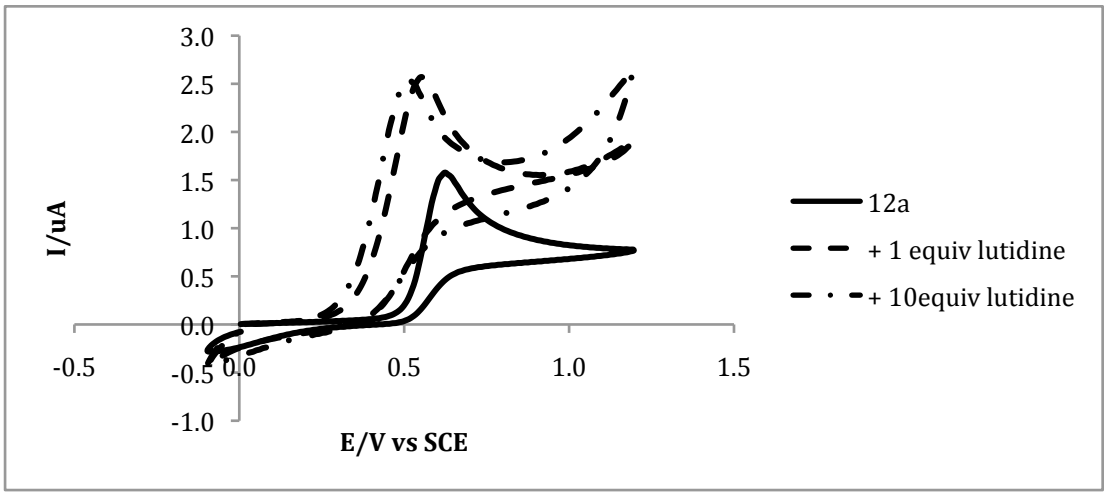

Figure 4.10 a) CV of **12a** (2 mM) (solid line), b) in the presence of lutidine (2 mM) (dashed line) and c) in the presence of lutidine (20 mM) (dotted dashed line). Conditions: study performed in DCM/[TBA][TFAB] (0.08 M); Pt electrode, 0.5 mm in diameter, scan rate 200 mV/s.

This also implies that oxidation of **12a** would allow the production of the corresponding radical **12a•** in the absence of a base. Indeed, upon addition of increasing amounts of 2,6-lutidine, the intensity of the oxidation wave of **12a** increased and shifted towards less positive potentials (Figure 4.10b). This base-dependent behavior, which is similar to that in the ferrocifens, clearly demonstrates that the presence of a base triggers a second electron transfer. In contrast to the ferrocifens, however, no new oxidation wave corresponding to oxidation of the quinone methide **12a-QM** was observed, at least at the cyclic voltammetry timescale. Since proton abstraction to

form the quinone methide should be fast, it is suspected that the QM was not formed at all, and that some other chemical reaction occurred upon addition of the base. The CV of an authentic sample of **12a-QM** also showed that, like the Ru analogue **11a-QM**, it is unstable under CV conditions.

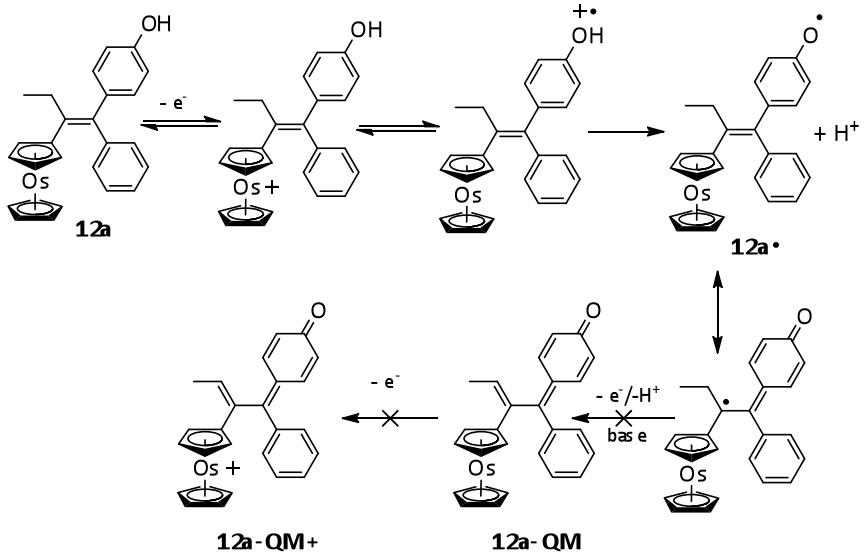

Scheme 4.4 Possible oxidation sequence of **12a**.

The above cyclic voltammetry experiments thus show that the ruthenocifens and osmocifens become highly unstable upon oxidation, and that their corresponding quinone methides are not formed electrochemically. Although the electrochemical conditions may not be truely representative biological oxidative conditions, the cyclic voltammetry experiments have demonstrated that ruthenocenium and osmocenium, unlike the ferrocenium, ions are extremely unstable and reactive and are thus unlikely to survive in the biological environment. Since the QMs are suspected to be the active species responsible for the antiproliferative activity, the inactivity of the phenol analogues of Ru and Os may be attributed to their inability to generate the quinone methides in situ.

4.3.4 Chemical reactivities - quinone methide formation

The QMs of the Ru and Os analogues can be synthesized chemically using Ag_2O as the oxidant (Scheme 4.5). It was observed, however, that their rates of formation were significantly slower than for the Fe analogues. The rate of formation of the three metallocifens was monitored by NMR spectroscopy; the methyl resonances for the QM and the starting material appeared as a doublet at

around 1.5 ppm, and as a triplet at around 0.9 ppm, respectively (Table 4.4).

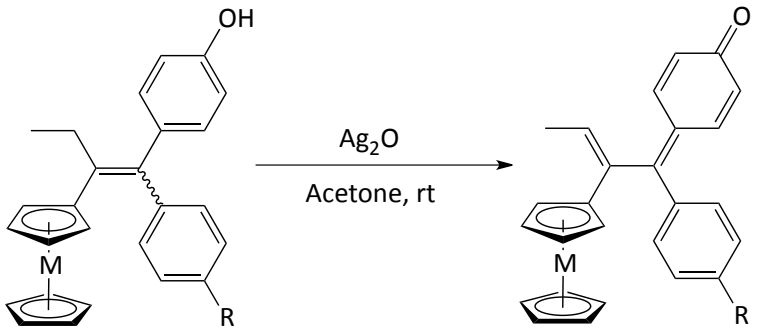

M = Fe, R = OH, **10b**
M = Fe, R = $O(CH_2)_3NMe_2$, **10c**
M = Ru, R = OH, **11b**
M = Ru, R = $O(CH_2)_3NMe_2$, **11c**
M = Os, R = OH, **12b**
M = Os, R = $O(CH_2)_3NMe_2$, **12c**

M = Fe, R = OH, **10b-QM**
M = Fe, R = $O(CH_2)_3NMe_2$, **10c-QM**
M = Ru, R = OH, **11b-QM**
M = Ru, R = $O(CH_2)_3NMe_2$, **11c-QM**
M = Os, R = OH, **12b-QM**
M = Os, R = $O(CH_2)_3NMe_2$, **12c-QM**

Scheme 4.5 Reaction of diphenol and amine chain analogues of the metallocifens with Ag_2O in acetone-d_6.

Table 4.4. Quinone methide formation: rate and rate constant

Cpd	R_1	R_2	Rate $M.s^{-1}$	Rate k* s^{-1}	$t_{1/2}$ (s)
10b-QM (Fe)	OH	OH	$38.7\ 10^{-6}$	$4.95\ 10^{-3}$	140
10c-QM (Fe)	OH	$O(CH_2)_3NMe_2$	$14.5\ 10^{-6}$	$1.61\ 10^{-3}$	431
11b-QM (Ru)	OH	OH	$3.5\ 10^{-6}$	$0.27\ 10^{-3}$	2567
11c-QM (Ru)	OH	$O(CH_2)_3NMe_2$	$3.0\ 10^{-6}$	$0.44\ 10^{-3}$	1575
12b-QM (Os)	OH	OH	$3.6\ 10^{-6}$	$0.32\ 10^{-3}$	2166
12c-QM (Os)	OH	$O(CH_2)_3NMe_2$	$3.2\ 10^{-6}$	$0.48\ 10^{-3}$	1444

* The reaction is assumed to follow first order kinetics.

The rate of oxidation to the quinone methides followed the order: Fe >> Ru ≈ Os, for both the

phenol and the amine chain analogues. It also correlates with the redox potential of the metal, where the oxidation potentials of the Fe compounds are lowest and therefore easiest to oxidize. The trend also correlates with the antiproliferative activity of the hydroxymetallocifen series, where **10c** is the most active, followed by **11c** and **12c**. However, the difference in antiproliferative activity of the diphenol analogues **11b** and **12b** cannot be fully explained by the ease of quinone methide formation since they have similar rates of formation (~3 x 10^{-6} Ms^{-1}). The inactivity of **11b** and **12b** may therefore be due to the instability of the QMs rather than whether the QMs were formed. This is corroborated by the observation that, in contrast to the iron quinone methide **10b-QM**, an orange solid precipitated from the acetone solutions of **11b-QM** and **12b-QM** upon standing (~60 min). On the other hand, the stability of **10c-QM**, **11c-QM** and **12c-QM** is remarkable; acetone solutions did not show signs of decomposition even after 24 h at room temperature. Indeed, it has been observed previously that while **10c-QM** could be isolated as a solid in its pure form, the phenol QMs could only be characterised spectroscopically but could not be isolated in their pure forms. This difference in stability between the QMs for the diphenol and amine chain analogues of the Ru and Os series may be one of the factors responsible for the difference in their activity. Similarly, the antiproliferative activity of the amine chain analogues is correlated to the rate of formation of the quinone methides. Both observations suggest that the quinone methides are involved, either directly or indirectly to the activity of the metallocifens.

4.4 Concluding remarks

This chapter revealed that the metal (Fe, Ru, Os) plays an important role in the antiproliferative activity of metallocene-based Tamoxifen. The difference in activity can be summarized as follows:

Table 4.5. Summary of difference in activity.	Complex (M)	Antiproliferative Activity		Senescence	
		ER+	ER-	1 μM	4 μM
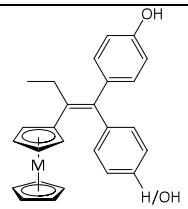	Fe	++	++	+	+
	Ru	Proliferative	-	-	-
	Os	Proliferative	-	-	-
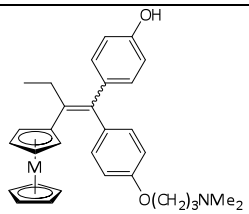	Fe	++	++	+	Change in shape
	Ru	+	+	+	
	Os	+	+	+	

The reasons for the difference in cytotoxicity of the complexes are multi-faceted. Although the side chain is the major contributor to the toxicity, the metallocene also plays a role. In particular, the differences in redox potential and electronegativity of the metal influences the formation of the quinone methides and their stability (chemically and electrochemically).

4.5 Experimental

Synthetic steps were carried out under an atmosphere of argon using standard Schlenk techniques. ^{1}H NMR spectra were recorded on a Bruker 300 NMR spectrometer as $(CD_3)_2CO$ solutions unless otherwise stated; chemical shifts reported were referenced against the residual proton signals of the solvent. The mass spectra (MS) were obtained on DSQII and ITQ 110 Thermo Scientific spectrometers for both electronic impact (EI) and chemical ionization (CI) methods. Starting material osmocene was obtained from Strem Chemicals; all other chemicals were purchased from other commercial sources and used as supplied. Ferrociphenol **10a**[5], ferrocidiphenol **10b**,[5] hydroxyferrocifen **10c**,[5] ruthenociphenol **11a**,[26] ruthenocidiphenol **11b**,[12] were synthesized according to literature methods.

4.5.1 Synthesis of propionyl osmocene 12

Osmocene (1000 mg, 3.12 mmol) and propionyl chloride (1.36 ml, 15.60 mmol) were first dissolved in dichloromethane (20 mL) in a schlenk vessel. Under Ar atmosphere, aluminum chloride (416 mg, 3.12 mmol) was added, and the mixture was allowed to reflux for 2 h. The mixture was then hydrolyzed with water (20 mL), extracted with dichloromethane (2 x 20 mL), and dried over $MgSO_4$. The solvent was removed under vacuum and the crude product was purified by column chromatography using pentane as eluent to elute unreacted osmocene (500 mg recovered) and a mixture of pentane/ethyl acetate (10:1, v/v) as eluent to elute propionyl osmocene (410mg). Yield: 41 %, isolated yield; 82 % yield based on amount of osmocene reacted. ^{1}H NMR (300 MHz, $CDCl_3$) δ: 1.10 (t, 3H, *J* = 7.3 Hz, $CH_2\mathit{CH_3}$), 2.50 (q, 2H, *J* = 7.3 Hz, $\mathit{CH_2}CH_3$), 4.76 (s, 5H, C_5H_5), 4.92 (t, 2H, *J* = 1.7 Hz, C_5H_4), 5.23 (t, 2H, *J* = 1.7 Hz, C_5H_4). ^{13}C NMR (75.47 MHz, $CDCl_3$) δ: 9.1 (CH_3), 31.9 (CH_2), 63.3 (CH, C_5H_4), 66.2 (CH, C_5H_5), 66.6 (CH, C_5H_4), 77.4 (C, C_5H_4), 202.9 (CO). Anal. Calcd for $C_{13}H_{14}OOs$: C, 41.47; H, 3.75 . Found: C, 41.47; H, 3.71.

4.5.2 Synthesis osmociphenol 12a

$TiCl_4$ (0.32 ml, 2.94 mmol) was added to a suspension of zinc powder (384 mg, 5.88 mmol) in THF (7 ml) in an ice bath. The mixture was then heated at reflux for 1 h to obtain a dark blue mixture. A second solution was prepared by dissolving 4-hydroxy-benzophenone (291 mg, 1.47 mmol) and propionyl osmocene **12** (370 mg, 0.98 mmol) in THF (2 ml). This latter solution was added to the first solution and the resulting mixture was heated for 30 min. After cooling to room temperature, the mixture was hydrolyzed with water (50 ml). After extraction with dichloromethane and solvent removal, the crude product was purified by column chromatography with petroleum ether/ether (2:1, v/v) as eluent. Pale yellow solid was obtained, yield: 390 mg (73 %), m. p. = 178°C, Z:E = 50: 50.

Z + E isomers: ^{1}H NMR δ: 0.96 + 0.99 (t, t, 3H, *J* = 7.5 Hz, CH_3, *Z* isomer + *E* isomer), 2.26 + 2.31 (q, q, 2H, *J* = 7.5 Hz, CH_2, *Z* isomer + *E* isomer), 4.44 (t, 1H, *J* = 1.5 Hz, C_5H_4), 4.51 (t, 1H, *J* = 1.5 Hz, C_5H_4), 4.54 (t, 1H, *J* = 1.5 Hz, C_5H_4), 4.57 (t, 1H, *J* = 1.5 Hz, C_5H_4), 4.69 + 4.60 (s, s, 5H, C_5H_5, *Z* isomer + *E*

isomer), 6.71 + 6.80 + 6.93 + 7.00 (4 d, 2H, *J* = 8.7 Hz, C_6H_4, *Z* isomer + *E* isomer), 7.08-7.25 (m, 3H, C_6H_5), 7.31 (t, 2H, C_6H_5), 8.25 + 8.28 (2s, 1H, OH, *Z* isomer + *E* isomer) .

^{13}C NMR δ: 16.0 (CH_3), 30.2 + 30.3 (CH_2), 64.1 (2CH, C_5H_4), 65.5 (5CH, C_5H_5), 66.6 (2CH, C_5H_4), 86.5 (C, C_5H_4), 115.6 + 115.8, 128.7 + 129.0, 129.9, 130.6, 131.0, 131.7 (CH, Ar), 126.8 + 126.9 (CH_p of C_6H_5), 136.4 + 136.6 (C), 136.9 (C), 137.4 (C), 138.4(C), 138.5(C), 145.6 (C), 145.9 (C), 156.7 + 156.8 (C-OH).

EI-MS: 544.2 $[M]^{\cdot+}$. Anal. Calcd for $C_{26}H_{24}OOs$: C, 57.54; H, 4.46. Found: C, 57.31; H, 4.44.

4.5.3 Synthesis of osmocidiphenol 12b

$TiCl_4$ (0.23 ml, 2.13 mmol) was added to a suspension of zinc powder (278 mg, 4.26 mmol) in THF (7 ml) in an ice bath. The mixture was then heated at reflux for 1 h to obtain a dark blue mixture. A second solution was prepared by dissolving 4,4-dihydroxy-benzophenone (228 mg, 1.07 mmol) and propionyl osmocene **12** (270 mg, 0.71 mmol) in THF (2 ml). This latter solution was added to the first solution and the resulting mixture was heated for 30 min. After cooling to room temperature, the mixture was hydrolyzed with water (25 ml). After extraction with dichloromethane (2 x 10 ml) and solvent removal, the crude product was purified by column chromatography with diethyl ether/petroleum ether (2:1, v/v) as eluent. White/Pale yellow solid was obtained, yield: 290 mg (73 %). M. p.: 238 °C (recrystallized from DCM/Hexane).

^{1}H NMR δ: 0.94 (t, 3H, *J* = 7.5 Hz, $CH_{3,}$), 2.26 (q, 2H, *J* = 7.5 Hz, CH_2), 4.47 (t, 2H, *J* = 1.5 Hz, C_5H_4), 4.65 (t, 2H, *J* = 1.5 Hz, C_5H_4), 4.65 (s, 5H, C_5H_5), 6.68 + 6.78 + 6.90 + 6.97 (4d, 4 x 2H, *J* = 8.5 Hz, C_6H_4), 8.18 (s, 2H, OH).

^{13}C NMR δ: 16.0 (CH_3), 30.4 (CH_2), 63.9 (2C, C_5H_4), 65.4(5C, C_5H_5), 66.6 (2C, C_5H_4), 87.0 (C, C_5H_4), 115.5 (2CH, C_6H_4), 115.7 (2CH, C_6H_4), 130.9 (2CH, C_6H_4), 131.7 (2CH, C_6H_4), 136.3 (C, C_6H_4), 136.8 (C, C_6H_4), 137.1 (C-alkene), 138.4 (C-alkene), 157.5 (C-OH), 157.6 (C-OH).

EI-MS: 561.04 $[M+H]^+$. Anal. Calcd for $C_{26}H_{24}O_2Os$: C, 55.89; H, 4.33. Found C, 55.47; H, 4.33.

4.5.4 Synthesis of hydroxyosmocifen 12c

In a schlenk vessel, **12b** (300 mg, 0.54 mmol) was dissolved in anhydrous DMF (2 ml). NaH (60 % oil, 48 mg, 0.81 mmol) was then added as a powder into the solution. The solution was then heated to 100 °C progressively. In another schlenk vessel, Et_3N (0.12 ml, 0.81 mmol) was added to a suspension of $Cl(CH_2)_3NMe_2.HCl$ (128.1 mg, 0.81 mmol) in THF (7 mL). After stirring for 1 h, the solution was added to the first solution maintained at 100 °C. After 1 h of heating, the mixture was concentrated using a rotary evaporator, hydrolyzed with water (50 ml), and extracted with ethyl acetate (2 x 75 ml). Combined organic extracts were washed with water (50 ml) and dried over $MgSO_4$. The crude mixture was vacuumed dried and purified by column chromatography using acetone/triethylamine (10:1, v/v) as eluent to give 3 bands. Band 1 corresponds to unreacted starting material. (135 mg recovered, 45 %), band 2 corresponds to **12c** (125 mg (66 % based on amount of starting material reacted, 36 % based on isolated yield)). Band 3 corresponds to di-alkylated product (47 mg, 12 %). **12c** was recrystallized using DCM/Hexane to obtain white solids. Melting point: 128 °C.

Z:E isomers: 50:50. *Z* + *E* isomers: ^{1}H NMR (400 MHz, CD_3SOCD_3) δ: 0.90 + 0.91 (2 t, 3H, *J* = 7.5 Hz, $CH_2\mathit{CH_3}$), 1.80 – 1.85 (m, 2H, $OCH_2\mathit{CH_2}CH_2N$), 2.15 + 2.16 (2s, 6H, $N(CH_3)_2$), 2.13 – 2.20 (m, 2H, $OCH_2CH_2\mathit{CH_2}N$), 2.34 – 2.39 (m, 2H, $\mathit{CH_2}CH_3$), 3.91 + 3.93 (2t, 2H, *J* = 6.4 Hz, $O\mathit{CH_2}CH_2CH_2N$), 4.38 + 4.39 (2t, 2H, *J* = 1.5 Hz, C_5H_4), 4.56 - 4.58 (m, 2H, C_5H_4), 4.69 (s, C_5H_5), 6.59 + 6.68 + 6.75 + 6.79 +6.84 + 6.88 + 6.89 + 6.98 (8d, 8H, *J* = 8.5 Hz, $2C_6H_4$), 9.26 + 9.30 (2s, 1H, OH).

Z + *E* isomers: ^{13}C NMR (100 MHz, CD_3SOCD_3) δ: 15.5 + 15.6 ($CH_2\mathit{CH_3}$), 26.8 ($OCH_2\mathit{CH_2}CH_2$), 29.0 + 29.1 ($\mathit{CH_2}CH_3$), 45.1 ($N(CH_3)_2$), 55.6 ($OCH_2CH_2\mathit{CH_2}N$), 63.3 ($O\mathit{CH_2}CH_2CH_2N$), 64.8 (7CH, C_5H_5 + C_5H_4), 65.5 (2CH, C_5H_4), 85.2 + 85.3 (C, C_5H_4), 113.7 + 114.0 (2CH, C_6H_4), 114.7 + 115.0 (2CH, C_6H_4), 129.7 (2CH, C_6H_4), 130.4 (2CH, C_6H_4), 134.7 + 134.9 +135.0 +136.4 + 136.7 + 136.8 (4C, C_6H_4 + C-alkene), 155.5 + 155.6 (C-O), 156.8 + 156.9 (C-O).

EI-MS: 646.04 $[M+H]^+$. Anal. Calcd for $C_{31}H_{35}NO_2Os$: C, 57.83; H5.48; N, 2.08. Found C, 57.42; H, 5.42; N, 2.08.

4.5.5 Synthesis of hydroxyruthenocifen 11c

This synthesis is an alternative to that previously reported.[11]

In a schlenk vessel, **11b** (300 mg, 0.64 mmol) was dissolved in anhydrous DMF (2 ml). NaH (60 % oil, 58 mg, 0.96 mmol) was then added as a powder into the solution. The solution was then heated to 100 °C progressively. In another schlenk vessel, Et_3N (0.13 ml, 0.96 mmol) was added to a suspension of $Cl(CH_2)_3NMe_2.HCl$ (151.7 mg, 0.96 mmol) in THF (7 mL). After stirring for 1 h, the solution was added to the first solution maintained at 100 °C. After 1 h of heating, the mixture was concentrated using a rotary evaporator, hydrolyzed with water (50 ml), and extracted with ethyl acetate (2 x 75 ml). Combined organic extracts were washed with water (50 ml) and dried over $MgSO_4$. The crude mixture was vacuumed dried and purified by column chromatography using acetone/triethylamine (10/1, v/v) as eluent. **11c** obtained (185 mg, 52 % yield) was recrystallized from dichloromethane/Hexane to give white solids. Melting point: 194 °C. Z:E or E:Z about 60:40.

Z + *E* isomers: ^{1}H NMR (400 MHz, CD_3SOCD_3) δ: 0.99 + 1.00 (2 t, 3H, *J* = 7.5 Hz, $CH_2\mathit{CH_3}$), 1.80 – 1.93 (m, 2H, $OCH_2\mathit{CH_2}CH_2N$), 2.18 + 2.19 (2s, 6H, $N(CH_3)_2$), 2.35 – 2.43 (m, 4H, $OCH_2CH_2\mathit{CH_2}N$ + $\mathit{CH_2}CH_3$), 3.96 - 4.03 (m, 2H, $O\mathit{CH_2}CH_2CH_2N$), 4.29 + 4.32 (m, 2H, C_5H_4), 4.36 - 4.39 (m, 2H, C_5H_4), 4.51 (s, C_5H_5), 6.68 + 6.76 + 6.79 + 6.87 +6.88 + 6.95 + 6.98 + 7.06 (8d, 8H, *J* = 8.6 Hz, $2C_6H_4$), 7.96 (s, 1H, OH).

Z + *E* isomers: ^{13}C NMR (100 MHz, CD_3SOCD_3) δ: 15.9 ($CH_2\mathit{CH_3}$), 28.2 ($\mathit{CH_2}CH_3$), 29.9 ($OCH_2\mathit{CH_2}CH_2$), 45.6 ($N(CH_3)_2$), 56.8 ($OCH_2CH_2\mathit{CH_2}N$), 66.6 ($O\mathit{CH_2}CH_2CH_2N$), 70.3 (2CH, C_5H_4), 71.8 (5CH, C_5H_5), 72.6 (2CH, C_5H_4), 93.4 (C, C_5H_4), 114.7 + 114.9 (2CH, C_6H_4), 115.6 + 115.8 (2CH, C_6H_4), 131.1 + 131.2 (2CH, C_6H_4), 131.7 + 131.8 (2CH, C_6H_4), 136.0 + 136.1 + 136.6 +138.2 +138.7 (4C, C_6H_4 + C-alkene), 156.7 + 156.8 (C-O), 158.5 + 158.6 (C-O).

EI-MS: 555.35 $[M]^{\cdot+}$

Anal. Calcd for $C_{31}H_{35}NO_2Ru$: C, 67.13; H, 6.36; N, 2.52. Found C, 67.18; H, 6.48; N, 2.43

4.5.6 Synthesis of osmocenyl quinone methide 12a-QM

12a (60 mg, 0.11 mmol) was dissolved in dry acetone (5 mL). Ag_2O (154 mg, 0.66 mmol) was added and the mixture was stirred for 2 h at room temperature. The red solution of quinone methide formed was separated from the solid by centrifugation (rt, 400 g, 5 min) and evaporated. A red oil (53 mg, 89% yield) of quinone methide was obtained. 1 mL of acetone was added to dissolve the quinone methide. Pentane was added to precipitate the quinone methide (red solid), Z + E isomers, E isomer is supposed to be the major isomer (E:Z 73:27).

^{1}H NMR δ: 1.59 (d, 3H, *J* = 7.0 Hz, CH_3, major isomer), 1.99 (d, *J* = 7.0 Hz, 3H, CH_3, minor isomer), 4.50 (s, 5H, C_5H_5, major isomer), 4.50 – 4.64 (m, 4H,C_5H_4), 4.64 (s, 5H, C_5H_5, minor isomer), 5.75 (q, *J* = 7.0 Hz, 1H, C<u>H</u>-Me, minor isomer), 6.28 (q, *J* = 7.0 Hz, 1H, C<u>H</u>-Me, major isomer), 6.30-6.39 (m, 2H, C_6H_4), 7.33 (dd, *J* = 10.0 Hz + *J* = 2.5 Hz, 1H, C_6H_4, minor isomer), 7.40-7.53 (m, 7H, C_6H_5+C_6H_4). ^{13}C NMR δ: 15.8 (CH_3), 63.6 + 64.0 + 64.5 66.5 (C_5H_4), 65.8 (C_5H_5, major isomer), 66.0 (C_5H_5, minor isomer), 85.7 (C, C_5H_5), 125.2 (CH_3-<u>C</u>H=C), 129.2, 129.4, 130.7, 131.6, 132.1, 139.9 (<u>C</u>H of C_6H_5 and C_6H_4), 138.4 (C), 139.1 (C), 140.0 (C), 157.3 (C), 186.8 (C=O).

EI-MS: 542.3 $[M]^{\cdot+}$

HRMS (ESI, $[C_{26}H_{22}OOs+H]^+$) calcd: 543.1359, found: 543.1338.

4.5.7 Synthesis of osmocenyl quinone methide 12b-QM

12b (26 mg, 0.04 mmol) was dissolved in dry acetone (1 mL). Ag_2O (92 mg, 0.40 mmol) was added and the mixture was stirred for 1 h at room temperature. The red solution of quinone methide formed was filtered by syringe to remove Ag_2O.

^{1}H NMR δ: 1.53 (d, *J* = 7.0 Hz, 3H, CH_3, major isomer), 1.98 (d, *J* = 7.0 Hz, 3H, CH_3, minor isomer), 4.28 (broad s, 1H, C_5H_4), 4.53 (s, 5H, C_5H_5, major isomer), 4.62 (s, 5H, C_5H_5, minor isomer), 4.53-4.66 (m, 2H, C_5H_4), 4.98 (broad s, 1H, C_5H_4), 6.26 (q, *J* = 7.0 Hz, 1H, C<u>H</u>-Me), 6.32 (m, 2H, C_6H_4), 6.98 (d, *J* = 8.0 Hz, 2H, C_6H_4), 7.32 (d, J = 8.0 Hz, 2H, C_6H_4), 7.45 (broad dd, 1H, C_6H_4), 7.53 (broad dd, 1H, C_6H_4), 8.5 s, 1H, OH).

MS (CI): m/z = 559.29 $[M+H]^+$.

HRMS (ESI, $[C_{26}H_{22}O_2Os+H]^+$) calcd: 559.1308, found: 559.1292.

4.5.8 Synthesis of osmocenyl quinone methide 12c-QM

12c (71 mg, 0.11 mmol) was dissolved in dry acetone (10 mL). Ag_2O (154 mg, 0.66 mmol) was added and the mixture was stirred for 2 h at room temperature. The red solution of quinone methide formed was separated from the solid by centrifugation (rt, 400 g, 5 min) and evaporated. A red oil (63 mg, 90% yield) of quinone methide was obtained. 1 mL of acetone was added to dissolve the quinone methide. Pentane was added to precipitate the quinone methide (red solid). ^{1}H NMR δ: 1.54 (d, *J* = 7.0 Hz, 3H, CH_3), 1.93 (m, 2H, CH_2), 2.17 (s, 6H, NMe_2), 2.41 (t, *J* = 6.9 Hz, 2H, CH_2), 4.14 (t, *J* = 6.4 Hz, 2H, OCH_2), 4.27 (broad s, 1H, C_5H_4), 4.53 (s, 5H, C_5H_5), 4.53-4.66 (m, 2H, C_5H_4), 4.97 (broad s, 1H, C_5H_4), 6.27 (q, *J* = 7.0 Hz, 1H, C<u>H</u>-Me), 6.27-6.36 (m, 2H, C_6H_4), 7.08 (d, *J* = 8.8 Hz, 2H, C_6H_4), 7.38 (d, J = 8.8 Hz, 2H, C_6H_4), 7.41 (dd, *J* = 10.0 and 2.8 Hz, 1H, C_6H_4), 7.51 (q, *J* = 10.0 and 2.8 Hz, 1H, C_6H_4). ^{13}C NMR δ: 15.7 (*CH_3*), 28.2 (OCH_2*CH_2*CH_2), 30.1 (*CH*), 45.7 ($N(CH_3)_2$), 56.7 (OCH_2CH_2*CH_2*N), 63.8 (2CH, C_5H_4), 65.8 (7CH, C_5H_5 + C_5H_4), 67.1 (O*CH_2*CH_2CH_2N), 115.4 (2CH, C_6H_4), 125.4 (CH_3-<u>C</u>H=C), 128.7 (CH), 129.4 (CH), 133.6 (2CH, C_6H_4), + 138.3 (CH), 161.9 (C-OCH_2).

MS (CI): m/z = 644.89 $[M+H]^+$.

HRMS (ESI, $[C_{31}H_{33}O_2Os+H]^+$) calcd: 644.2200, found: 644.2187.

4.5.9 X-Ray crystal determination

Colourless needles were grown by slow cooling of a DCM/ hexane solution at 4 °C. The crystals chosen were mounted on a quartz fiber. X-ray diffraction data were collected on a Bruker X8 APEX Single-Crystal X-ray Diffractometer at 103(2) K, using Mo Kα radiation, with the SMART program.[28] Reflections data was processed and corrected for Lorentz and polarization effects with SAINT,[29] and for absorption effects with SADABS.[30] The structure was solved by direct methods, and subsequent difference maps were used for locating the rest of the non-hydrogen atoms to complete the structure. Hydrogen atoms were placed in calculated positions and refined with a riding model. In

the final model, all non-hydrogen atoms were given anisotropic displacement parameters. The crystal of **12a** exhibited twinning; the twin law was determined to be a two-fold about the x-axis. There was also disorder of the OH group. This was modeled with alternative positions at the two phenyl rings, corresponding to the presence of an E- and Z-isomer. The occupancies were refined to be almost equal. The crystal of **12b** exhibited disorder of the ethyl group, which was modeled with two alternative sites, with their occupancies summed to unity. Appropriate restraints were placed on all disordered parts. Structural solution and refinement were carried out using the SHELXTL suite of programs.[31] Crystallographic data have been deposited with the Cambridge Crystallographic Data Centre (CCDC-1013129 and CCDC-1013130), and can be obtained free of charge via www.ccdc.cam.ac.uk/data_request/cif.

4.5.10 Determination of log $P_{o/w}$ values

Log $P_{o/w}$ values of the compounds were determined by reverse-phase HPLC on a C18 column (NUCLEODUR C18 HTec 5 μm) according to the method described by Minick[32] and Pomper.[33] Measurement of the chromatographic capacity (kN) for each compound was done at various concentrations in the range of 70 – 95 % methanol (containing 0.25 % octanol) and an aqueous phase consisting of 0.15 % n-decyl-amine in 0.02 M MOPS (3-morpholinopropanesulfonic acid) buffer pH 7.4 (prepared in 1-octanol-saturated water). These capacity factors (kN) were extrapolated to 100 % of the aqueous component to give the value of kN_w. Log $P_{o/w}$ (y) was then obtained with the formula: $\log P_{o/w} = 0.13418 + 0.98452 \log kN_w$.

4.5.11 Cell viability assays

MDA-MB-231 and MCF-7 breast cancer cells were maintained in monolayer in DMEM with phenol red (Gibco BRL) supplemented with fetal calf serum (10 %, Gibco BRL) and L-glutamine (1 %, Sigma Aldrich) at 37 °C in a 5 % CO_2 incubator. For antiproliferation assays, the cells were first plated in DMEM (1 mL; with phenol red for MCF-7, and without phenol red for MDA-MB-231), supplemented with decomplemented and hormone depleted fetal calf serum (10 %) and L-glutamine (1 %). It was

allowed to incubate for 24 h, after which 1 ml of media containing the compounds to be tested was added to the plates. After 3 days, the incubation medium was removed and fresh medium containing the compounds was added. Amount of viable cells were analyzed on the fourth day for MDA-MB-231 and fifth day for MCF-7, as follows. Cell media was removed and the cell monolayer was then fixed using methylene blue (1 ml, 1mg/ml in 1:1 MeOH/H_2O v/v) for 1 h. Methylene blue was then removed and the wells were rinsed twice with ultra pure water. Hydrochloric acid (2 ml, 0.1 M) was then added and the absorbance of each well was measured at 650 nm with microplate reader (Biorad). The results were then expressed as the percentage of proteins versus the control.

4.5.12 Senescence-associated β-galactosidase staining

MDA-MB-231 cells were first plated into a 24-well plate at a density of 25000 cells/well, in DMEM without phenol red, supplemented with decomplemented and hormone-depleted fetal calf serum (10 %), L-glutamine (1 %) and Penicillin/Streptomycin (1 %). They were incubated for 24 h, after which they were treated with **10a** – **12c** at various concentrations (0.5 μM – 8 μM) for 4 days. After treatment, cells were fixed with 3 % paraformaldehyde (pH 7.2). Cells were then washed and stained with a solution of 1 mg/mL 5-bromo-4chloro-inolyl-β-galactoside (pH 6, X-gal) in 5 mM potassium ferrocyanide, 5 mM potassium ferricyanide, 150 mM NaCl, 40 mM citric acid and 2 mM $MgCl_2$ (37 °C, 24 h). Senescence-associated β-galactosidase activity was then assessed under an optical microscope.

4.5.13 Chemical cyclic voltammetry experiments

Cyclic voltammetry experiments were performed at room temperature under an argon atmosphere in a three-electrode cell by using an Autolab potentiostat (PGSTAT 20). The reference electrode was an SCE (saturated calomel electrode; Tacussel), which was separated from the solution by a bridge compartment filled with the same solvent/supporting electrolyte solution as used in the cell. The counter electrode was a platinum grid (ca. 0.5 cm2, Goodfellow). The glass-sealed platinum working

electrodes disks (0.5 mm diameter, Goodfellow) were home-made. $TBA^+B(C_6F_4)^-$ electrolyte was synthesized according to reported literature.[25]

4.5.14 Chemical oxidation experiments

To the compounds dissolved in acetone-d_6 (0.010 - 0.015 M), 10 equivalents of freshly prepared Ag_2O were added at 20 °C. The formation of quinone methide was then followed by drawing aliquots (0.7 mL) at specific times for NMR recording. The intensity of the methyl signal was used for the calculation of rates and rate constants.

4.6 References

1 S. Top, A. Vessières, C. Cabestaing, I. Laios, G. Leclercq, C. Provot, G. Jaouen, *J. Organomet. Chem*. **2001**, *637*, 500.

2 E. A. Hillard, P. Pigeon, A. Vessières, A. Amatore, G. Jaouen, *Dalton Trans*, **2007**, 5073

3 A. Nguyen, A. Vessières, E. A. Hillard, S. Top, P. Pigeon, G. Jaouen, *Chimia.* **2007**, *61*, 716

4 A. Vessières, *J. Organomet. Chem.* **2013**, *734*, 3

5 S. Top, A. Vessières, G. Leclercq, J. Quivy, J. Tang, J. Vaissermann, M. Huché, G. Jaouen, *Chem Eur J*. **2003**, *9*, 5223.

6 E. A. Hillard, A. Vessières, L. Thouin, G. Jaouen, C. Amatore, *Angew. Chem. Int. Ed.* **2006**, *45*, 285.

7 P. Pigeon, S. Top, O. Zekri, E, A. Hillard, A. Vessières, M. A. Plamont, O. Buriez, E. Labbé, M. Huche, S. Boutamine, C. Amatore, G. Jaouen, *J. Organomet. Chem*. **2009**, *694*, 895

8 J. de J. Cázares-Marinero, E. Labbé, S. Top, O. Buriez, C. Amatore, G. Jaouen, *J. Organomet. Chem*. **2013**, *744*, 92-100

9 J. de J. Cázares-Marinero, O. Buriez, E. Labbé, S. Top, C. Amatore, G. Jaouen, *Organometallics*. **2013**, *32*, 5926-5934

10 D. Hamels, P. M. Dansette, E, A. Hillard, S. Top, A. Vessières, P. Herson, G. Jaouen, D. Mansuy, *Angew. Chem.* **2009**, *121*, 9288; *Angew. Chem. Int. Ed.* **2009**, *48*, 9124.

11 P. Pigeon, S. Top, A. Vessières, M. Huché, E. A. Hillard, E. Salomon, G. Jaouen, *J. Med. Chem.* **2005**, *48*, 2814.

12 A. Vessieres, S. Top, P. Pigeon, E. Hillard, L. Boubeker, D. Spera, G. Jaouen, *J. Med. Chem.* **2005**, *48*, 3937.

13 E. A. Hillard, A. Vessieres, S. Top, P. Pigeon, K. Kowalski, M. Huche, G. Jaouen, *J. Organomet. Chem,* **2007**, *692*, 1315.

14 A. Vessieres, C. Corbet, J. M. Heidt, N. Lories, N. JOuy, I. Laios, G. Leclercq, G. Jaouen, R. A. Toillon, *J. Inorg. Biochem,* **2010**, *104*, 503.

15 C. Lu, J.-M. Heldt, M. Guille-Collignon, F. Lemaitre, G. Jaouen, A. Vessieres, C. Amatore, *Chemmedchem* **2014**, *9*, 1286-1293.

16 Q. Michard, G. Jaouen, A. Vessières, B. A. Bernard, *J. Inorg. Biochem.* **2008**, *102*, 1980-1985.

17 P. Leeson, *Nature*, **2012**, *481*, 455.

18 O Buriez, J. M. Heldt, E. Labbe, A. Vessieres, G. Jaouen, C. Amatore, *Chem. Eur. J.* **2008**, *14*, 8195.

19 a) O Buriez, E. Labbe, P. Pigeon, G. Jaouen, C. Amatore, *J. Electroanal. Chem,* **2008**, *619*; b)O. Mertins, O. Buriez, E. Labbe, P.-P. Fang, E. Hillard, A. Vessieres, G. Jaouen, Z.-Q. Tian, C. Amatore, *J. Electroanal. Chem*. **2009**, *635*, 13; c) O. Mertins, P. Messina, E. Labbe, V. Vivier, S. Arbault, F. Lemaître, O. Buriez, C. Amatore, *Inorg. Chim. Acta* **2011**, *374*, 59.

20 D. Plazuk, A. Vessieres, E. A. Hillard, O. Buriez, E. Labbe, P. Pigeon, M. A. Plamont, C. Amatore, J. Zakrzewski, G. Jaouen, *J. Med. Chem.* **2009**, *52*, 4964.

21 J. C. Swarts, A. Nafady, J. H. Roudebush, S. Trupia, W. E. Geiger, *Inorg. Chem.* **2009**, *48*, 2156.

22 M. D. Todd, Y. Dong, J. T. Hupp. *Inorg. Chem.* **1991**, *30,* 4688.

23 S. Trupia, A. Nafady, W. E. Geiger. *Inorg. Chem.* **2003**, *42*, 5480.

24 M. G. Hill, W. M. Lamanna, K. R. Mann, *Inorg. Chem.* **1991**, *30*, 4687.

25 R. J. LeSuer, C. Buttolph, W. E. Geiger, *Anal. Chem.* **2004**, *76*, 6395.

26 H. Z. S. Lee, O. Buriez, E. Labbe, S. Top, P. Pigeon, G. Jaouen, C. Amatore, W. K. Leong, *Organometallics*, **2014**, *33*, 4940.

27 P. Messina, E. Labbe, O. Buriez, E. A. Hillard, A. Vessieres, D. Hamels, S. Top, G. Jaouen, Y. M. Frapart, D. Mansuy, C. Amatore, *Chem. Eur. J.* **2012***, 18*, 6581.

28 SMART, version 5.628 ed., Bruker AXS Inc., Madison, WI, **2001**.

29 SAINT+, version 6.22a ed., Bruker AXS Inc., Madison, WI, **2001**.

30 G. M. Sheldrick, SADABS, **1996**.

31 SHELXTL, version 5.1 ed., Bruker AXS Inc., Madison, WI, **1997**.

32 D. J. Minick, J. H. Frenz, M. A. Patrick, D. A. Brent, *J. Med. Chem.* **1988**, *31*, 1923.

33 M. G. Pomper, H. VanBrocklin, A. M. Thieme, R. D. Thomas, D. O. Kiesewetter, K. E. Carlson, C. J. Mathias, M. J. Welch, J. A. Katzenellenbogen, *J. Med. Chem.* **1990**, *33*, 3143.

Chapter 5. Conclusion

In this work, two classes of organometallic compounds of osmium, i.e., the triosmium carbonyl clusters and the hydroxyosmocifens, were examined in relation to their activity as anticancer agents. The role of the osmium was different for the two classes of compounds; the triosmium carbonyl clusters exert their activity by virtue of the metal centre, while the metal does not play a direct role in the activity of the osmocifens but serves to modulate the activity of the organic fragment – Tamoxifen.

A number of osmium carbonyl clusters, viz., $Os_3(CO)_{10}(NCMe)_2$ **2**, $Os_3(CO)_{11}(NCMe)(\mu\text{-}H)^+$ **1'** and $Os_3(CO)_9(\mu\text{-}H)(\mu\text{-}\gamma\text{-}C_6H_5O_3)$ **5**, were found to exhibit high cytotoxicity, and they appear to have intracellular sulfhydryl residues as the common target. This can be understood on the basis that osmium is a soft Lewis acid; it binds weakly to hard Lewis bases such as acetonitrile, hence these dissociate easily and allows the creation of a vacant coordination site for binding to sulfhydryl residues which are soft Lewis bases. This binding with protein targets in turn causes downstream reactions, which ultimately leads to cell death.

The difference among these clusters lie in the key step that triggers their reactivity (Scheme 5.1). For **2**, the weakly bound acetonitrile ligands readily dissociate, giving two vacant coordination sites for the binding with thiols. For **1'**, initial deprotonation to the neutral species **1** is required in order for the acetonitrile ligand to be displaced; **1** is the active form that reacts with the thiol, while the positive charge just imparts solubility to the compound. Finally for **5**, a stronger nucleophile such as a thiolate is required. As may be expected, solubility was also found to play an important role in the activity of these osmium clusters; therefore the lipophilicities (the balance between solubility and the ability to penetrate the cell membrane) will have to be investigated. Most importantly, these osmium carbonyl clusters were found to be selective towards cancer cells over normal cells; the reason for this selectivity requires further examination.

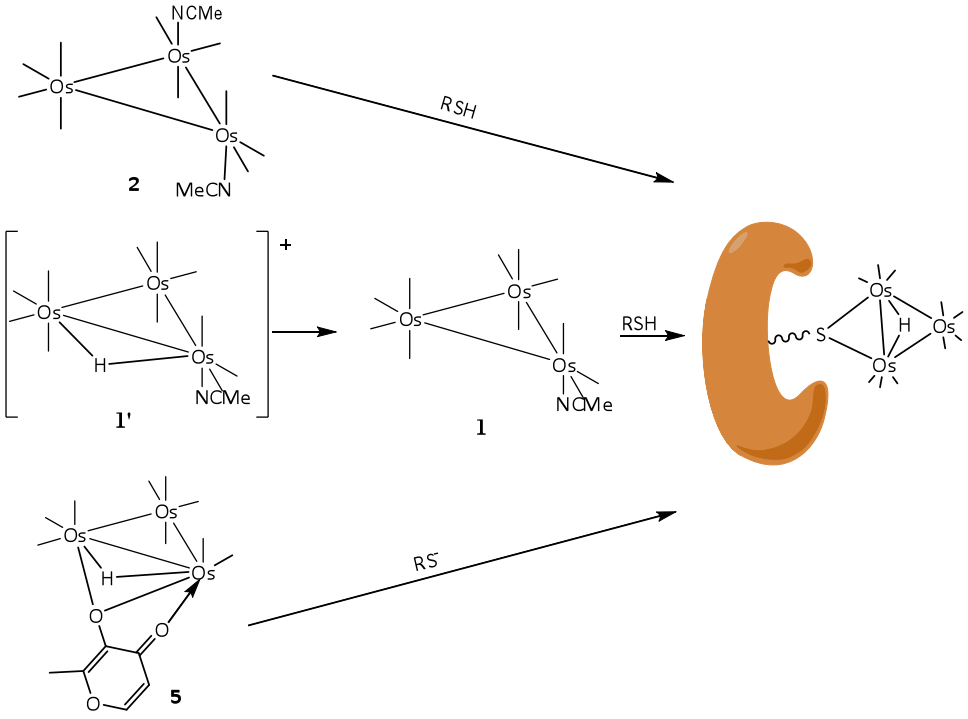

Scheme 5.1. Reaction of osmium carbonyl clusters **2**, **1'** and **5** with thiols.

Their different triggers also have implications on future drug design. Firstly, the fact that only one vacant coordination site/labile ligand instead of two is required already widens the possibility of many more osmium carbonyl clusters as potential drug candidates. Secondly, that **1'** is only activated under basic conditions suggests that it will be interesting to explore osmium carbonyl clusters that can be triggered under different physiological conditions. Since cancer cells are usually more acidic than normal cells, clusters that are activated under acidic conditions may exhibit selectivity for cancer cells.[1] The reaction of alcohols with the cluster $Os_3(CO)_{10}(\mu\text{-}H)(\mu\text{-}OH)$ **7b**, for example, is known to be catalyzed by the addition of a few drops of HBF_4, and preliminary cell viability assays showed that it did gave some selectivity. Therefore, it would be interesting to extend this investigation. Finally, that **5** responded to thiolate and not to thiol suggest that carbonyl clusters may be tuned to respond to different biologically important functional groups. This would allow for targeting of specific proteins or other biological molecules.

Earlier studies on the ferrocifens have suggested that their activity was ascribable to the formation of quinone methides. The ability to form the quinone methides is a function of the redox potential of the metal; the three metallocifens (Fe, Ru, Os) exhibited similar structural and physical characteristics but very different antiproliferative activity (Table 5.1). The ferrocifens greatly enhanced the cytotoxicity of Tamoxifen, and became very active against the hormone independent (ER-) breast cancer cells. On the other hand, only the ruthenocifen and osmocifen are active while the monophenol and diphenol analogues are almost inactive against the breast cancer cells. This result shows that the cytotoxic effect of the metallocifens not only came from the metallocene but also the amine chain; and this effect is more pronounced for the ferrocene series. This could be attributed to the higher redox potentials of Ru and Os – oxidation to the active quinone methides was more difficult, and the stability of these were also lower. Lastly, the senescence effect seems to be an important characteristic too; only compounds that induce senescence showed cytotoxicity.

Table 5.1 Summary of difference in activity

Compound	Metal (M)	Antiproliferative Activity		Senescence	QM formation electrochemically	QM stability
		ER+	ER-			
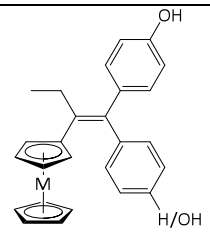	Fe	++	++	+	✓	✓
	Ru	Proliferative	-	-	× (**11a**)	Unstable
					- (**11b**)	(for **11b**)
	Os	Proliferative	-	-	× (**12a**)	Unstable
					- (**12b**)	(for **12b**)
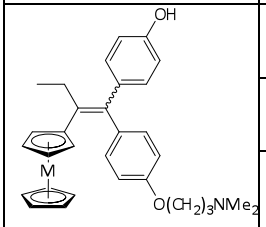	Fe	++	++	+	✓	✓
	Ru	+	+	+	-	✓
	Os	+	+	+	-	✓

Since the osmocifens were found to be similar in physical properties as the ferrocifens, the more electron-rich osmium may have potential structural mimics for bioimaging purposes; it has been a challenge to establish the target or distribution of ferrocifen due to the abundance of iron ions in the body.

---

1 L. E. Gerweck, K. Seetharaman, *Cancer Research*, **1996**, *56*, 1194; I. F. Tannock, D. Rotin, *Cancer Research*, **1989**, *49*,4373.